Direct Imaging Analysis of the Circumstellar Disks and Planetary-mass Companions on Wide Orbit Around a Disk-host Star

Daehyeon OH

Doctor of Philosophy

Department of Astronomical Science
School of Physical Sciences
SOKENDAI (The Graduate University for Advanced Studies)

THE GRADUATE UNIVERSITY FOR ADVANCED STUDIES

Direct Imaging Analysis of the Circumstellar Disks and Planetary-mass Companions on Wide Orbit Around a Disk-host Star

by

Daehyeon OH

A thesis submitted in partial fulfillment for the
degree of Doctor of Philosophy

in the
Department of Astronomical Science

June 20, 2016

"Look again at that dot. That's here. That's home. That's us."

Carl Sagan

"My God — it's full of stars!"

David Bowman

Submission:	January 8, 2015
Examination of doctoral dissertation:	January 22, 2016
Conferment of doctoral degree:	March 24, 2016
Minor update:	June 20, 2016

THE GRADUATE UNIVERSITY FOR ADVANCED STUDIES

Abstract

Department of Astronomical Science

Doctor of Philosophy

by Daehyeon OH

During the last decades, remarkable progress of observational techniques has pioneered the new fields of circumstellar objects such as protoplanetary disks and planets. The diverse structures of protoplanetary disks have been obtained by observations at near-infrared to millimeter wavelengths. Especially, Infrared Astronomical Satellite had revealed the presence of a transition phase between primordial disk and debris disk. In the so-called *transitional disks*, evidence of a large inner hole has been discovered through modeling analysis of the infrared spectral energy distributions and interferometry at millimeter wavelengths. Subsequently, the presence of another transition phase *pre-transitional disks* has been reported; evidence of a large gap and an optically thick inner disk has been discovered. The most convincible cause of holes and gaps in (pre-)transitional disks is disk-planet interaction, and thus the evolution of such disks are eventually connected with the origin of planetary systems, such as our solar-system. However, it is not clear whether the cause of structural diversity is disk evolution or different disk clearing mechanisms. Furthermore, there is no clear evidence showing that a pre-transitional disk is the actual former phase of a transitional disk.

In this thesis, I embark on observational studies to reveal the cause of different disk cavities in typical disks, whether disk evolution or disk clearing mechanisms, by high-resolution near-infrared polarimetric imaging. At the same time, I also embark on the property of planets inside and outside disks, because the presence of a planet is one of the major factors in disk evolution and disk clearing. I chose three typical objects from three disk categories; DoAr 25 from cavity-less full disks, LkCa 15 from pre-transitional disks, and GM Aur for transitional disk to concentrate the disk structure.

As results of observations, I have found that each of disks has individual physical properties and that only DoAr 25 has a visible planetary-mass companion with wide separation over 1430 AU. For DoAr 25, I have found a cavity-less full disk with a flared surface and dust shell remnant which indicate the youth of the disk. Strong forward scattering from the disk surface also suggests that this disk is still in early stage of dust grain growth. A newly discovered planetary-mass companion around DoAr 25 is called DoAr 25 b. On the basis of additional observations including common proper motion test, I confirmed that DoAr 25 b is a co-moving 13 $M_{\rm Jup}$ companion with possible circumplanetary disk, and its convincible origin is a molecular cloud core, not the disk around DoAr 25. For LkCa 15, I have found a large gap whose radius is consistent with the result of previous sub-mm interferometry imaging studies. I also have found that the optically thick inner disk is significantly tilted with the outer disk. This is the first direct detection of so-called warped disk associated with young T Tauri star. Such morphological features indicate the presence of multiple planets less massive than 1 $M_{\rm Jup}$ in the LkCa 15 system. Furthermore, physical inconsistency, such as degrees of flared surfaces of inner and outer disks, suggests that some possible unknown physical mechanisms could be working on it. For GM Aur, I have found a large inner hole at near-infrared wavelengths for the first time, which has a significantly smaller radius than that of previous sub-mm interferometry images. This inconsistency may indicate the presence of a few-$M_{\rm Jup}$ planet in the GM Aur disk cavity.

I have searched a possible connections between resolved disk structures and disk evolution from comparative study of three disks, but there is no common chronological sense in comparisons of physical parameters (cavities, mass accretion rates, and degrees of flared surface) which could be interpreted as an evolutionary path. On the other hand, I have discussed and suggested an alternative explanation; the more convincible cause of diversity in structures is different clearing conditions (the presence of massive planets, masses and orbital radii of planets). Furthermore, the presence of planetary-mass companion outside the disk indicates that the range of planetary system is wider than previous understanding, and that there are still unrevealed fields in the disk-planet connection and the origin of planets.

Acknowledgements

This work would not have been possible without an enormous amount of support that I received from many wonderful people around me. First of all, I would like to sincere thank to my supervisor Prof. Motohide Tamura for his endless advice and encouragement throughout the years that got things right and led to the submission of thesis. His invaluable insight into the star and planet formation have motivated me start this work. I am truly fortunate to have had such a generous and insightful scientist as my supervisor. I also deeply thank to Dr. Jun Hashimoto and Dr. Masayuki Kuzuhara who have guided me stay on the track and develop my research more professionally. Thanks to their highly accurate advices and incredibly scrupulous care, I could rise up from endless difficulties so many times.

I am also indebted to Dr. Nobuhiko Kusakabe, Dr. Tomoyuki Kudo, Dr. Tea-Soo Pyo, Dr. Yasuhiro Takahashi, Dr. Takuya Suenaga, and Dr. Jungmi Kwon who has kindly helped me observe my targets using the Subaru Telescope, and has taught the astronomical data reduction from the very beginning. If it had not been their help, I couldn't even have started the research. I want to thank to many SEEDS coworkers over the world, including Dr. John Wisniewski, Dr. Christian Thalmann, and Dr. Satoshi Mayama who generously advised to the both of the research and my english. Even though I am not able to mention all the wonderful people, I would like to thank here. I hope they know how I appreciate them.

In the last 4 years, I have been economically supported by private foundations; Takaku Foundation (2012), The Korean Scholarship Foundation (2013-2014), and Honjo International Scholarship Foundation (2015). The worth of their great and generous supports to international students in Japan is immeasurable, and I am very proud of being one of their scholarship student.

Last but never the least, I deeply grateful to my family and my friends. Their constant encouragement has made me never lose the light even in the deepest darkness.

Contents

List of Figures

List of Tables

Part I

General Introduction

Chapter 1

General Introduction

1.1 Formation and Classification of YSOs

The current understanding of the low-mass star formation is standing on the remarkable progresses of theoretical and observational works over the last few decades. The formation of young stellar objects (YSOs) begins with the collapse of molecular dense core. Interstellar molecular clouds have local non-uniformity due to its own gravitational instability, or external pressures such as stellar wind. When gravitational force overcomes that of thermal expansion, the first step for low-mass star formation begins. When the core density gets close to the stellar density, it is called a protostar or a protostellar object. During the gravitational collapse, collapsing materials revolve around the center of dense core because of angular momentum conservation. Those rotating and accreting materials form flattened disk extending for tens to hundreds of astronomical units, which is known as an accretion disk or a circumstellar disk.

The general evolutionary sequences of protostars and pre-main-sequence stars are divided into distinct groups based on the spectral slope α (or spectral index) of the spectral energy distribution (SED) at NIR and MIR wavelength; Class I, II, III (Lada, 1987), and Class FS (Greene et al., 1994), which are given as;

$$\begin{aligned} \alpha =& \frac{d\log \lambda F_\lambda}{d\log \lambda}, \\ \alpha >& \ 0.3 \text{ for Class I;} \\ -0.3 <& \ \alpha < 0.3 \text{ for Class FS;} \\ -1.6 <& \ \alpha < -0.3 \text{ for Class II;} \\ \alpha <& \ -1.6 \text{ for Class III.} \end{aligned} \tag{1.1}$$

Figure 1.1 describes the current schematic of formation of low-mass star (Dauphas and Chaussidon, 2011). Class I is the earliest evolutionary stage detected in the infrared and characterised by $\alpha > 0.3$. Class I YSOs are surrounded by a heavy (a few tenths of a solar mass) circumstellar envelope, and powerful molecular outflows are associated with it. Thus, they have strong mid-IR excess over the estimated blackbody emission of stellar photosphere. When the evolutionary stage proceeds to next stage, known as Class II, a notable IR excess still exists, but IR-SED slope is apparently declining with increasing wavelengths ($-1.6 < \alpha < -0.3$). This is due to the circumstellar envelope dissipating and the growth of flatter accretion disk. Class FS is the intermediate stage between Class I and II. When the accretion disk is dissipated, the evolutionary stage turns into the final stage, Class III. In this pre-main-sequence stage, YSOs are not surrounded by circumstellar envelope anymore, but only by the remnants of circumstellar disk. Thus they have a steep spectral slope ($\alpha < -1.6$).

In the optical observations, there is a T Tauri category for also young and low-mass (0.2-2 $M_\odot$) stars in pre-main-sequence. T Tauri stars were easily identified by their strong emission lines, in particular Hα. They are classified as Classical T Tauri stars (CTTSs, alias Class II YSOs) with stronger emission lines, and weak-line T Tauri stars (WTTSs, alias Class III YSOs) with relatively weak emission lines. Their emission is believed to come from the hot accreting circumstellar disk with the radii of a few hundred AU and the mass of 0.001 to 0.1 $M_\odot$. Thus the stronger emission lines of CTTSs indicate an earlier stage of stellar evolutional phase than WTTSs

1.2 Circumstellar Disk

Circumstellar disks are considered as the birth-place of planets. Understanding the physical processes that occurs through the disk evolution is crucial for understanding

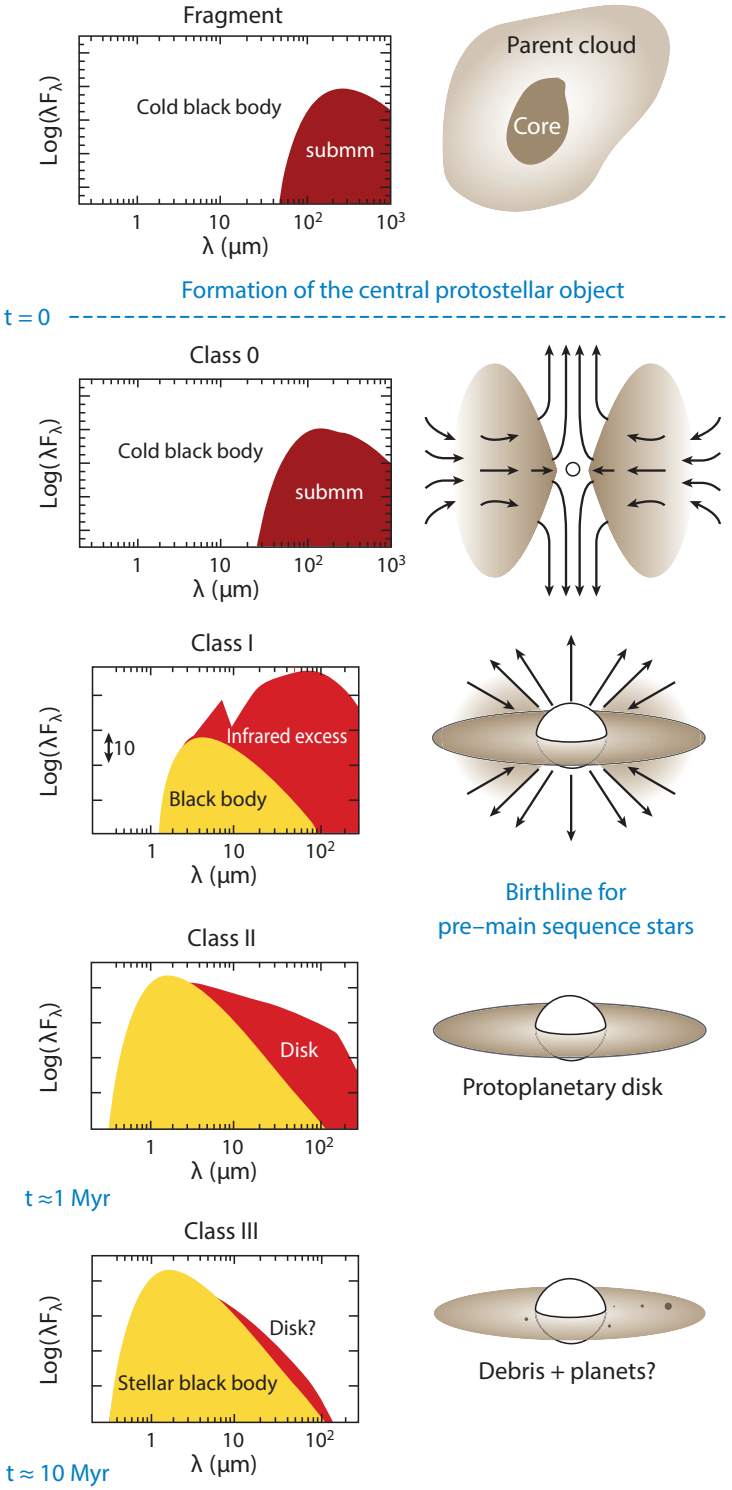

FIGURE 1.1: Schematic of formation of low-mass star. (Figure adapted from Dauphas and Chaussidon, 2011)

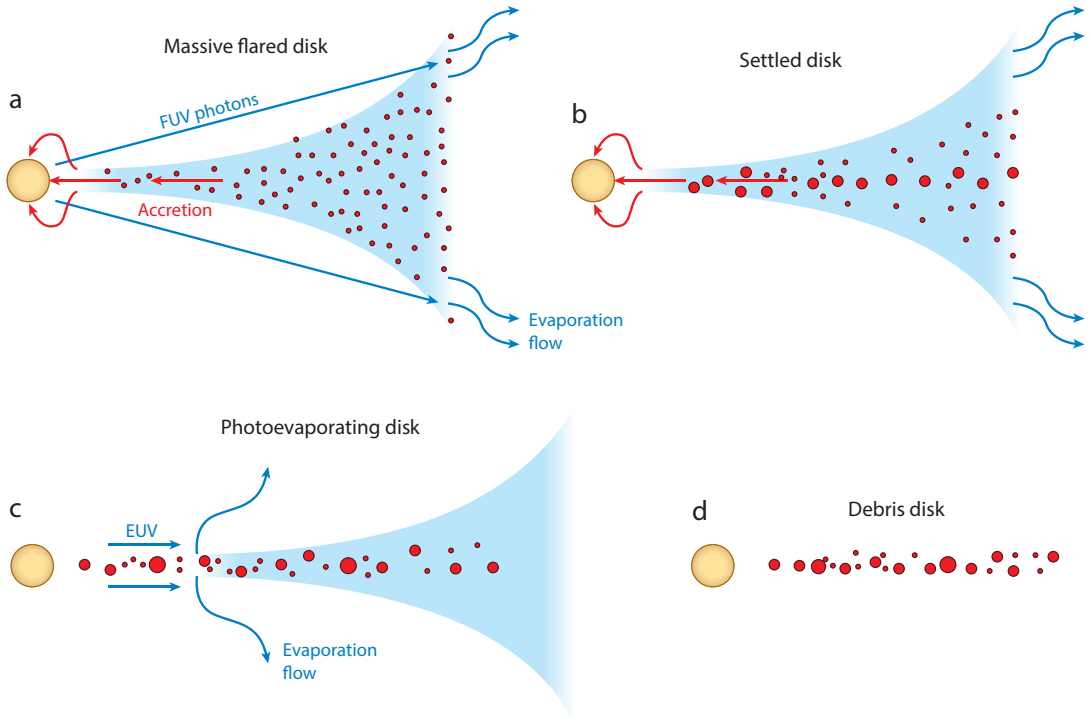

FIGURE 1.2: Schematic of typical evolution of circumstellar disk. The gas distribution is shown in blue and the dust in red. (a): The disk loses mass through accretion onto the star and FUV photoevaporation. (b): Dust grains grow into larger bodies and settle down to the mid-plane of the disk. (c): As mass accretion rate decrease, photoevaporation becomes more dominant, and the inner disk quickly dissipates from the inside out. (d): After gas and small grains are disappeared by photoevaporation and radiation pressure, the gas poor disk with larger grains and planetesimals/planets is left behind. (Figure adapted from Williams and Cieza, 2011).

the origin and the formation of planets. The Infrared Astronomical Satellite (IRAS) and ground-based observations (e.g., Skrutskie et al., 1990, Strom et al., 1989) opened up the identification and statistical studies of circumstellar disks. Disks emit strong radiations at a range of wavelengths from microns to millimeters, because they have a range of surface temperatures, observations at a wide range of wavelengths allowed detailed constructions of their physical models, even from unresolved photometry.

1.2.1 Typical Evolution of Circumstellar Disks

Circumstellar disks are believed to evolve through various processes, such as viscous accretion, dust grain growth, photoevaporation, and gravitational interaction with lower-mass companions. Those physical processes are well constrained observationally, but they explain only few parts from the entire disk evolution. Although the complex evolution of circumstellar disks is still well not understood, there is a suggested coherent

picture – typical evolution – based on observational trends and many models including above physical processes.

In the early evolutionary stage, the disk loses mass through accretion onto star and FUV photoevaporation (Massive flared disk; Figure 1.2a). At this phase, the object would be classified as a CTTS based on its high accretion rate. At the same time, dust grains start to settle down onto the mid-plane of the disk as they grow into lager grains. This makes the flared dusty disk becomes sharper and flatter (Settled disk; Figure 1.2b). Accretion rate may be variable on a short time scale, but it declines in long-term trends. Once the accretion rate matches the photoevaporation rate at an inner region, the resupply of material from the outer disk is prevented by photoevaporation (Alexander et al., 2006a, Owen et al., 2010), and the inner disk drains onto the star within a viscous timescale ($\lesssim 10^5$ year), leaving an inner hole with the radius of a few AU surrounded by the low mass outer disk (Photoevaporating disk; Figure 1.2c). This short timescale evolution is believed as the counterpart of the rapid transition between the CTTS and the WTTS stage. After disappearing of optically thick inner disk, the energetic photons impact the outer disk, increase the photoevaporation rate, and make fast the mass dissipation of the disk. The WTTS objects in this disk dissipation stage show a various SED curves at near to mid-infrared wavelengths, as expected for disks with inner holes of different sizes (Cieza et al., 2008, Padgett et al., 2008, Wahhaj et al., 2010). After remaining gas and small grains are blown out by photoevaporation and radiation pressure, larger grains and planetesimals/planets are left behind in the gas poor disk (Debris disk; Figure 1.2d).

1.2.2 Transitional Disks

The observed properties of some circumstellar disks are not consistent with the evolutionary paths briefed in Section 1.2.1 and Figure 1.2. Among those outliers, the most intriguing subgroup is the *transitional disks* : objects that have large inner cavities with the size of tens AU, but still preserve massive outer disks with large accretion rates. By IRAS and ground based observations, unique objects with little or no excess emission at near-IR ($\lambda < 10\mu$m) but significant excess at mid- and far-IR ($\lambda \gtrsim 10\mu$m) were identified as transitional disks (Calvet et al., 2005, Espaillat et al., 2007a, Strom et al., 1989, Wolk and Walter, 1996). Although the transitional disks represents a small percentage of the

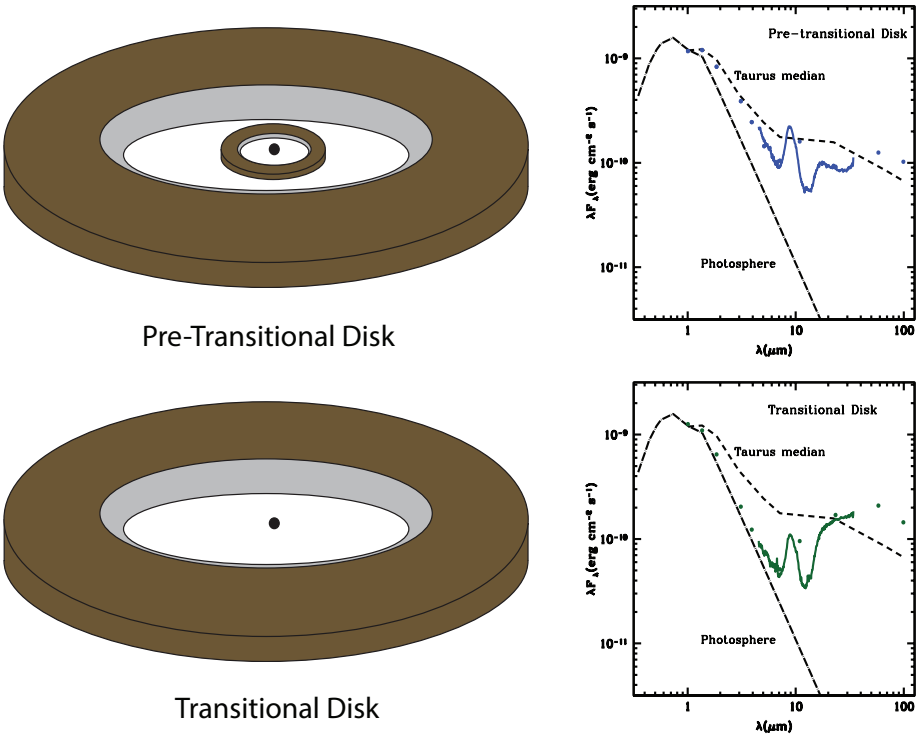

FIGURE 1.3: Schematic of pre-transitional (*top*), and transitional (*bottom*) disk structures with observed SED examples. SEDs are from LkCa 15; Espaillat et al. (2007a), GM Aur; Calvet et al. (2005), respectively. *Light gray* represents the disk wall. *Pre-transitional disk* is characterized by small but detectable near IR excesses ($<10\mu$m) and significant mid- and far-IR excesses ($\gtrsim 10\mu$m). *Pre-transitional disk* shows similar SED but less or no near-IR excesses(Figure adapted from Espaillat et al., 2014a).

observed disk population, but they have been considered as crucial targets to understanding the disk evolution because the lack of near-IR excess could be interpreted as a diagnostic of the disk clearing by planet formation. The Infrared Space Observations (ISO) and the Spitzer Space Telescope (Spitzer) allowed to infer a large cavity such as holes (e.g., Calvet et al., 2005, D'Alessio et al., 2005, Espaillat et al., 2007b, Uchida et al., 2004) and annular gaps (e.g., Brown et al., 2007, Espaillat et al., 2007a) based on disk SEDs. Espaillat et al. (2007a) additionally suggested the *pre-transitional disks*: objects that have large gap rather than inner cavities, based on their small but still detectable near-IR excess which indicate optically thick inner disks beyond large gaps (See Figure 1.3).

Cieza et al. (2007) introduced SED morphologic two-parameter scheme, $\lambda_{\text{turn-off}}$ and α_{excess}, to define the transitional disk, and this definition is also applicable to the pre-transitional disk (Figure 1.4 and Table 1.1; Also see Williams and Cieza, 2011). A $\lambda_{\text{turn-off}}$ represents the longest wavelength wavelength without significant infrared excess

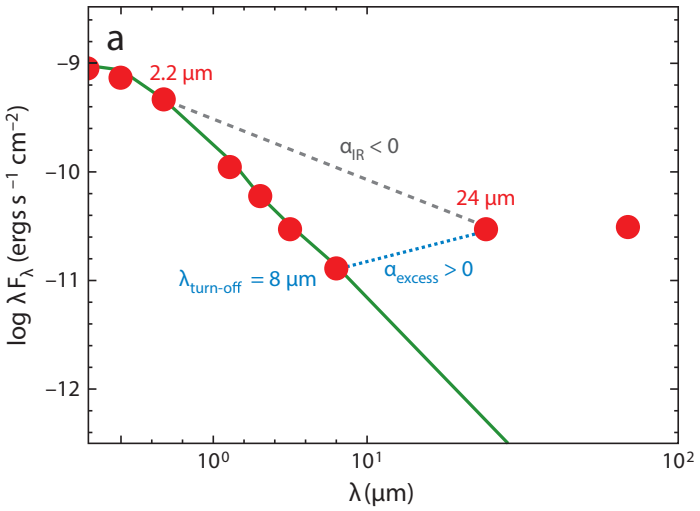

FIGURE 1.4: Schematic of $\lambda_{\text{turn-off}}$ and α_{excess} parameter scheme. A α_{IR} represents the slope of infrared excess over the emission of stellar object. (Figure adapted from Williams and Cieza, 2011).

TABLE 1.1: Schematic classification of (pre-)transitional disks.

	$\lambda_{\text{turn-off}}$	α_{excess}	Structure
FD[a]	$\lesssim 1\mu$m	none.	No significant inner hole.
PTD[b]	$1\mu\text{m} < \lambda_{\text{turn-off}} < 4.5\mu\text{m}$	>0	Inner disk, large gap, and massive outer disk.
TD[c]	$4.5\mu\text{m} \lesssim \lambda_{\text{turn-off}} \lesssim 8\mu\text{m}$	>0	Large inner cavity and massive outer disk.

[a] Full disk.
[b] Pre-transitional disk.
[c] Transitional disk.

on dereddened SED, and α_{excess} represents the slope of SED longward of $\lambda_{\text{turn-off}}$.

SED modeling is a powerful method and provides many evidences for the presence of inner cavities in transitional disks. However, it is essentially indirect estimation, and the results are strongly model-dependent. The more detailed direct studies of resolved disk images became possible as high-contrast direct and/or polarimetric imaging at infrared wavelengths (e.g., Fukagawa et al., 2006, Hashimoto et al., 2015, Thalmann et al., 2010) and interferometry at submillimeter wavelengths (Andrews and Williams, 2007b, Andrews et al., 2011a,b, Piétu et al., 2005) became available. The submillimeter observations provide detailed information, in particular, the distribution of large dust ($\gtrsim$ sub-mm) and its cavities (e.g., Andrews et al., 2011b). Infrared observations, on the other hand, provide high spatial resolution images of smaller dust ($\lesssim$ sub-μm) distribution, and inner region including central cavity within inner disk edge to central star

(e.g., Hashimoto et al., 2011, 2012).

Interestingly, it is revealed that the disk image at different wavelengths in some of (pre-)transitional disks often shows different structures. In particular, some of inner cavities detected at submillimeter wavelengths are missing at NIR wavelengths, even though the inner working angle of the NIR images is significantly smaller than the inferred cavity sizes from submillimeter observations (e.g., Dong et al., 2012a). This differences in the observations can be explained by the spatial differentiation of the grain sizes in the disk, since the observations with various techniques at different wavelengths resolve different aspects of the dust distribution (e.g., de Juan Ovelar et al., 2013b). The spatial differentiation of the grain sizes is considered as a result of pressure bumps which arise from the presence of the planet. Moreover, the result of 2D two fluid (gas + particles) hydrodynamical calculations with three-dimensional Monte Carlo Radiative Transfer simulation provides that multiple planets can open up the wide detectable gap at both of millimeter and NIR wavelengths, although a single planet ($\sim 0.2 M_{\rm Jup}$) only produces a gap at millimeter wavelengths and almost no features at NIR wavelengths (e.g., Dong et al., 2015). Therefore, the disk-planet interaction and the cavity-clearing mechanisms are the closely connected, and also are the core part of the essential issues to understand the origin and evolution of planetary system.

1.2.3 Veiled Disk Clearing Mechanisms

Many questions still exist in the physical transitions that occurs between transitional disk and pre-transitional disk (earlier evolutionary phase). The formation of the cavity in (pre-)transitional disk is not well understood currently. For example, in (pre-)transitional disks, a typical photoevaporation rate is not high enough to sustain the cavity against high mass accretion from the outer disk. Currently, several alternative disk clearing mechanisms are under consideration to explain the formation of a large cavity in transitional disks.

Grain growth models (e.g., Birnstiel et al., 2012, Dullemond and Dominik, 2005, Strom et al., 1989) have predicted a rapid depletion of small grains in the inner disk (e.g., Dullemond and Dominik, 2005, Tanaka et al., 2005). Birnstiel et al. (2012) showed that grain growth models can explain the loss of near- and mid-IR excess in the SED of transitional disks.

Protoplanetary disk wind via magneto-rotational instability (MRI) is more appropriate to massive outer disks (Chiang and Murray-Clay, 2007, Suzuki et al., 2010b). The MRI is driven by coupling between magnetic fields and disk rotation. Although it is purely an evacuation mechanism, the MRI working on the inner disk edge predicts substantial accretion rate and inner dust clearing by stellar radiation pressure.

Dynamical interactions between disks and companions are the most conceivable explanation to date for clearing large cavity in the disk (e.g., Dong et al., 2015, Kley and Nelson, 2012, Papaloizou et al., 2007). On the basis of two-dimensional disk-planet hydrodynamical simulations performed by Zhu et al. (2011) and Dodson-Robinson and Salyk (2011), a system of four or more planets may open wide a combined or common gap in the disks, whereas a single planet may open up a narrow gap. Dong et al. (2015) demonstrated that multiple planets can produce a wide common gap with few tens of AU at millimeter and near-infrared wavelengths, while a single low-mass planet ($\sim 0.2 M_{\rm Jup}$) can carve a deep gap at millimeter wavelengths and almost no features (e.g., too narrow gap to be detected) at near-infrared. And a large gap may play a role as a catalyst for inner disk clearing by inside-out MRI evaporation. At the outer edge of a planet-induced gap, dust particles drift outward by the gas pressure gradient, then some of particles are decoupled with infalling gas and stay at the gap edge. This dust filtration effect (Paardekooper and Mellema, 2006, Rice et al., 2006) leaves a dust-depleted inner cavity with no large dust grain supply from outer disk (Pinilla et al., 2012a, Zhu et al., 2012). After decoupled inner region diminished by *some* inside-out clearing, an evacuated central hole surrounded by a massive outer disk remains.

These mechanisms partially explain the observational results; however, there is no decisive observational evidence yet. At the moment, the only mechanism to sustain a wide cavity in the disk is dynamical formation of wide gaps by disk-planet interaction(Papaloizou et al., 2007). Therefore, the practical next pathway, and of particular interest, is to distinguish the disk-planet interactions from other proposed cavity-clearing mechanisms, by , e.g., detecting a planetary companion in the inner cavity region (e.g., Kraus and Ireland, 2012) or an annular gap between optically thick inner and outer disks (e.g., Espaillat et al., 2007a, Thalmann et al., 2015).

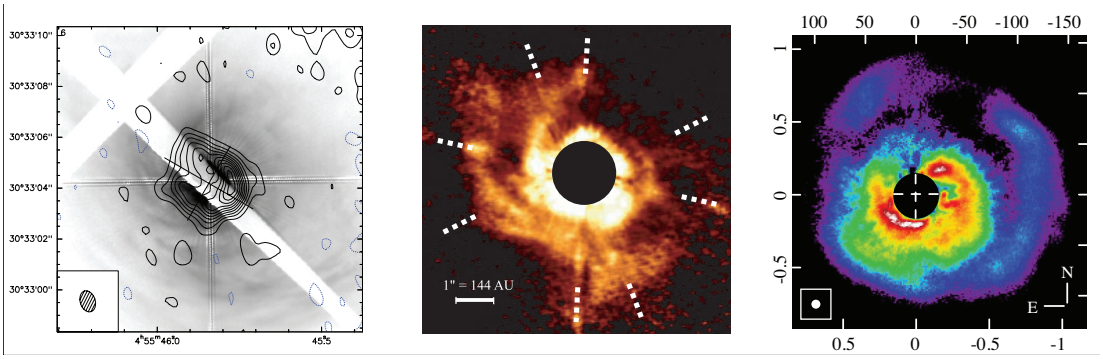

FIGURE 1.5: Observed images of AB Aurigae disk, (*left*): using submillimeter; (*center*): using near-infrared; (*right*) using polarized near-infrared. At infrared wavelengths, polarimetry technique provides more detailed image. Figures are adapted from Fukagawa et al. (2004), Piétu et al. (2005) and (Hashimoto et al., 2011), respectively. Even on the same target, each observation capture different properties of the disk.

1.2.4 Incomplete Understanding of Disk Evolution

Previous studies using submillimeter interferometric imaging (e.g., Andrews et al., 2009, 2010, 2011b) have revealed various structures, including large inner holes in transitional disks, from many of disk-host objects. The disk mass usually decided by the gas which is observable at submillimeter wavelengths. Thus submillimeter interferometry is a powerful method to reveal disk structure. However, resolving detailed spatial gas distribution is still difficult observational task. Although near-infrared observation cannot detect the gas, it can trace small dust particles which are coupled with the gas. Therefore, we can use a small dust particle distribution to derive a gas distribution in the disk. In general, submillimeter interferometry traces large particles (mm-size) in the disk, and has relatively low resolution in imaging ($\sim$40 AU at the distance of 140 pc). Since the disk evolution progresses in various dust particle sizes, a imaging-based studies must be combined with different wavelengths observations. Especially, de Juan Ovelar et al. (2013a) showed that planet-induced disk structures look different at different wavelengths, and that the range of difference is dominantly decided by the physical properties of embedded planet. Therefore, even though submillimeter interferometry is a powerful method to reveal disk structure, its results could drive us incomplete understanding of disk structures evolution without additional wavelengths observations, such as near-infrared wavelengths which trace smaller (μm-size) particles in the disk (See Figure 1.5).

Although recent imaging observations at multiple wavelengths imaging observations (micron to millimeter) have revealed the diversity of the disk structures over various ages, it is yet unclear what evolutionary pathway they pass through in their lifetime, varying

from $\lesssim$1 Myr to $\sim$ 10 Myr (Williams and Cieza, 2011). To construct a chronological view of the disk evolution, a highly accurate age measurement must be done. Before that, we can only estimate the position in schematic evolutionary tree of circumstellar disks, on the basis of morphological history analysis, such as origin and forming process of certain structures.

1.3 Planetary Mass Companions

1.3.1 Extrasolar Planet

The presence of planets orbiting stars other than the sun (extrasolar planets or exoplanets), had been discussed, and many challenges were conducted. After the verification of the first extrasolar planet around solar-like star (51 Pegasi b ; Mayor and Queloz, 1995), the significant progresses in the observation and data analysis techniques have been achieved and provided magnificent results. Especially, NASA's Kepler mission has found incredibly many extrasolar planets (confirmed and candidate), even more than the number of previously discovered planets. Currently, more than 1900 of confirmed planets (See Figure 1.6), and more than a twice the number of planet candidates were discovered. These discoveries have revealed an unexpected diversity in planet population, such as hot Jupiters (e.g., Jackson et al., 2008), hot Neptunes (e.g., Butler et al., 2004), and Super-Earths (e.g., Rivera et al., 2010). The presence of these exotic planets indicates our immature understanding on the planet formation mechanisms.

Most of extrasolar planets have been detected using radial velocity (RV) or planetary transits variations of the host star. One of the most powerful points of both methods is an excellent feasibility on medium-to-small telescopes and space telescopes. The large number of planet detection by both techniques has allowed the statistical studies. However, both methods usually require multiple observations over several orbital periods. Moreover, the high level of intrinsic stellar activity of young stars, such as T Tauri stars, makes the survey complicate on particular host stars. The RV method is also not suitable for planets around massive host stars due to the paucity of stellar absorption lines which play the role of the measurement scale in the RV method. This is why the distribution of the planets currently detected is strongly biased toward short-period planets at small separations around old and quiet host stars.

On the contrary, the direct imaging requires 8-m class telescopes with adaptive optics, and higher contrast imaging instruments. Thus, the current detection feasibility of

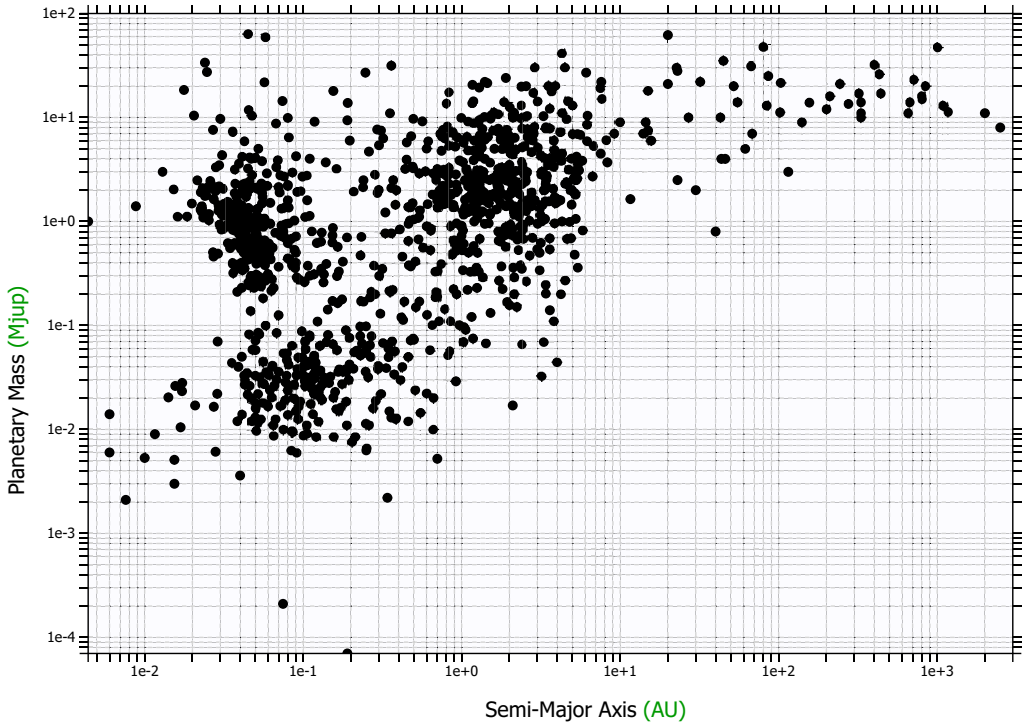

FIGURE 1.6: The orbit-radius to mass distribution of confirmed exoplanets (From exoplanet.eu). Different detecting methods have different detecting biases, thus there are some crowds. The planets detected by direct imaging biased toward heavy planets on wide orbit. The direct imaging became possible very recently and still not easy task, thus counterpart is relatively empty in the diagram.

the direct imaging is not as good as that of two methods mentioned above. However, the direct imaging can be applied to both young and old stars, and allows the direct measurements of the light from the planet itself, such as color, luminosities and spectra. Thus direct imaging is the essential and the ultimate method to study extrasolar planets. The total number of planets directly imaged is growing up slowly, but steadily, since the first direct detection of planets situated at the solar-system planetary orbit scale (e.g., Kalas et al., 2008, Marois et al., 2008).

1.3.2 Planets and Brown Dwarfs

Brown dwarfs are substellar objects that have mass lower than main-sequence stars. The presence of brown dwarfs was theoretically predicted and discussed earlier (e.g., Hayashi and Nakano, 1963, Kumar, 1963a,b). Brown dwarfs are not massive enough to sustain hydrogen fusion reaction in their interior. Due to that, the radiation from brown dwarfs steadily fades out as time passes out. This makes the detection of a brown dwarfs difficult and takes a long time. The first detection of cold brown dwarf

was reported in 1995 (GI 299B, Nakajima et al., 1995, Oppenheimer et al., 1995), the same year of the first extrasolar planet detection. On the other hand, the first detection of L-dwarfs, a colder brown dwarf, had been reported 1992 (GD 165B Zuckerman and Becklin, 1992). However, as the sensitivity of detections of substellar objects improved, the lower limit of brown dwarfs's mass decreased and approached to the mass of giant gas planets. Nowadays, the mass ranges of low-mass brown dwarfs and massive giant gas planets are partially overlapped. Various definitions have been suggested and strained by the discoveries of objects of intermediate masses (10∼15 $M_{\rm Jup}$). The Working Group on Extrasolar Planets of the International Astronomical Union stated a definitions of planets, brown dwarfs, and sub-brown dwarfs as follow (Boss et al., 2007):

> 1) Objects with true masses below the limiting mass for thermonuclear fusion of deuterium (currently calculated to be 13 Jupiter masses for objects of solar metallicity) that orbit stars or stellar remnants are "planets" (no matter how they formed). The minimum mass/size required for an extrasolar object to be considered a planet should be the same as that used in our Solar System.
>
> 2) Substellar objects with true masses above the limiting mass for thermonuclear fusion of deuterium are "brown dwarfs", no matter how they formed nor where they are located.
>
> 3) Free-floating objects in young star clusters with masses below the limiting mass for thermonuclear fusion of deuterium are not "planets", but are "sub-brown dwarfs" (or whatever name is most appropriate).

These statements are still working definitions and could be changed or updated, hence not the final definitions. Moreover, the deuterium fusion mass depends on several factors, such as the abundances of the helium and the initial deuterium, and on the model metallicity. Also, the error range of the mass estimation of low-mass objects is still significantly large. Thus, at the moment, it is difficult to clarify whether a certain intermediate mass object is brown dwarf or giant gas planet. Most of directly detected planets around solar-like stars are fall into this intermediate mass range. These objects, include low-mass brown dwarfs orbiting main-sequence stars, are also termed as planetary mass companions (PMCs) for convenience.

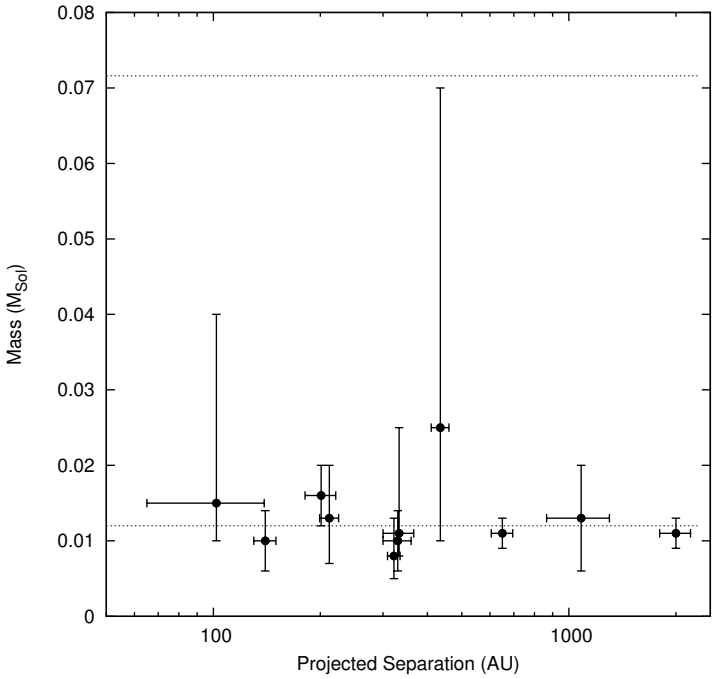

FIGURE 1.7: The separation to mass diagram of imaged PMCs around YSOs. Upper and bottom dashed line indicates the mass boundary of stellar object to brown dwarf, and brown dwarf to gas giant planet, respectively. See Section 7.14 for detailed object information.

1.3.3 Wide-orbit Planetary Mass Companions

The direct imaging technique revealed another unexpected distribution of extrasolar planets. Aforementioned kind of exotic planets, discovered by indirect method such as RV or planetary transit, are orbiting very close to their host stars, <1 AU, due to the detection bias mentioned above. Neptune, the farthest planet in our solar system, is $\sim$ 20 AU away from the sun. Conversely, some of the directly imaged planets are incredibly far from their host star, from few tens to two thousands of AU (e.g., Kuzuhara et al., 2011, Naud et al., 2014). These planets are generally termed wide-orbit planets, or wide-orbit PMCs.

The extremely wide orbital radius (>100 AU) is a huge challenge to current planet formation mechanisms. The conventional models for planet formation are the core-accretion model (e.g., Ida and Lin, 2004a,b, Kokubo and Ida, 2002), and the disk gravitational instability model (e.g., Boss, 1997, Cameron, 1978, Inutsuka et al., 2010). The core-accretion model explains the formation of giant planets as a result of multistage process; particle growth from dust grains into rocks, rocks into planetesimals, and finally planetesimals into protoplanetary cores (Williams and Cieza, 2011), but this model

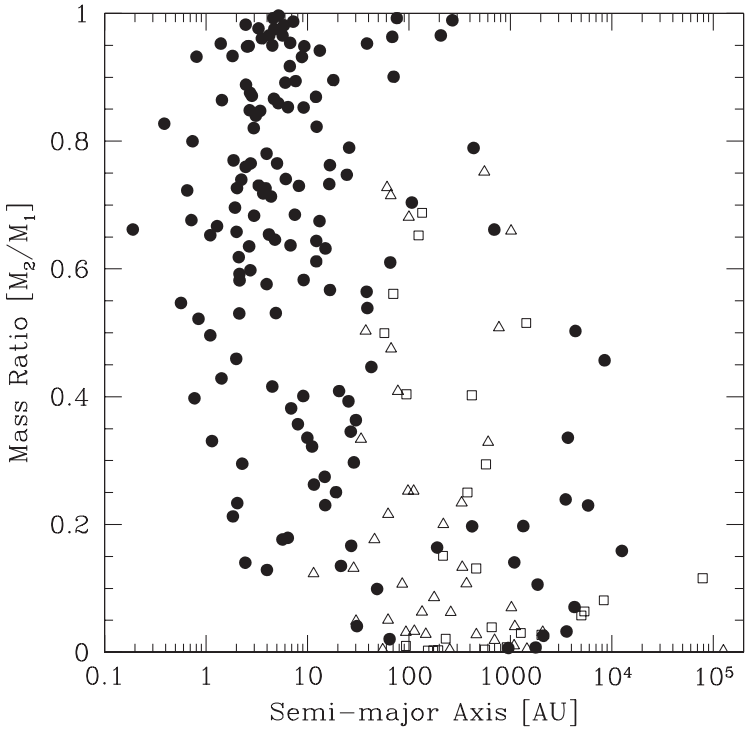

FIGURE 1.8: The mass ratio to separation diagram from Bate (2009)'s results of the hydrodynamical simulation of star cluster formation. (*filled circles*): Binaries; (*open triangle*): Triples; (*open squares*): quadruples. A few extremely low-mass companion (<5% of primary star) with extremely wide separation ($\gtrsim$1000 AU) is formed.

shows a very steep increase in the formation time scale with increasing distance from the host star, even Neptune has always been the difficult planet to form in the age of solar system (e.g., Pollack et al., 1996). The gravitational instability model produce giant planets via the gravitational collapse of perturbations (Williams and Cieza, 2011), but the disk needs to be massive enough to be Toomre unstable (Q<1; Safronov, 1960, Toomre, 1964) at planet forming location. However disks around young Class II stars (e.g., Andrews and Williams, 2005, 2007b, Andrews et al., 2009, 2010) do not have enough mass density to be Toomre unstable at a long orbital separations at hundreds of AU (e.g., Dodson-Robinson et al., 2009, Meru and Bate, 2010).

The origin of wide-orbit PMCs is still not well understood; thus it will provide new constraints to formation models for low mass objects. The first plausible scenario is that wide orbit PMCs originated in a planetary disk but ejected to outer orbit due to dynamic interaction with other massive companion such as binary star (e.g., Kuzuhara et al., 2011, Reipurth and Clarke, 2001). But most of wide-orbit PMCs are orbiting around single

stars and do not have other confirmed massive nearby objects. Thereby, this ejection scenario is ruled out. The second one is that wide orbit PMCs and their primary stars were both formed from molecular cloud core fragmentation (e.g., Bate, 2009, Bate et al., 2003, See Figure 1.8). The planet formation makes complex asymmetric structures such as gaps, spiral arms and holes in disk (e.g., Follette et al., 2015, Hashimoto et al., 2011, 2012, 2015, Pérez et al., 2014) and the planet-scattering from initial location within disk also causes the disk disrupting (e.g., Jilkova and Zwart, 2015, Raymond et al., 2012). Thus if wide orbit PMCs around young star are originated from stellar disk of primary star and then migrated outward, stellar disk of host star would be disappeared or has complex asymmetric structures. Besides, if wide-orbit-PMC-host star had significant symmetric disk, it indicates that a wide orbit PMC has non-stellar-disk origin, such as molecular cloud core fragmentation.

Chapter 2

Purpose and Approaching of This Thesis

In this thesis, I discuss the diversity of (proto-)planetary systems in two different points of view; protoplanetary disks and planetary objects beyond protoplanetary disk. I first aim to constrain the morphologic diversity of protoplanetary disks by resolving detailed spatial structures, and reveal the cause of the observed disk diversity; evolutionary phase or different clearing mechanism. By studying high resolution near-infrared polarimetric images, we have made possible to estimate the origin and connections of characteristic disk structures on the basis of imaging diagnostics for transitional disks at different wavelengths. Especially, disk cavities such as gaps and holes are the sign of disk-planet interaction which is one of the major interests in this thesis. Additionally, the surface radial profile of the disk may give us more hints about evolutionary phase. Typical protoplanetary disks are flared (Williams and Cieza, 2011), but flaring angle of the disk decreases as dust settling progresses in the disk. The slope of radial surface brightness profile, or of the radial polarized intensity profile in case of polarimetry, can be used for evaluating the flared disk (Dong et al., 2012a), because the flared disk surface scatters light more efficiently than the flat disk surface due to the lower incident angle of light. If other physical parameters of the disks are similar to each other, we can expect that more-evolved disk has less-flared disk than that less-evolved disk have.

Since many of protoplanetary disks have already been resolved at (sub-)mm wavelengths and have been analysed with SED, we could choose candidate objects that are suitable for our requirements: (1) they are in different disk categories; (2) they have similar disk masses; (3) their mass accretion rates are known; (4) ages of their host

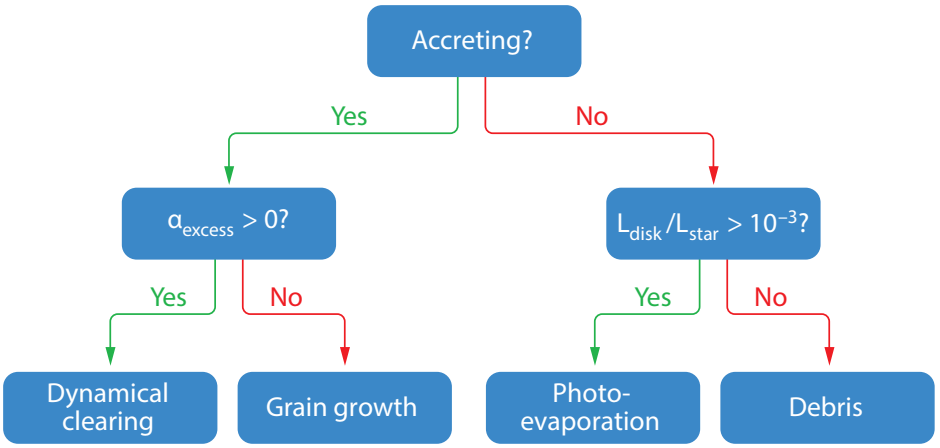

FIGURE 2.1: Decision tree to determine the dominant physical process for transition disks based on the study of Cieza et al. (2010). They suggested that diverse properties of transitional disks can be understood as a result of different disk evolutionary process and stages. Figure adapted from Williams and Cieza (2011).

stars are known; (5) cavity sizes in (sub-)mm disk images have been measured; and (6) $\alpha_{\rm excess} \gtrsim 0$. Cieza et al. (2010, 2012) and Romero et al. (2012) studied a large sample of disks in many star forming molecular clouds, and categorized on the basis of the dominant physical process (See Figure 2.1). To simplify the tree of possibility, we concentrated on dynamical clearing which is dominant in disks with $\alpha \gtrsim 0$. Finally selected targets are DoAr 25 full disk, LkCa 15 pre-transitional disk, and GM Aur transitional disk. The number of observed disk-host objects is ∼1500, and that of transitional disks is about ∼480 (Koepferl et al., 2013). Beside, the number of observationally and spatially resolved disks is only ∼20 (Espaillat et al., 2014a). Thus, at the present, well-resolved three disks could be a valuable statistical sample in transitional disk population.

Previous studies by Najita et al. (2007) and Espaillat et al. (2012) showed that mass accretion rates of similar-mass disks tend to decrease from full disks to transitional disks. Since the disk dispersing and the disk evolution are closely related to each other, this could be an indicative of the transitional order of the disk. Thus we set mass accretion rates as free parameter for comparison with the results based on our near-infrared observations.

Secondly, I aim to reveal the circumstellar planetary system beyond the protoplanetary disk by confirming wide-orbit planetary mass companion and searching their origin. Two faint objects were detected around DoAr 25 at the separations of ∼5″ and ∼11″.

If they are wide-orbit PMCs associated with DoAr 25, it would be a great laboratory for studying the possible origin of wide-orbit PMCs around young stars. Because if wide-orbit PMCs are originated in protoplanetary disk and migrated outer orbit later, there must be footprints in the disk. A typical companionship verification using common proper motion may not be enough, because some of nearby isolated objects share similar proper motions in dense star forming region, such as ρ Ophiuchus where DoAr 25 is located in. Thus I attached importance to additional companionship verifications by using multiple bands photometry. Furthermore, by combining with near-infrared spectroscopy, I will discuss the properties of confirmed object and its alternative origin.

Although these two subjects—protoplanetary disks and planetary mass companions beyond the disks— are related as diversity of circumstellar systems, I separated this thesis into two parts, because each subject deserves to be discussed independently. This thesis consists of the following parts and chapters:

In Part II

Chapter 3 introduces the observational results of the full disk associated with DoAr 25. This is the first near-infrared polarimetric imaging on this object. I report newly discovered possible dust shell remnant (*disk wing*), which indicates the youth of the system. On the basis of results from high resolution image, I suggest that the DoAr 25 disk is a young cavity-less disk in early grain growth progress with envelope remnant.

Chapter 4 presents the evidence of interaction between disk unseen multiple planets by the near-infrared polarized intensity image of LkCa 15 pre-transitional disk. In this chapter, I provide the estimation of possible properties of unseen planets on the basis of planet-disk interaction scenarios and disk diagnostics with previous sub-mm observational studies. A part of this chapter has been accepted for publication in Publications of the Astronomical Society of Japan (Oh et al., 2016, ; DOI:10.1093/pasj/psv133).

Chapter 5 reports the inconsistency of disk structures between the near-infrared polarized intensity image in this work and previous imaging studies such as the sub-mm interferometry image and the near-infrared intensity image. This inconsistency can be interpreted as the important sign of current disk evolution processes in GM Aur disk because different wavelengths and methods traces different properties of the disk.

Chapter 6 briefly summarises previous three chapters, and discusses possible morphologic evolutionary pathways and alternative evolutionary indices. I found that discussed physical parameters cannot be major indices for a common disk evolution, and

suggest that this an indicative of different formation histories for different disks.

In Part III

Chapter 7 reports the discovery of new wide-orbit PMC beyond the protoplanetary disk. I searched around above three targets by using previous sky survey archives, and found that only DoAr 25 has a nearby faint point source. Furthermore, by deep imaging observation, I also found an additional point source around DoAr 25. This chapter presents verifications of the companionship of two wide-orbit PMC candidates detected around DoAr 25 by multiple methods, and discusses the properties of a confirmed wide-orbit PMC by near-infrared spectroscopy. By considering DoAr 25 disk study in Chapter 3, we concluded that wide-orbit PMC around DoAr 25 can not be originated from the young protoplanetary disk associated with DoAr 25. This result brings on the necessity of an alternative formation scenario, and I suggest the simultaneous formation with primary star by cloud core fragmentation as a convincible scenario.

In Thesis Summary

Chapter 8 provides short summary of discussions in this thesis and future works.

Part II

Direct Imaging Analysis of the Circumstellar Disks: Various Disk Clearing Processes

Chapter 3

Structures of DoAr 25 Circumstellar Disk Revealed By Near-IR Imaging Polarimetry

Abstract

We present the high resolution *H*-band polarized intensity image of the circumstellar disk associated with the young T Tauri star DoAr 25. We obtained the first spatially resolved disk image at 1.6 μm wavelengths with the effective inner working angle of 0.28″ ($\sim$35 AU at 125 pc distance). We discovered a mysterious disk wing structure along the minor axis of the disk. Polarization vector map and radial polarization $Q_{\rm r}$ image propose that this structure is a circumstellar component associated with DoAr 25. We found that DoAr 25 disk shows only near-half side of the surface which indicates an extreme brightness asymmetry between near and far side of the disk possibly due to forward scattering effect on micron-size particles. We extended cavity-less surface radius into 18 AU on the basis of resolved images and simple SED comparison. We discuss these results as the characteristic of a young protoplanetary disk in early grain growth phase.

3.1 Introduction

3.1.1 Background

Circumstellar disks are a natural post process of the star formation. When a molecular cloud core collapses, a rotating and accreting circumstellar disk rises by angular momentum conservation of falling gas and dust. The disk material dissipates over 1-10 Myr of time through several processes such as mass accretion onto the central star, photoevaporation, or the disk-planet interaction. The study on the dust dissipating in disks is dramatically improved by detailed infrared spectral energy distributions (SEDs). Typical disk-host T Tauri stars have an optically thick full disk (i.e., a disk without significant radial discontinuities in its dust distribution, Espaillat et al., 2014a). The near-infrared excess of full disks is dominated by the wall or inner edge where high temperature sublimates dust in inner radius. The Spitzer Infrared Spectrograph (IRS; Houck et al., 2004) and the Infrared Space Observation (ISO Kessler et al., 1996) have provided strong evidence of dust dissipation in several disks, which is referred to as transitional disks. Transitional disks have a significant deficit of flux in the near-infrared wavelengths (e.g., Espaillat et al., 2007a,b), which has been interpreted as optically thick disk with large inner cavity by SED modeling (e.g., Calvet et al., 2005, D'Alessio et al., 2005, Uchida et al., 2004). Subsequently, transitional disk is subdivided into the transitional disk and pre-transitional disk that have large gaps and an optically thick inner disk (Espaillat et al., 2007b). Najita et al. (2007) found that mass accretion rates of full disk are ~ 10 times higher than those of (pre-)transitional disks at the same disk mass, and indicated a possible connection to the evolutionary transition.

Millimeter interferometry observations revealed spatially resolved disk images, which show the spatial distribution of mass (Andrews and Williams, 2007a, Andrews et al., 2009, 2010). Recent high resolution direct imaging using optical to near-infrared polarimetry and interferometry have provided more detailed spatial structures including inner cavities in (pre-)transitional disks (Hashimoto et al., 2012, 2015, Rich et al., 2015, Thalmann et al., 2015), and have started playing a crucial role in understanding disk evolution. However, even though high resolution observations have revealed that some of inner holes in disks are induced by stellar companions (CoKu Tau 4 Ireland and Kraus, 2008), what physical mechanism(s) brings inner cavities to full disks and make it change into transitional disks is not clearly understood yet.

Studying physical characters of full and (pre-)transitional disks is of great interest because planet formation and disk evolution may be excited by the inner material clearing mechanism between full disks and (pre-)transitional disks, and their early process is largely determined by the physical conditions of the disk (e.g., Casassus et al., 2012, Cieza et al., 2012, Dodson-Robinson and Salyk, 2011, Matter et al., 2015, Williams and Cieza, 2011, Zhu et al., 2011). Therefore, to study early disk evolution, at first, we decided to figure out the structure of the disk in earlier phase on the basis of SED.

3.1.2 History of Study on DoAr 25

DoAr 25 (K5, $0.65M_{\odot}$; Wilking et al., 2005) is T Tauri star in the L1688 dark cloud in the large ρ Ophiuchus cloud complex. The recent measured distance to the cloud is $\sim$125pc (Loinard et al., 2008, Lombardi et al., 2008, Mamajek, 2008), but DoAr 25 may be somewhat closer because its low visual extinction value A_v=2.9 indicates that it lies at the surface of the cloud (Wilking et al., 2005). Although a median age of the cloud surface population appears to have 2-5 Myr (Wilking et al., 2008), the estimated age of DoAr 25 is $\lesssim$1 Myr, relatively younger than the others (Wilking et al., 2005).

DoAr 25 has a significant excess over the stellar photosphere emission from μm to mm wavelengths (Andrews and Williams, 2007a, McClure et al., 2010, Olofsson et al.,

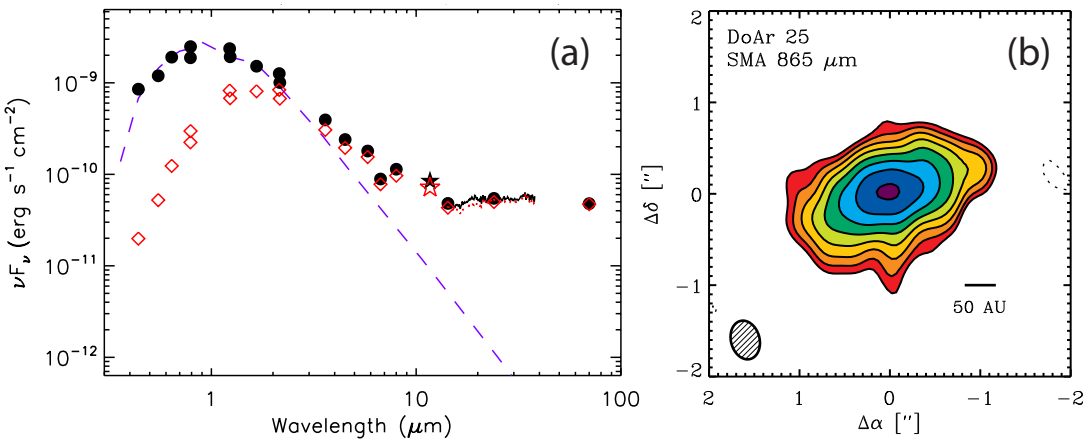

FIGURE 3.1: (a): The SED of DoAr 25. Empty red squares and dotted lines represent the original and extinguished data, while filled circles and solid lines are the extinction-corrected data (A_V = 3.4, SpT = K5). There is a significant infrared excess over the stellar emission. A deficit at mid-infrared is relatively shallower than other (pre-)transitional disks (e.g., LkCa15 and GM Aur; See Chapter 4 and 5). Figure adapted from McClure et al. (2010). (b): The 865 μm SMA disk image of the DoAr 25. A inner cavity has not seen in any (sub-)millimeter interferometry images, including this. Figure adapted from Andrews et al. (2008).

2009), which indicates the presence of circumstellar disk associated with it. Andrews et al. (2008) pointed out that a low mass accretion rate ($\dot{M} \sim 10^{-10}$-$10^{-9} M_{\odot}\mathrm{yr}^{-1}$; Greene and Lada, 1996, Luhman and Rieke, 1999, Natta et al., 2006) may indicate the inner disk is in an advanced state of evolution, and proposed that DoAr 25 disk can be considered less-evolved version of transitional disk based on the submillimeter visibilities and the SED. The observed SED (Figure 3.1a) shows deficit at mid-infrared wavelengths, but it is very shallow (α_{excess} ~0, See Section 1.2.2). At the present, an inner cavity such as hole or gap is not seen in the (sub-)millimeter interferometry observations (Andrews and Williams, 2007a, Andrews et al., 2008, 2009, 2010, Pérez et al., 2015). Consequently, DoAr 25 disk might be in the boundary between the full disk and (pre-)transitional disk. To constrict the presence of an inner cavity and to explore early evolutionary structures of the DoAr25 disk, higher angular resolution of observations are required.

3.1.3 In this work

We present the first spatially resolved *H*-band (1.6μm) polarized scattered light image of the DoAr 25 circumstellar disk. By using the 8.2-m Subaru Telescope with HiCIAO (High Contrast Instrument for the Subaru Next Generation Adaptive Optics; Tamura et al., 2006)+AO188 (Hayano et al., 2010), we succeed in resolving the disk with higher resolution and deeper inner working angle than previous works. We report the butterfly-like distribution of disk brightness and the discovery of strange pillar-like structure. We discuss the youth and the evolutionary phase of the DoAr 25 disk, and the possibility of the presence of planets embedded in the disk.

3.2 Observation and Data Reduction

The *H*-band direct imaging observations were conducted in 2012 May 16 with HiCIAO installed on the Subaru Telescope. To detect polarized scattered light from the disk surface, we adopted PDI (Polarimetric Differential Imaging; See Figure 3.2) technique, which uses the half-wave plate at four angular positions for four serial images to efficiently obtain full polarization angle coverage. Since the stellar emission is incomparably brighter than the scattered light from the disk, combining multiple short exposures may not possible to reduce saturated radius sufficiently. To obtain the minimum inner working angle, we utilized double Wollaston prism to split light into four channels: two sets of ordinary and extraordinary rays. Consequently, one data set consists of four serial

images obtained through four different half-wave plate angle, and each image consists of four independent channels with $5''\times5''$ field of view. We obtained 25 data sets with 20 s exposure for each image. The total integration time of the resultant polarization intensity image was 2000 s.

To reduce the polarimetric data, we adopted the standard approach for differential polarimetry (e.g., Hinkley et al., 2009). Scattered light from the circumstellar disk is polarized perpendicular to the disk surface. In PDI mode, one data set consist of four frames obtained through the half-waveplate at different angles (0°, 45°, 22.5°, and 67.5°). Then, Wollaston prism split polarized light into two perpendicular components (qPDI mode uses double Wollaston prism for taking longer exposure time with a smaller saturation radius). In data reduction, we first calculate Stokes parameters Q and U, then evaluate polarized intensity (PI), polarization angle (θ), and degree of polarization (P) as follow;

$$\begin{aligned} \mathrm{P} &= \sqrt{\left(\frac{Q}{I}\right)^2 + \left(\frac{U}{I}\right)^2}, \\ \theta &= \frac{1}{2}\arctan\left(\frac{U}{Q}\right), \\ \mathrm{PI} &= \sqrt{Q^2+U^2}. \end{aligned} \tag{3.1}$$

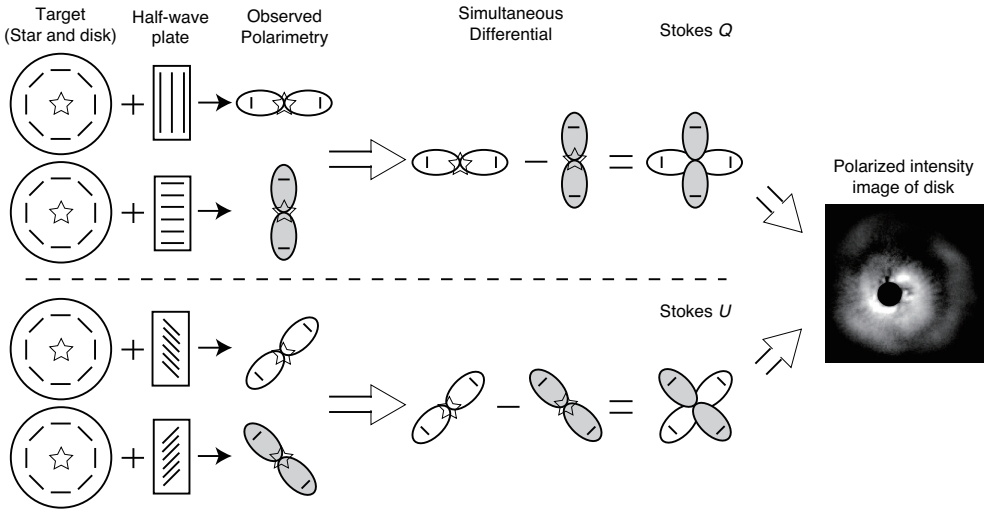

FIGURE 3.2: Schematic of simultaneous polarimetric differential imaging. Figure provided by J.Hashimoto and reproduced with permission.

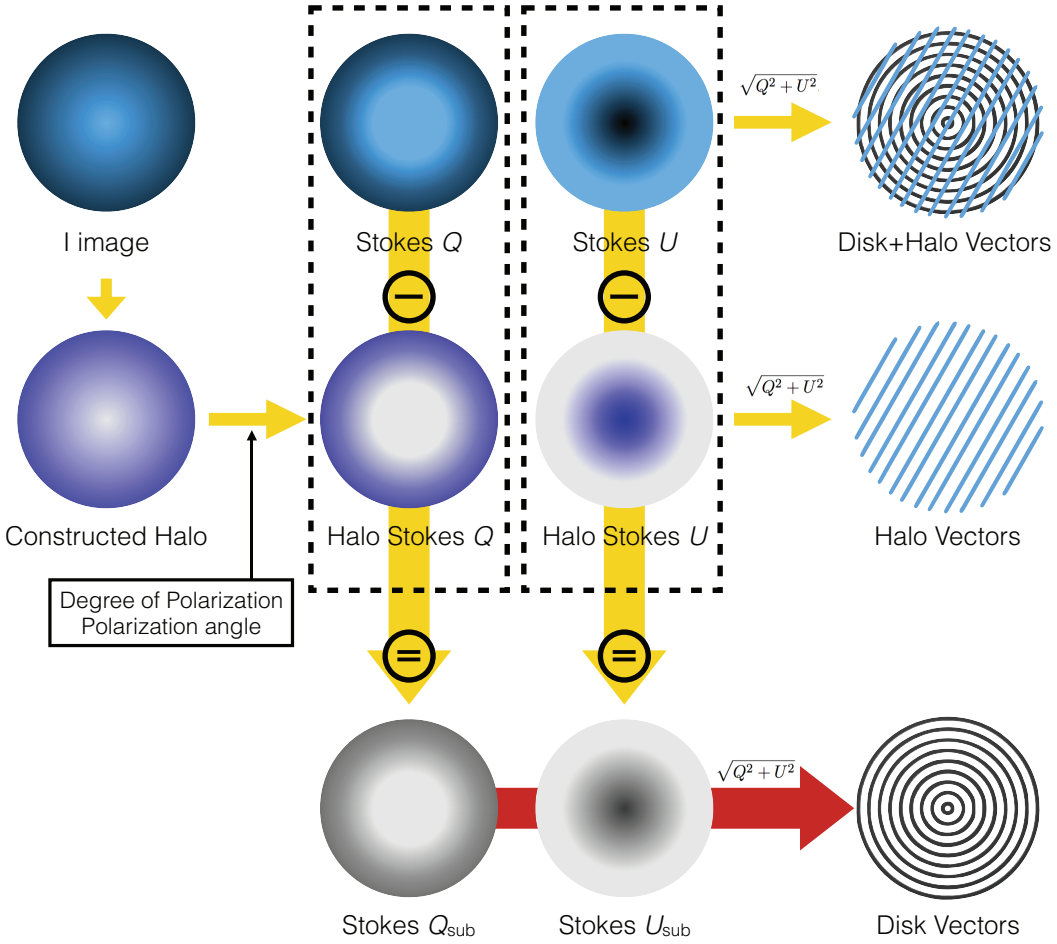

FIGURE 3.3: Schematic of halo subtraction process. Blue color represents polarized halo components, and gray color represents disk polarization components. Color gradient is only used for distinction of components, and is not represents any physical features.

PI represents the intensity of scattered light, thus the geometry and the signal intensity of the resultant PI image are interpreted as a scattering disk surface and a density of μm-size dust in the disk, respectively.

The reduction was made using the IRAF (Image Reduction and Analysis Facility)[1] software and the custom script pipeline optimized for HiCIAO polarimetric data (designed and provided by Hashimoto et al., 2011). Figure 3.4a and b show the resultant PI image and polarization vector map, respectively, obtained from the Stokes Q and U images.

[1]The IRAF software is distributed by the National Optical Astronomy Observatory, which is operated by the Association of Universities for Research in Astronomy (AURA) under a cooperative agreement with the National Science Foundation.

In ideal condition, the stellar emission must be subtracted by above procedure. However calculated polarization vectors are showing a tendency to align toward a certain direction, not a circular symmetry as expected from Fresnel reflection on circular disk surface. This polarization tendency arises from a residual stellar emission in reduced images. Because the convolved PSF might contain contributions from the polarized flux by seeing, a standard differential polarimetry procedure cannot perfectly remove the effect of polarized stellar halo. In order to solve this problem, we first conduct halo based on average radial profile of I image, and derived the average polarization strength P and average polarization angle θ from unsaturated frames by using aperture polarimetry. Then we builded a simple polarization halo model (halo Q and halo U) of DoAr 25 by using its derived polarization of P=1.57%±0.01% with θ=13.7±0.5°. By subtracting this halo model from the Stokes Q and U images, we finally obtained halo-subtracted PI image. Schematic of this process is shown in Figure 3.3.

Simultaneously, we calculated and conducted the radial polarization images, the Stokes Q_r and U_r given by

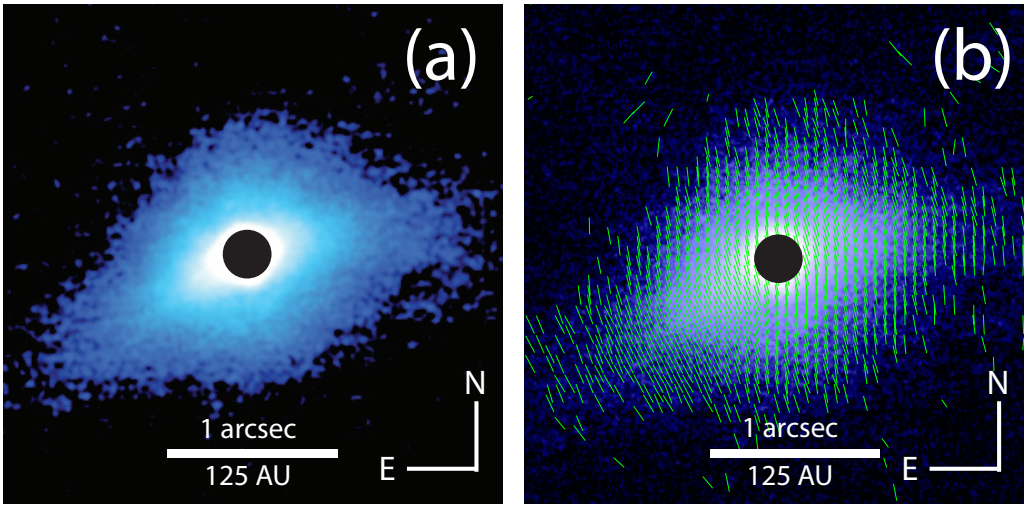

FIGURE 3.4: The PI image of DoAr 25 disk and its polarization vector map. The saturated region is occulted by a software mask (r∼0.15″). The vectors are binned with spatial resolution, and the lengths are arbitrary for presentation purpose. The polarization vectors are strongly aligned along a certain direction.

$$
\begin{aligned}
Q_{\mathrm{r}} &= +Q\cos 2\phi + U\sin 2\phi, \\
U_{\mathrm{r}} &= -Q\sin 2\phi + U\cos 2\phi, \\
\phi &= \arctan\frac{x-x_0}{y-y_0}.
\end{aligned}
\tag{3.2}
$$

where x_0 and y_0 are the coordinates of the apparent disk center. Q_{r} indicates a radial plarization perpendicular to the azimuthal direction, while U_r corresponds to the polarization $\pm 45°$ with respect to the radial direction (Schmid et al., 2006). Thus, the Q_{r} image must show the scattering polarization which should similar to PI_{sub} image, while the U_{r} image would contains less or no scattered light from the disk (Avenhaus et al., 2014). The Q_{r} and PI images contain basically similar informations in ideal situation, thus it is available as comparative verification of the results.

Additionally, we also reduced same data by using classical ADI (Angular Differential Imaging Marois et al., 2006) and LOCI (Locally Optimized Combination of Images Lafrenière et al., 2007) to verify the presence of planets which potentially can contribute to the disk evolution. Figure 3.8 shows the results of that. Because we are focussing on the disk in this section, we only check the presence of detectable planets at here. See Chapter 7 for detailed descriptions about ADI/LOCI and more discussions focused on planetary companions.

3.3 Results

3.3.1 Polarimetric Imaging of DoAr 25 disk

The resultant *H*-band PI image is presented in Figure 3.5a. Despite the strong effect of polarized stellar halo in highly inclined disk, post procedure for halo subtracting allowed us to remove polarized stellar halo over the radius of $0.28''$ effectively and find a large and flared butterfly-like disk around DoAr 25. Figure 3.5b presents a polarization vector map. Some vectors close around the star ($\mathrm{r} \lesssim 0.28''$) still look like to have some tendency induced by possible stellar halo remnant, but generally it shows a clear circular symmetry on the bright disk surface. Thus we choose to use the regions over $\mathrm{r} \gtrsim 0.28''$ for discussion to prevent possible effect of unsubtracted stellar halo. A least-squares estimation elliptical fit with five free parameters to the bright surfaces indicates an inclination (i) of $83\pm2°$ at a position angle (PA) of $114\pm3°$. A position angle is

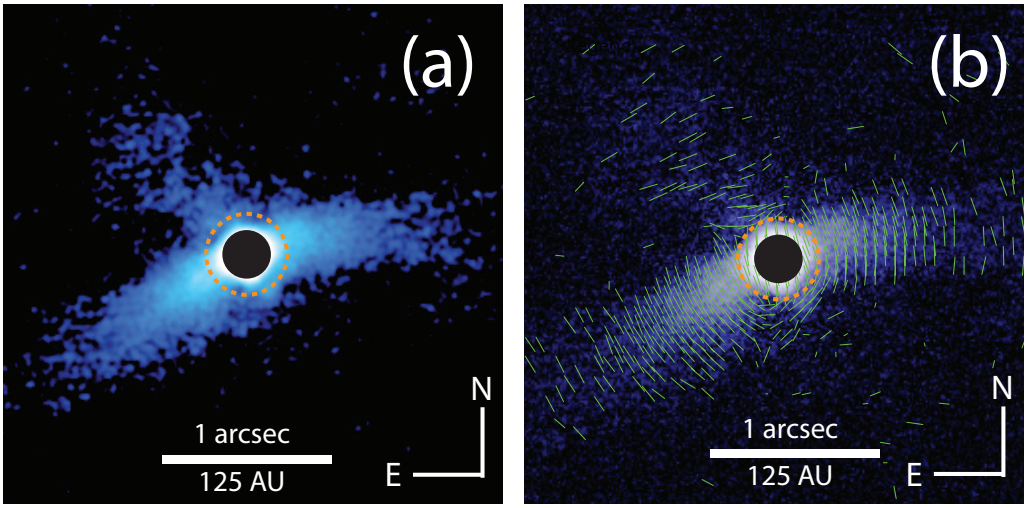

FIGURE 3.5: The halo-subtracted PI image of DoAr 25 disk and its polarization vector map. The saturated region is occulted by a software mask (r∼0.15″), and the halo remnant region is marked with yellow dotted circle. The DoAr 25 disk finally unveiled from the strong effect of polarized stellar halo. A significant difference in PI images before and after halo subtraction is due to a high inclination of the disk. A mysterious perpendicular component is founded (northeast side of the disk). The vectors are binned with spatial resolution, and the lengths are arbitrary for presentation purpose. The polarization vectors are clearly circular symmetric on the disk surface.

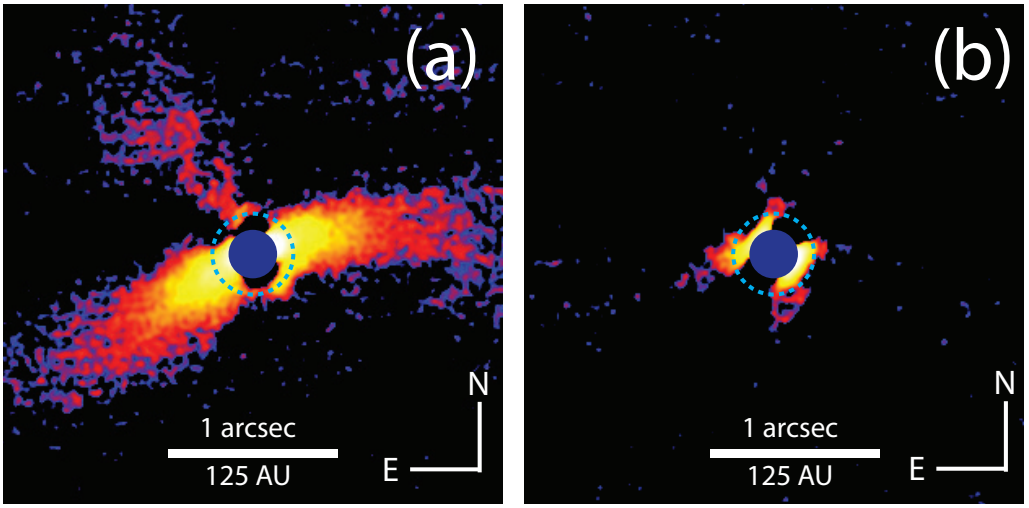

FIGURE 3.6: The radial polarization Stokes Q and U images (a and b, respectively). The saturated region is occulted by a software mask (r∼0.15″), and the halo remnant region is marked with blue dotted circle. The Q_r image shows similar disk components including perpendicular component. This consistency may indicates that this perpendicular structure is real disk component. Beside, U_r image shows no disk-like component. Signals around masked region in U_r image may be due to incompleteness in stellar halo subtraction.

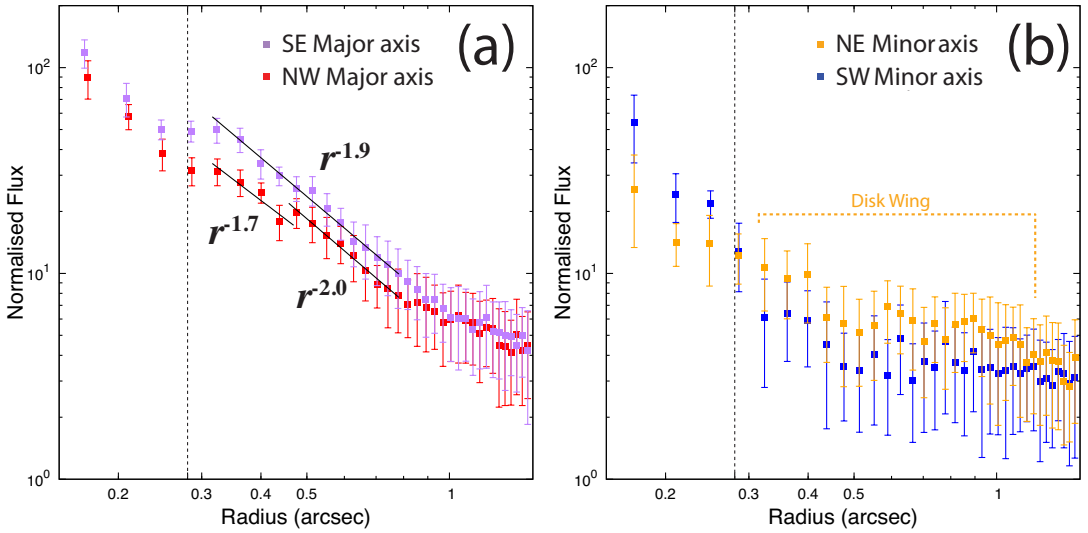

FIGURE 3.7: Radial surface brightness profiles of DoAr 25 disk along the major axis (a) and minor axis (b), with simple power-law fit on each slope between breakpoints. Vertical dashed lines indicate the boundary (∼0.28″) between halo-clear regions (right) and possible halo-remnant regions (left).

consistent with the previous sub-mm observation, but an inclination is significantly higher than that (PA=111±3°; i=62±3°, Andrews et al., 2008). It should be noted that a high inclination of the disk brings large uncertainties in polarimetric and geometric calculation, especially along the minor axis in the vicinity of disk center.

Interestingly, we also found a elongated perpendicular component along the northeast minor axis of the disk (hereafter, a disk wing). The polarization vector map (Figure 3.5b) and the radial Stokes Q_r image (Figure 3.6a) are showing similar structures. Beside, the radial Stokes U_r image is not showing any similar structures, but showing possible stellar halo remnant signals around saturation mask. This suggests that a disk wing is a possible circumstellar component associated with DoAr 25, even though it is faint.

The radial surface brightness profiles (Figure 3.7) shows generally symmetric disk surface along the major axis. However, the brightness of southeast surface is *slightly* brighter than minor axis ($\sigma \lesssim 2$), and there are some breakpoints on the brightness slopes (Figure 3.7a). On the other hand, that of minor axis shows no significant surface brightness slope. The brightness of northwest side, in which a disk wing was found, is constantly brighter than that of southwest side, although the flux differences are similar to the range of error, (Figure 3.7b).

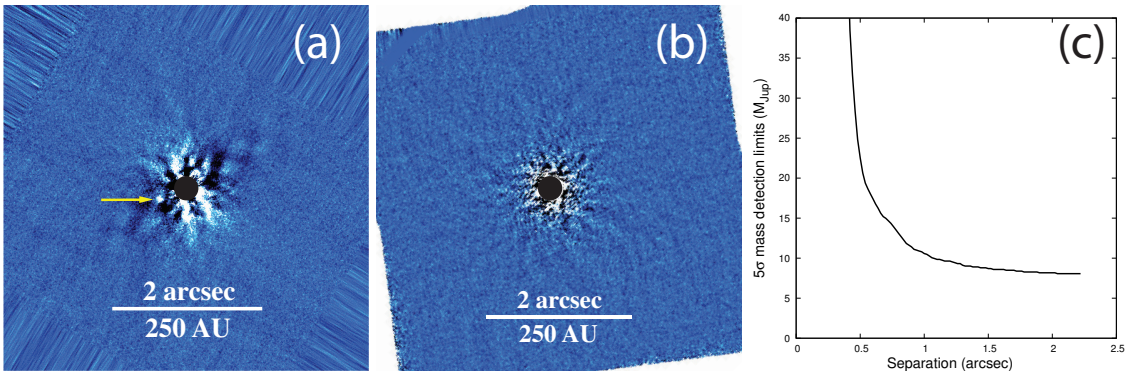

FIGURE 3.8: Classical ADI image, LOCI image of DoAr 25, and upper mass limit of detection (a, b, and c, respectively). We couldn't find any significant evidence of planetary companion around DoAr 25. A planet-like point source exist in ADI image (*yellow arrow*), but it is not detected in LOCI image. Thus it is a pseudo-signal which may be induced by speckle noises. We ruled out the presence of planets massive than 5-10$M_{\rm Jup}$ on the basis of detection limit.

3.3.2 Constraints on the presence of planets

The LOCI image provides upper detection limit on the possible point sources in around DoAr 25. By using the DUSTY evolutionary models (Chabrier et al., 2000), we calculated that excludable masses of unseen planets at 5σ level as a function of separation from the star (Figure 3.8c). We couldn't find any statistically significant point source signals that could be considerable as planet candidates, thus we concluded that there is no planet massive than 8-10 $M_{\rm Jup}$ nearby the disk, and no close substellar companion massive than 20 $M_{\rm Jup}$ and 10 $M_{\rm Jup}$ beyond $0.5''$ ($\sim$60 AU) and $1''$ ($\sim$120 AU) separation, respectively. A planet-like point source seen in the classical ADI image (yellow arrow in Figure 3.8a) is considered as a pseudo-signal accidentally induced by speckle noises.

From the wide FOV imaging observations using IRCS (the Infrared Camera and Spectrograp; Kobayashi et al., 2000, Tokunaga et al., 1998), we found two possible companion candidates with planetary-mass beyond the disk of DoAr 25. We will discuss their companionship and non-disk origin in Part III.

3.4 Discussion

3.4.1 Young cavity-less dust disk

It is interesting whether DoAr 25 disk has small inner cavity or not, because of a very low mass accretion rate for its massive disk (Espaillat et al., 2014a). However any of high resolution imaging observations couldn't resolved the inner disk or hole from this

system (Andrews et al., 2008, 2009, 2010, Pérez et al., 2015, , and this work). From radial brightness profile (Figure 3.7a), we also couldn't find a decreasing brightness slope toward inner side which indicates inner cavity, over the radius of 0.28″ (∼ 35 AU). MIR deficit of DoAr 25 disk is significantly weaker than that of GM Aur disk which has similar disk mass and a large inner hole with the radius of 18 AU (See Section 5). Moreover, a shallow radial brightness slope (power indices of $r \sim -1.9$) indicates flared scattering surface because a that of typical flat scattering surface is ~ -3 (Dong et al., 2012a). A flared disk can be interpreted as a youth of the disk because opening angle of disk surface decreases as dust settling to the midplane progresses. However, it also should be noted that fast dust settling on inner disk can produce flared disk even in relatively evolved disk (e.g., Akiyama et al., 2015). If we assume dust settling is generally constant with the radius, we can conclude that DoAr 25 disk is very young and flared, and has no cavity at least beyond the radius of ∼ 18 AU.

3.4.2 Disk Wing

We have detected faint (3-4σ) wing-like structure which is elongated diffuse component lying along the northeast minor axis of the DoAr 25 disk. The validity of the result has been confirmed by comparative verifications; vector map, the Stokes Q_r image. Hence, we concluded that this wing structure is possible disk component in DoAr 25 system. Although, there is no clear counterparts in other observational features yet, several similar elongate structures have been reported. Using Hubble Space Telescope (HST) and near-infrared camera NICMOS, Schneider et al. (2003) reported centrally condensed but diffuse *polar lobes* along the minor axis in opposite directions around GM Aurigae disk, and noted that polar lobes are much brighter in F160W filter (∼ 1.6 μm), which is similar to the *H*-band, than in F110W filter (∼ 1.1 μm). They proposed that polar lobe features are primarily due to shocked emission from jets of outflow material. Jet and/or outflows are accompanied by a large fraction of young stellar objects, including disk-host T Tauri stars (e.g., RY Tau, St-Onge and Bastien, 2008). Sako et al. (2005) also showed the complex circumstellar envelope surrounding M17-S01, and noted that the presence of *antennae* features which may be induced by a collimated jet.

Most recently, de Leon et al. (2015) reported a pair of narrow bipolar *tail* structures extending east and west from the disk associated with the T Tauri star SU Aur. Figure 3.9 shows the comparison of DoAr 25 disk and SU Aur disk with overlaid contour and

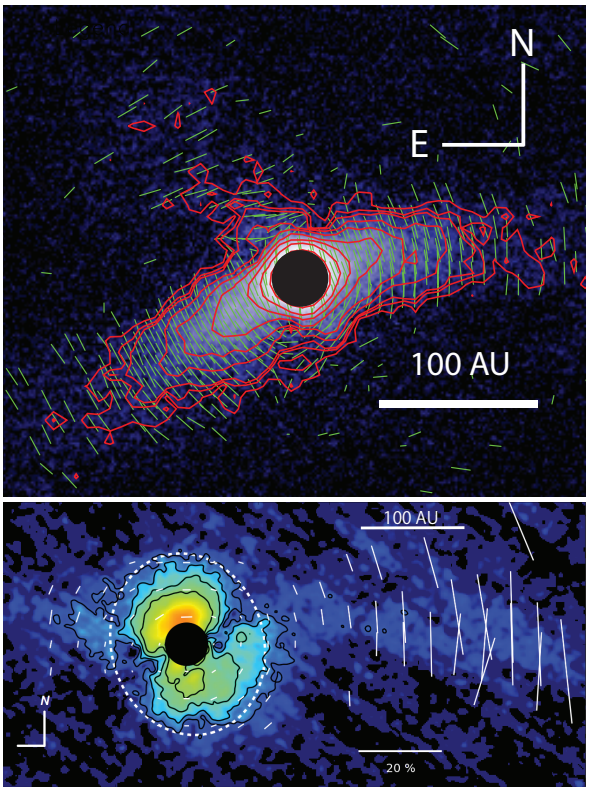

FIGURE 3.9: DoAr 25 disk (*top*) and SU Aur disk (*bottom*) with overlaid contour and polarization vector maps. *Wing* structure of DoAr 25 is extending northeast from the disk, *tail* structures of SU Aur are extending east and west from the disk.

polarization vector maps. They suggested three possible explanations; outflow cavities, collimated jets, and tidal interaction with a brown dwarf. The wide orbit planetary-mass companion DoAr 25 b at ∼1430 AU away (See Part III) would affect the DoAr 25 disk structure. However, gravitational effect from the DoAr 25 b is unlikely because a narrow elongated structure on a symmetric cavity-less surface of the DoAr 25 disk can be indicative of the presence of local dynamic effect on the wing, not the global gravitational effect from extremely far away planetary-mass companion. Thus the ohter two, outflow cavities and collimated jets, are more suitable for the DoAr 25 system.

Since observations at different wavelengths trace different grain sizes, an infrared-only detection may indicate that the main material in the disk wing is dust particles with sizes of 1-10 μm in general. This may propose that those dust particles had previously underwent the grain growth to μm-size after accretion onto the disk, and then swept up by jet or outflow. Given measurable properties in infrared-only detection are very limited, thus additional observations might lead us to a clearer answer. In the case of GM Aurigae, ^{13}CO molecular emission line was detected from just beyond the location

of the polar lobe, at the same position angle, suggesting the presence of a jet-like outflow phenomenon (Schneider et al., 2003). However, there are no published literatures reporting molecular observational results on DoAr 25. Furthermore, ^{12}CO and ^{13}CO emission map of L1688 in ρ Ophiuchus, in which DoAr 25 is located, indicates that extended and diffused molecular cloud may inhabit that direction (Ridge et al., 2006), suggesting that the observed line emission from the direction of DoAr 25 could be substantially confused by the extend molecular cloud (Andrews et al., 2008). Therefore, by the line emission observation, it is difficult to verify that the jet or outflow inducing a disk wing are still exist in DoAr 25 system. At present, the most conceivable candidate of the disk wing is a dust shell remnant which consisted of outflow-entrained material from circumstellar disk or a primeval envelope.

3.4.3 Disk geometry: Extreme brightness asymmetry

In previous (sub-)millimeter observations (Andrews et al., 2008, 2009, Pérez et al., 2015), measured inclinations and position angles were well consistent with each others, as $i = 62\pm3^\circ$ and PA $= 110\pm3^\circ$. Figures 3.10a and b show NIR contour maps overlaid on optical and model image adapted from Andrews et al. (2008). HST image is partially saturated, but the position angle consistence with NIR image ($114\pm3^\circ$) is obviously confirmable (Figure 3.10a). Besides, NIR image only covers a near-half of the model image (Figure 3.10b). On large dust grain disk, the forward scattered light from the near-side surface is several times brighter than the backward scattered light from the far-side surface (Mie scattering). Therefore, the comparison with disk models indicates that NIR scattered emission from the DoAr 25 disk is dominated by forward scattering, and that we are watching the near-half side of the DoAr25 disk surface. This extreme brightness asymmetry of near- and far-side surfaces suggests that micron-size particles are still dominant in the disk (Min et al., 2007), thus we can conclude that DoAr 25 disk still has young dust composition.

In general, a disk inclination is calculated from the estimated ellipticity of the observed disk image. But in this case, it is difficult determine the disk inclination from observed disk geometry due to the strong forward scattering effect mentioned above.

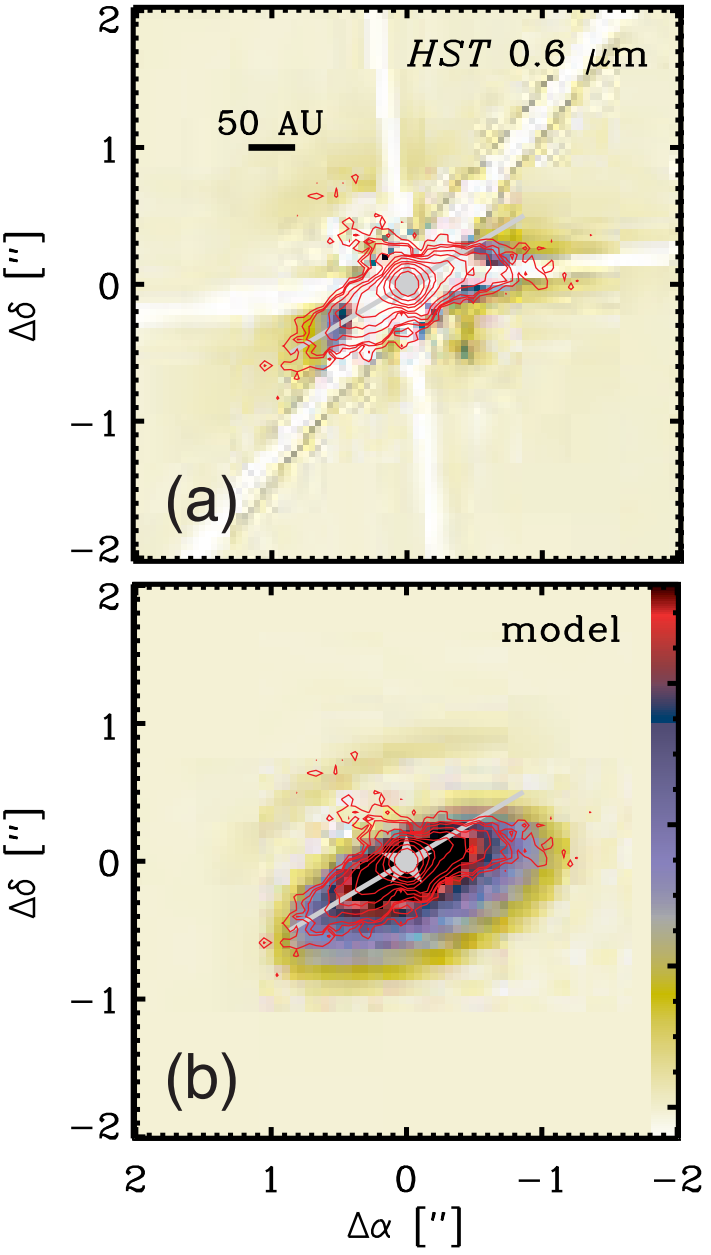

FIGURE 3.10: NIR contour maps of DoAr 25 disk overlaid on optical image (*top*; HST; 0.6μm) and model image (*bottom*). HST and model images are adapted from Andrews et al. (2008). Star symbols indicate the stellar position, and gray line indicate the position angle of the disk. The comparison with the HST image show good agreement in general disk geometry. Besides, the comparison with the model image indicates that the forward scattering effect is strong and dominant in NIR scattered light.

3.5 Conclusion

We have presented the first near-infrared scattered light image DoAr 25 in high resolution. We found a new disk wing component which is considered as a dust shell remnant induced by outflow or jet. A significantly strong forward scattering effect on disk surface suggests a less-evolved grain-growth phase. Therefore, the DoAr 25 disk may serve an excellent laboratory for studying the circumstellar disk evolution in early stage.

High angular resolution observations by ALMA (the Atacama Large Millimeter Array) can play a key role in the studies on more detailed disk structures including unresolved inner regions in previous imaging studies. Ground-based instruments with the Extreme Adaptive Optics (ExAO) system such as the Subaru Coronagraphic ExAO (SCExAO; Jovanovic et al., 2015) are also required. The combination of these advanced imaging observations at different wavelengths will be the most efficient route to reach the understanding of disk evolution.

Chapter 4

Near-Infrared Imaging Polarimetry of LkCa 15: A Possible Warped Inner Disk

A letter version of this chapter has been accepted for publication to the Publications of the Astronomical Society of Japan (Oh et al., 2016, ;DOI:10.1093/pasj/psv133).

Abstract

We present high-contrast H-band polarized intensity images of the pre-transitional disk around the young solar-like star LkCa 15. By utilizing Subaru/HiCIAO for polarimetric differential imaging (PDI), both the angular resolution and the inner working angle reach 0.07″ and r=0.1″, respectively. We obtained a clearly resolved gap (width $\lesssim$ 27 AU) at 47 AU from the central star. This gap is consistent with images reported in previous studies. We also confirmed the existence of a bright and optically thick inner disk with a large misaligned position angle of 13±4° with respect to that of the outer disk, i.e., the inner disk is possibly warped. The large gap and the warped inner disk both point to the existence of a multiple planetary system with a mass of $\lesssim 1 M_{\rm Jup}$.

4.1 Introduction

4.1.1 Background

The circumstellar disks around young stars are the main birthplace of giant gas planets. In the typical disk evolution, a mass accretion onto the star tends to decrease as disk evolves. When accretion rate become lower than photoevaporation rate, photoevaporation clears inner disk, and change it to small inner cavity. However, recent analysis of spectral energy distribution (SED) and the results at infrared to millimeter wavelengths reveal the evidence of large cavity and gap structures in circumstellar disks which have a high accretion rate. Such disks have been called (pre-)transitional disks, and are thought to be an intermediate phase between gas-rich primordial disks and gas-poor debris disks with planetesimals/planets (e.g., Andrews and Williams, 2007b, Espaillat et al., 2014a, Williams and Cieza, 2011). Especially, when newly formed planet(s) are embedded in the disks, a gap structure (i.e., optically thick inner and outer disks separated by an optically thin gap; pre-transitional disks) instead of a cavity (i.e., a complete lack of an inner disk; transitional disks) is predicted to form by disk-planet interactions (Kley and Nelson, 2012). Therefore, disks with a gap structure could indicate the birth of the giant gas planets. Hence, understanding the detailed structures of the pre-transitional disks with large gap could unveil the origin of our planetary system.

The remarkable progress of high-contrast imaging in the last decade allows us to see more details in the transitional disks. By direct imaging, the incredible diversity of the disk morphology, such as inner hole, spiral and gap structures, has been revealed (e.g., Currie et al., 2014, Fukagawa et al., 2006, Hashimoto et al., 2012, Muto et al., 2012). Thus, direct imaging of the pre-transitional disks could provides essential hints to understanding its detailed structure.

4.1.2 History of Study on LkCa 15 Disk

LkCa 15 (K5, 0.97 $M_{\odot}$, 2−5 Myr old; Simon et al., 2000), a young solar-like star located in the Taurus-Auriga region ∼140 pc away from the solar system, is one of the most intensively studied (pre-)transitional disk systems around the T Tauri star.

Espaillat et al. (2007a, 2008b) conducted a detailed analysis of SED in LkCa 15 and suggested the existence of a large gap structure at ∼ 46AU, and categorized this disk system as possible pre-transitional disk. Such a gap structure has been confirmed

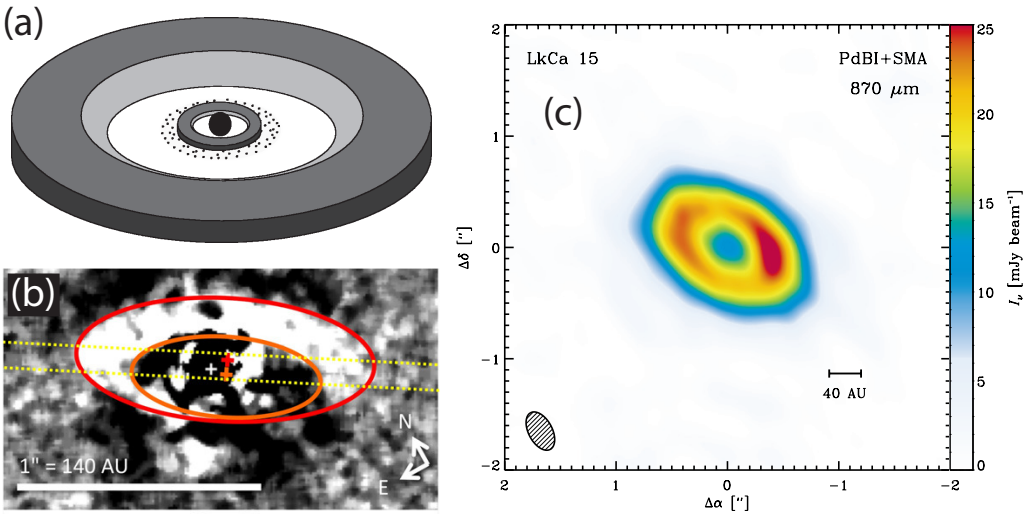

FIGURE 4.1: Schematic and imaging results from previous studies. *Left*: Schematic of LkCa 15 on the basis of SED analysis (Espaillat et al., 2008b). *center*: Direct imaging result at NIR wavelengths (Thalmann et al., 2010). *right*: Result of Interferometry at mm wavelengths (Andrews et al., 2011a). The inner disk in LkCa 15 system has been expected from SED analysis (a), but had not resolved at NIR and mm wavelengths (b and c) until Thalmann et al. (2015) (See Figure 4.2). But large cavity was clearly resolved. Figures adopted from each article.

by millimeter (mm) interferometry (Piétu et al., 2006) and near-infrared (NIR) high-contrast direct imaging (Thalmann et al., 2010) (Figure 4.1), but optically thick inner disk was not resolved. It is challenging to determine which of side of the disk is near to us. Mulders et al. (2010) provided modeling results of two possible disk orientations with forward scattering (southeast is near) and illuminated wall scenarios (northwest is near), and Thalmann et al. (2010) supported illuminated wall scenario as the more likely explanation of the observed bright nebulosity. This means that the bright northwest side is the illuminated inner wall of far side of the outer disk, and forward-scattering is suppressed by high inner wall (See Figure 4.1 a and b).

Subsequently, Thalmann et al. (2014) concluded that the bright arc region (northwest) is a result of strong forward scattering of the near side of the disk on the basis of additional observations and extensive forward modeling results. The inner disk, which is predicted by SED analysis, was finally resolved just recently by Thalmann et al. (2015) using direct polarimetric imaging at optical wavelengths (590-890 nm). Furthermore, protoplanet candidates LkCa 15 b and c ($\lesssim$5$\sim$10$M_{\rm Jup}$) were discovered (Kraus and Ireland, 2012, Sallum et al., 2015)

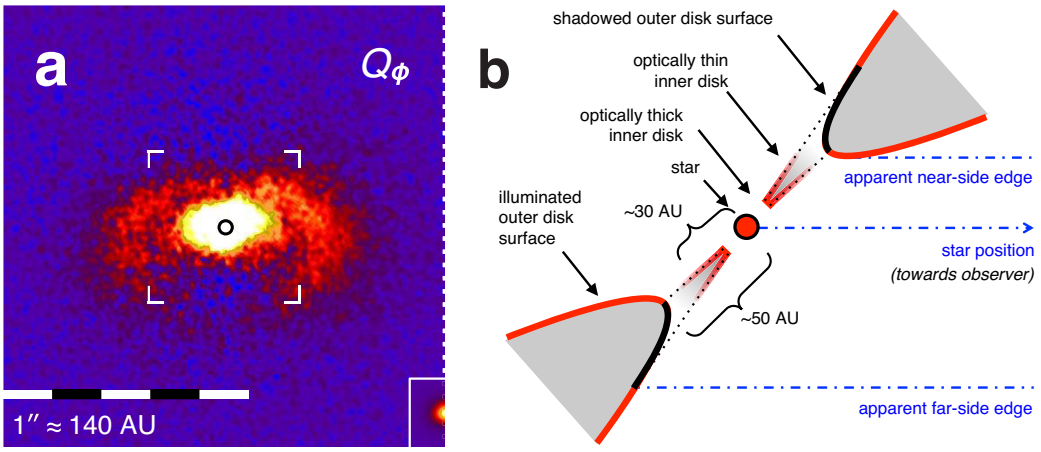

FIGURE 4.2: The first resolved inner disk image (Q_r, or Q_ϕ image) by direct polarimetric imaging at optical wavelengths (590-890 nm) (*left*) and schematic the proposed architecture (*right*). Figures adopted from Thalmann et al. (2015).

Therefore, LkCa 15 disk system may serve an excellent laboratory for studying the interaction between infant planets and the protoplanetary disk structure they sculp.

4.1.3 In This Work

Here, we present the results of new high-contrast NIR (1.6μm) polarization imaging carried out on the LkCa15 disk system by Subaru Telescope at Mauna Kea, Hawaii. We set our goals as the quantitative analysis of the gap and inner disk and finding the sign of disk evolution mechanism, such as unseen planets. The combination of the High Contrast Instrument for the Subaru Next Generation Adaptive Optics (HiCIAO; Tamura et al., 2006), AO188 (Hayano et al., 2010) and Polarimetric Differential Imaging (PDI) provides a high-contrast image that is unprecedented in quality at infrared wavelengths and enables us to both clearly confirm and quantitatively analyze the wide gap structure and the inner disk. We report the warped inner disk and discuss the potential origin of a gapped and warped disk around LkCa 15. The gapped and warped disk suggests the existence of a multiple planetary system.

4.2 Observation and Data Reduction

The PDI observations of LkCa 15 were performed in the *H*-band on 2013 November 22 with HiCIAO on the Subaru Telescope combined with AO188. In PDI mode, we used a double Wollaston prism to split incident light into four images, two o- and e-rays sets, to reduce the saturated radius (quad-PDI). Each image has a 5″×5″ field of view

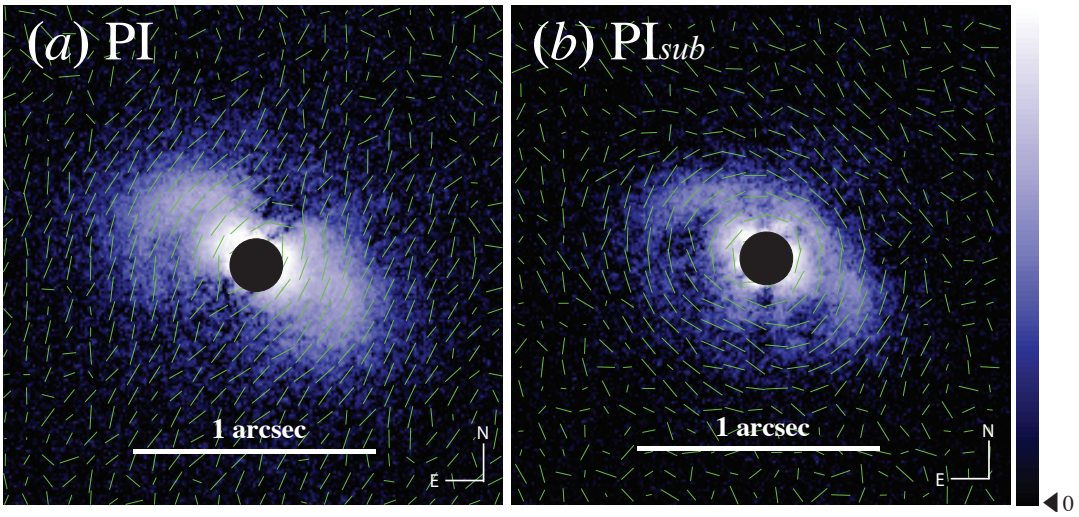

FIGURE 4.3: PI and overlapped polarization vector map images (2.0″×2.0″) before (*a*) and after (*b*) halo subtraction. The saturated region is occulted by a software mask (r∼0.1″), the vectors are binned with spatial resolution, and the lengths are arbitrary for presentation purposes. (*a*): The effect of a polarized halo appears to have a tendency toward the minor axis of the disk. (*b*): The polarization tendency to the minor axis was removed, and the disk-origin polarization along the disk surface was revealed.

(FOV) with a pixel scale of 9.5 mas/pixel. We obtained 17 data sets with 30 s exposure. The total integration time on the source of the polarization intensity image was 2040 s. All of our observations were conducted under the program of the SEEDS (Strategic Explorations of Exoplanets and Disks with Subaru; Tamura, 2009) project.

The polarimetric data were reduced in the standard manner of infrared image reduction that uses the custom IRAF[1] pipeline designed by Hashimoto et al. (2011). The Stokes Q and U images were obtained by the standard method for differential polarimetry (Hinkley et al., 2009). The polarized intensity (PI) image was obtained as $(Q^2 + U^2)^{1/2}$. Because the convolved point spread function (PSF) cannot be perfectly removed by standard procedures, a residual stellar halo was sometimes observed in the obtained PI images. From the PI image (Figure 4.3*a*), the effect of the polarized stellar halo along the minor axis axis of the disk is confirmable from overlapped vector map. To remove the effect of this polarized halo, we constructed the polarization halo model by using the average polarization strength (0.67±0.03%) and average polarization angle (149.1±0.5°) derived from Stokes I image and unsaturated frames, and subtracted this from the Stokes Q and U images. From the halo-subtracted Stokes Q_{sub} and U_{sub} images,

[1]The IRAF software is distributed by the National Optical Astronomy Observatory, which is operated by the Association of Universities for Research in Astronomy (AURA) under a cooperative agreement with the National Science Foundation.

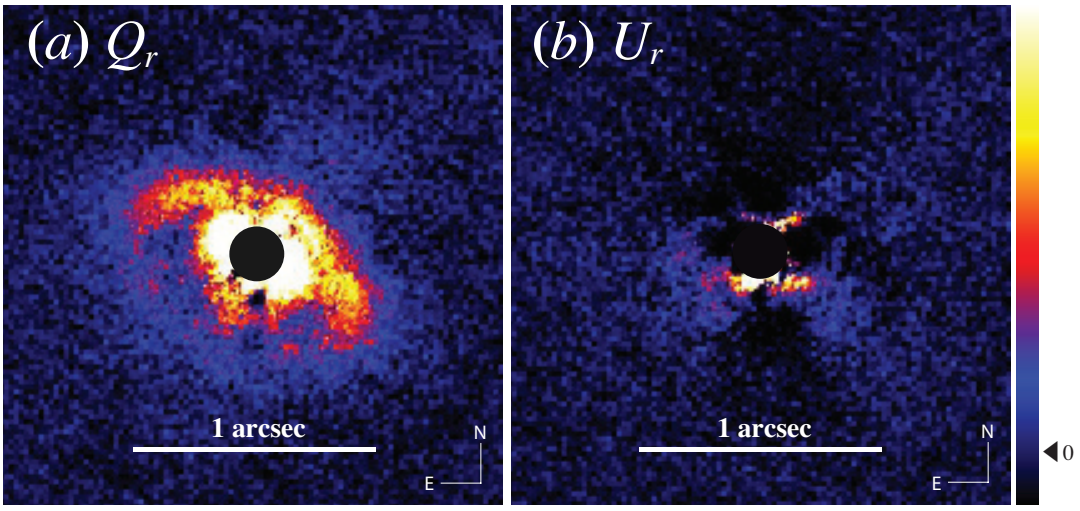

FIGURE 4.4: The radial Stokes Q_r (c) and U_r (d) images of LkCa 15 disk. The saturated region is occulted by a software mask (r∼0.1°). In the Q_r image, both the outer and inner disks are significantly detected as expected from the PI image. On the other hand, the U_r image shows no disk-like component.

the final halo-subtracted PI_{sub} image was generated. Figure 4.3b shows the final PI_{sub} image and overlapped halo-subtracted vector map which is clearly circular symmetric, unlikely that of the previous PI image.

To verify this result, we converted the coordinate system of the Stokes parameters from the celestial coordinate system (the Stokes Q and U) to the radial coordinate system originate from disk center (the Stokes Q_r and U_r), and compared the results. Because the Stokes Q_r and U_r describe the polarization in tangential and radial direction, respectively, the Stokes Q_r image must show scattering polarization similar to the PI_{sub} image, while the Stokes U_r image should contain less or no scattered light from the disk (Avenhaus et al., 2014, Schmid et al., 2006). In our results (Figure 4.4a and b), the disk components are clearly visible in the Stokes Q_r image, whereas the Stokes U_r image does not show any circular structures and its signals are faint and noisy. Therefore, we concluded that the final PI_{sub} image is robust.

4.3 Results

The final H-band PI_{sub} image of the LkCA 15 disk with a software mask (r∼0.1″) is shown in the right panel of Figure 4.3b) and 4.5, and two elliptical disk structures are clearly resolved. Both the angular resolution and the inner working angle reach 0.07″ and r=0.1″, respectively. The brightness of the northwest side is significantly brighter than

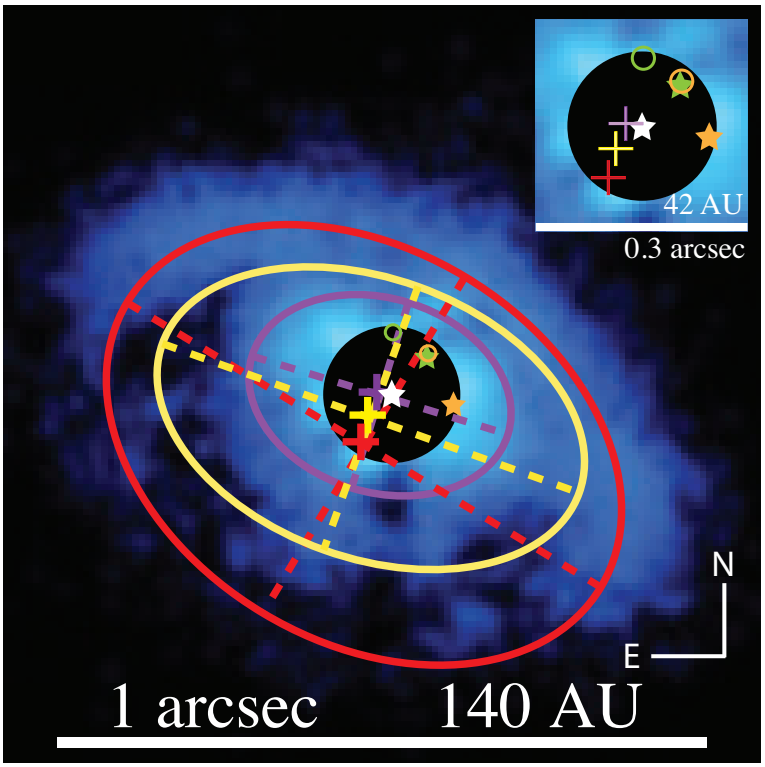

FIGURE 4.5: Elliptical fitting results of the inner disk (*purple*), the gap (*yellow*), and the outer disk (*red*). The image has been smoothed by a gaussian with r=2 pixels to reduce the effects of speckles on the inferred structure of the disk. The central region is also shown in the right top panel. *White star* indicates the location of LkCa 15. *Green and orange stars* indicate where the planet candidates LkCa 15 b and c were detected in 2014, respectively (Sallum et al., 2015). *Open green and orange circles* indicate the locations of two infrared sources seen in 2009-2010 (Kraus and Ireland, 2012), which are assumed as LkCa 15 b and c, respectively.

TABLE 4.1: Elliptical fitting results of two disks and gap[a].

Parameter	Outer Disk	Gap	Inner Disk
Radius of semi-major axis (AU)	59.0±1.4	48.3±0.7	29.8±2.0
PA of semi-major axis (°)[b]	59±2	67±3	72±2
Inclination (°)[c]	44±1	51±2	44±2
Geometric center offset (mas)[d]	(-37±4,-83±6)	(-24±6,-42±6)	(-13±2,-8±2)

[a] The peak, bottom, and half maximum positions (for the outer disk, gap, and inner disk, respectively) were obtained first from the radial profile at position angles every 10°. Then we conducted an elliptical fit by using the non-leaner least-squares Gauss-Newton algorithm with five free geometric parameters.
[b] Counterclockwise from north axis.
[c] Derived from the ellipticity. The inclination of a face-on disk is 0°, and that of an edge-on disk is 90°.
[d] (ΔR.A., ΔDec.). The origin of the coordinate corresponds to the position of the central star.

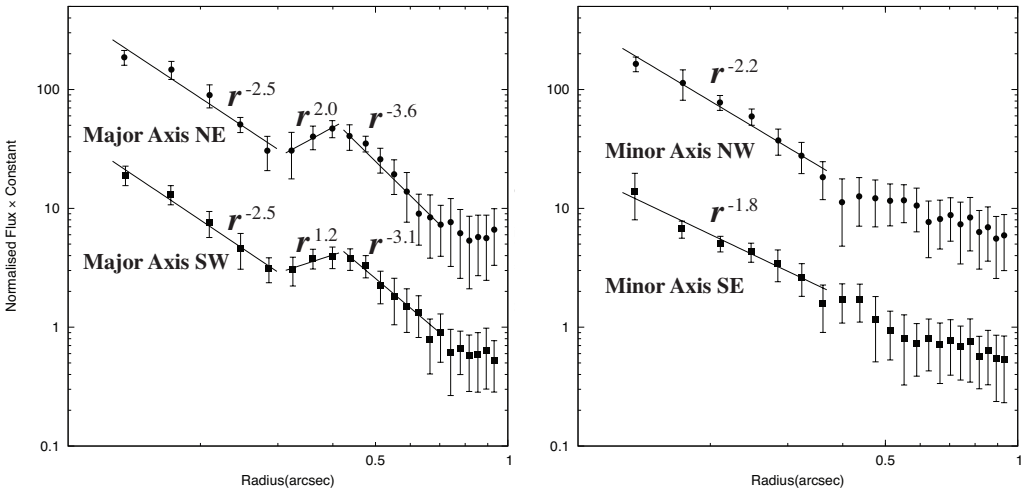

FIGURE 4.6: Radial surface brightness profiles with 1σ error bars at major and minor axes. The values were measured at each axis within the range of $\pm 10^\circ$, and were binned with a width of dr=4 pixels. The typical error of of power index is $\sim$0.05. The gap and inner disk slopes are confirmable along the major axis (*left pannel*).

that of the southeast side, this characteristic crescent-shape of scattered light brightness is consistent with the optical imaging results of Thalmann et al. (2015).

The elliptical shape could be due to the system's inclination (i). Thus, we fitted elliptical isophotes on a resulting image in order to measure the inclinations and position angles (PAs) of each disk. The elliptical fitting results are shown in Table 4.1 and Figure 4.5. We newly discovered significant misalignment from major axis PAs of the two disks ($13\pm4^\circ$), which indicate the strongly warped disk. The center of all three disk components appear on southeast side from the central star (See right top panel of Figure 4.3). The inclinations of the two disks are similar ($\sim 44^\circ$), but that of the gap shows larger angle ($\sim 51^\circ$). Note that Thalmann et al. (2014) reported eccentricities from the shape of the gap edge associated with LkCa 15, therefore the inclination estimated from the elliptical fitting could be biased.

Figure 4.6 shows the radial surface brightness profiles on the major and minor axes with a power-law fit at each slope. In the profiles of major axes (left panel of Figure 4.6), the gap appears as a depletion in the middle of each profile. The slopes of the gap regions in profiles show a significant change between northeast and southwest axes (power indices of r=2.0 and 1.2, respectively), and the slopes of the disk regions also show a change between inner and outer disks (r=-2.5 for inner disks, r=-3.1 and -3.6 for outer disks).

4.4 Discussion

4.4.1 Disk Geometry: Which side is near to us?

We revisited the question of which side of the disk faces us, northwest or southeast. The brightness asymmetry of the disk could be a clue, but Mulders et al. (2010) proposed that both orientations can explain well the SED of LkCa 15. The first interpretation — southeast is near-side — corresponds to the scenario of the backward illumination of the gap wall; backward illumination indicates that the bright side is the wall of the far side of the gap (Quanz et al., 2011). The second interpretation — northwest is near-side — corresponds to the scenario of the forward scattering, which indicates that the bright side is the surface of the disk's near side (e.g., Fukagawa et al., 2006). If backward illumination is the true explanation, the outer disk's inner wall would be optically thick and vertically high enough to conceal and reflect back the light from the star. Therefore, we can detect illuminated inner wall of outer disk more efficiently than forward scattering from near-side disk surface. On the other hand, if forward scattering is the true explanation for this asymmetry, the inner wall of the outer disk would have a relatively low vertical height; therefore, more star light would arrive on the disk surface over the gap wall and more forward-scattered light would come toward the observer. On large grains of μm to mm, forward scattering can be several times efficient than backward scattering. Beside, the optically inner disk casts shadow on inner wall of outer disk, and make it hard to detect. Therefore, both explanations are still under debate.

To try to elucidate which side faces us, we utilized the star-disk offset along the minor axis. On the projection of inclined disk, the central star comes to near side of the disk's minor axis (Dong et al., 2012b). In Figure 4.5, the central star is roughly on the northwest minor axes of three disk components, therefore we can conclude that the northwest side of the disk of LkCa 15 could be the one facing us. This supports forward scattering as the explanation of the brightness asymmetry and is also consistent with 3D radiative transfer modeling (Thalmann et al., 2014).

The warped disk is also can be a hint for this discussion; if there is the shadow of the warped inner disk on the outer disk's surface, and it makes asymmetric brightness in the outer disk along the southeast side of major axis. However, in the surface brightness profiles on possible shadow regions (Figure 4.7), we found no significant asymmetry over the range of the error. Therefore, the shadow of optically thick inner disk may cast only

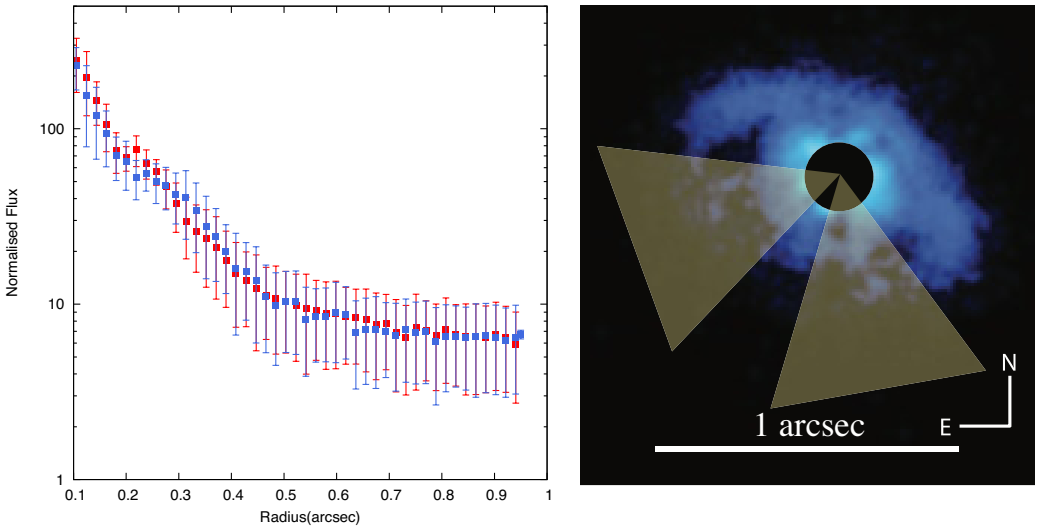

FIGURE 4.7: Radial surface brightness profiles of possible shadowed regions (*left*). Yellow triangles in *right* panel are represent the regions where radial profiles are obtained.

over the inner wall not the surface of outer disk. This is also reconcile with forward scattering scenario.

4.4.2 Surface brightness behavior

We found the slope of the brightness changes between northeast and southwest gaps, and between inner and outer disks. Furthermore, our measured slopes are not consistent with those of SPHERE/ZIMPOL results (power indices of inner disk, gap, and outer disk $\sim$ -2.4, 3.2 and -3.5 for northeast axis, -1.9, 2.1, and -4.1 for southwest axis, respectively, with typical error $\sim$ 0.1; Thalmann et al., 2015, private communication)

A number of reasons have been suggested to explain the change in brightness slopes, such as different extinction levels, surface densities, flaring angles or dust properties. The geometrical properties of inner disk could change the extinction level between the star and outer region and affect the brightness of outer disk (e.g., Krist et al., 2000); an actual change in the surface density slope can be translated into a change in the surface brightness slope, and a change of the flaring angle cause a change in the scattering of the disk's surface (Apai et al., 2004); a radial distribution of small dust particles and dust properties can affect the brightness slope (Akiyama et al., 2015). Although the brightness behavior could provide some physical properties of the disks, a detailed analysis of the reason of the brightness behavior is beyond the scope of this letter, and it will be discussed elsewhere.

4.4.3 The large gapped disk

In the PI$_{sub}$ image and radial profiles, LkCa 15 has a large gapped (width ∼27 AU) disk. Among some mechanisms (e.g., grain growth, photoevaporation, disk-planet interaction; see Espaillat et al., 2014a) that have been proposed to explain the clearing of the gaps in transitional disks, only gravitational interaction between disks and orbiting *multiple* planets (at least four) can clear a large inner gap of $\gtrsim$ 15 AU or more (Dodson-Robinson and Salyk, 2011, Zhu et al., 2011) and preserve optically thick inner disk around high-accretion T Tauri star. Dust grain growth fails to reproduce the large emission cavity (Birnstiel et al., 2012) observed by mm interferometric image (Andrews et al., 2011a). Photoevaporation can not make large cavity with the radius of 20 AU or more, and is difficult to reconcile with both massive outer disk and high accretion rate.

Furthermore, de Juan Ovelar et al. (2013a) simulated observations of various planet-hosting disk models, and suggested a 1 $M_{\rm Jup}$ planet would create a similar size of outer gap edge at NIR and (sub-)mm wavelengths; conversely planets more massive than 1 $M_{\rm Jup}$ would make different radial grain-size distribution in the dusty disk, and observations at different wavelengths capture different parts of this grain-size distribution. Since the sizes of the outer gap edge of LkCa 15 are ∼50 AU at sub-mm (50 AU and 46±3 AU; Andrews et al., 2011a, Piétu et al., 2006, respectively) and 48.3±0.7 AU at NIR (this work), a 1 $M_{\rm Jup}$ planet might create a gap around LkCa 15. By combining the upper mass limits of LkCa 15 companions, as Thalmann et al. (2010) suggested on the basis of their NIR imaging result and COND evolutionary model by Baraffe et al. (2003), we concluded that assuming multiple planets with a mass of $\lesssim 1 M_{\rm Jup}$ could account for LkCa 15's large gapped disk with an outer gap edge similar in size at both NIR and (sub-)mm wavelengths.

4.4.4 The warped disk

We found a significant misalignment between two position angles of inner and outer disks (=13±4°) which indicates that the inner disk is possibly warped along the disk major axis. If inner disk was also warped along the minor axis, we would see a misaligned inclination. However, the inclination of the inner disk is consistent with that of outer disk (∼44°). Currently, the disk system of LkCa 15 is the first observed warped disk associated with young T Tauri star. Warped disks, such as β Pictoris (e.g., Mouillet et al., 1997), AB Aurigae (e.g., Hashimoto et al., 2011), and HD 142527 (e.g., Marino

et al., 2015) have been reported on several old or heavy stars surrounded by transitional disks and debris disks. These warped inner disks may be explained by the gravitational perturbation from planets (e.g., Mouillet et al., 1997). β Pictoris, whose planetary mass companion β Pictoris b has a similar inclination to and possibly responsible for the inner warped disk (e.g., Lagrange et al., 2012), is a possible evidence for this scenario. Additionally, Ahmic et al. (2009) also suggested the possibility of multiple planets/planetesimals in β Pictoris to explain two separate inclined disks, although the mechanism they used is different — the collisional dynamics of bodies in the disks.

To summarise, since LkCa 15 may possess multiple planets with a mass of $\lesssim 1 M_{\rm Jup}$ in the large gap, the warped inner disk could be the result of potential planets around LkCa 15.

4.5 Conclusion

We have presented a warped inner component beyond the large gap from the LkCa 15 disk system revealed by angular differential imaging in the H-band with HiCIAO installed on a Subaru Telescope. We derived $13 \pm 4^\circ$ as the PA offset between the outer disk and the warped inner disk. This unique gap plus the warped disk configuration of the LkCa 15 system combined with the previous observations at mm and optical wavelengths indicates the existence of a multiple planetary system possibly composed of $\lesssim 1 M_{\rm Jup}$ planets on the solar system scale. To directly observe and reveal the origin and evolution of possible multiple planetary systems, future ground-based observations with the Extreme Adaptive Optics (ExAO) system such as the Subaru Coronagraphic ExAO (SCExAO; Jovanovic et al., 2015) are required.

Chapter 5

Resolved Near-IR Image of Inner hole in GM Aur Transitional Disk

Abstract

We present high-contrast H-band polarized intensity images of the transitional disk around the young solar-like star GM Aur. The polarimetric direct imaging of the disk was derived by polarimetric differential imaging (PDI) using 8.2-m Subaru Telescope and HiCIAO, and its angular resolution and inner working angle reach 0.07″ and r∼0.05″, respectively. We obtained a clearly resolved large inner hole, and the radius of hole (∼18 AU) is smaller than that of sub-mm interferometric image. This inconsistency of the hole radii at NIR and sub-mm wavelengths may induced by a 3-4 $M_{\rm Jup}$ planet. The presence of near-infrared inner hole could be strong constraint on the hypotheses of inner hole formation in a transitional disk. Especially, dust filtration mechanism have been proposed to explain the large hole in sub-mm image, but our results suggest that it must be combined with additional process. We found that the polarized intensity slope of outer disk is significantly different with the intensity slope obtained from HST/NICMOS, and this difference may be a sign of grain growth progress in the disk.

5.1 Introduction

5.1.1 Background

The presence of the circumstellar disks had been predicted as an inevitable consequence of angular momentum conservation during gravitational collapse in the star formation, and now it is considered as the initial phase of the planet evolution. Typical circumstellar disks have nearly photometric emission at infrared wavelengths, but some disks have substantial mid- and far-infrared (>10μm) excesses above the stellar emission (Strom et al., 1989). Spectral energy distribution (SED) modeling studies of the Spitzer Infrared Spectrograph (IRS; Houck et al., 2004) and the Infrared Space Observations (ISO: Kessler et al., 1996) proposed that the spectral dent at near-infrared (<10μm) can be explained by optically thin inner cavities with the radius of 10 AU or more in optically thick disks (Calvet et al., 2005, D'Alessio et al., 2005, Espaillat et al., 2007b, Uchida et al., 2004). Such disks are referred to as transitional disks (Espaillat et al., 2007a, Strom et al., 1989), and now have become central to understanding of the evolutionary transition between dusty protoplanetary disk and cold debris disk. The inside-out disk clearing in transitional disk must occur in very short time scale (< 10 Myr), since transitional disks appear around only young stellar objects with ages of 1-10 Myr. Also the small frequency of transitional disks may reflect that not all disks actually experience an inner disk clearing at young ages (Muzerolle et al., 2010). However it is not well understood which physical mechanism(s) drives disk clearing process.

One of the promising mechanisms is dust filtration by the outer edge of a planet-induced gap (Paardekooper and Mellema, 2006, Rice et al., 2006, Zhu et al., 2012). This mechanism was proposed to explain the both of the dust dynamics and the gas dynamics in the disk. Because the radial density and pressure gradient of the gas is negative at the outer edge of a planet-induced gap, dust particles drift outward by gain of angular momentum from the gas. When drifted dust particles overcome the coupling with the gas, they will stay at the gap outer edge while the gas fall into the star through the gap. This process works like dust filter, and it depletes the inner dust disk to the radius of the planet-induced gap, producing a dustless inner hole. It should be noted that this mechanism is effective only if dust particles are large enough to have significant drift velocities. Zhu et al. (2012) showed that 0.01-0.1 mm particles and above can be filtered by a reasonable gap. Consequently, dust filtration can explain the large-dust-depleted

inner hole seen in sub-mm observations, but it cannot explain the small-dust-depleted inner hole seen in near-infrared observations.

Thus, even though modeling analysis on the basis of SED is indispensable, the spatial distribution of gas and various-size dust in the disk must be evaluated by high resolution imaging observations at multiple wavelengths (de Juan Ovelar et al., 2013a) to constraint physical mechanisms occur at transitional phases.

5.1.2 History of Study on GM Aur Disk

GM Auriga (K5, 0.84 $M_{\odot}$ Simon et al., 2000) is a T Tauri star located in Taurus-Auriga molecular cloud ∼140 pc away from us, initially revealed to have a rotating gaseous disk with inner hole(Koerner et al., 1993). Estimates for the age of GM Aur vary from 3 to 10 Myr (e.g., Hartmann, 2003, Simon et al., 2000).

Since the discovery of GM Aur disk, the inner hole in the disk have been studied intensively by SED analysis. Koerner et al. (1993) used simple flared accretion disk model, and proposed a deficiency of dust at ∼0.4 AU from the star. Chiang and Goldreich (1999) conducted a hydrostatic radiative equilibrium model of SED, and suggested 4.8 AU as the radius of inner hole. Calvet et al. (2005) raised up the estimated radius to 24 AU on the basis of Spitzer IRS spectrum and the radiative transfer model (D'Alessio et al., 2005).

A (sub-)millimeter interferometry allowed more direct analysis using spatially resolved images (See Figure 5.1). Hughes et al. (2009) resolved the inner hole by the Submillimeter Array (SMA) at a wavelength of 860 μm and the Plateau de Bure Interferometer (PdBI) at a wavelength of 1.3 mm, and suggested the hole radius as 20 AU. They also suggested dust filtration effect by planet-induced gap edge as the convincible explanation for inner disk clearing. Andrews et al. (2011b) revisited this with 2D Monte-Carlo radiative transfer calculation and new high angular resolution SMA observations at a wavelength of 880 μm, and derived 28 AU.

The spatial resolution of near-infrared imaging (∼10 AU) is higher than that of typical (sub-)mm interferometry observations (∼40 AU), and observations with various techniques at different wavelengths (μm to mm) resolve different aspects of the dust distribution (de Juan Ovelar et al., 2013b). Schneider et al. (2003) provided non-polarimetric scattered light observations using HST/NICMOS with near-infrared spectral bands (1.1 μm and 1.6 μm), but they conducted coronagraphic imaging with hole

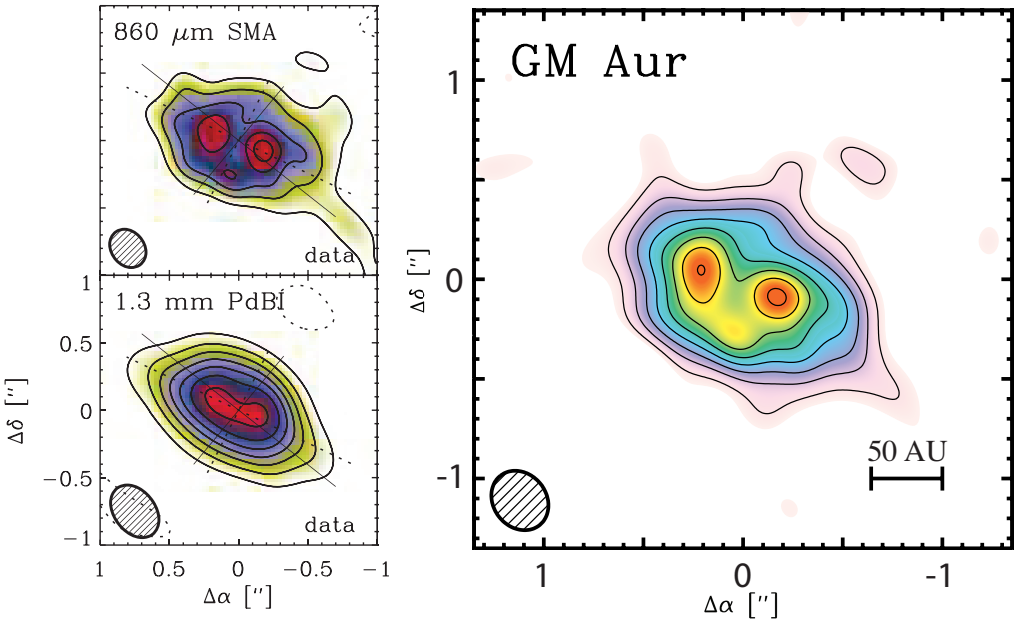

FIGURE 5.1: Continuum emission images of GM Aur disk by (sub-)mm interferometry. *left top*: 860 μm SMA, *left bottom*: 1.3 mm PdBI, and *right*: 880 μm SMA. The synthesized beam dimensions are marked in the lower left corner. The 880 μm observation (*right*) provides more accurate location for visibility null (i.e., dust hole). Figures adopted from Hughes et al. (2009) and Andrews et al. (2011b)

radius of 0.3″, which is too large to verify inner hole with the radius of $\lesssim$ 28 AU ($\sim$ 0.2″). Beside, the polarimetric direct imaging with high resolution on GM Aur disk at near-infrared wavelengths has not been challenged yet. Therefore, resolving inner hole in GM Aur with near-infrared imaging polarimetry may serve a further understanding for disk clearing in transitional disks.

5.1.3 In This Work

We present the results of the first high-contrast NIR (1.6μm) polarization imaging conducted on the transition disk associated with young T Tauri star GM Aur by 8.2-m Subaru Telescope at Mauna Kea, Hawaii. The priority goal is the quantitative analysis of spatial structure including inner hole to discuss the dust distribution at different aspects with previous works. The High Contrast Instrument for the Subaru Next Generation Adaptive Optics (HiCIAO; Tamura et al., 2006) combined with AO188 (Hayano et al., 2010) provides high-resolution and -contrast image, and resolved more inner side of the disk, where previous near-infrared HST/NICMOS observation couldn't resolve.

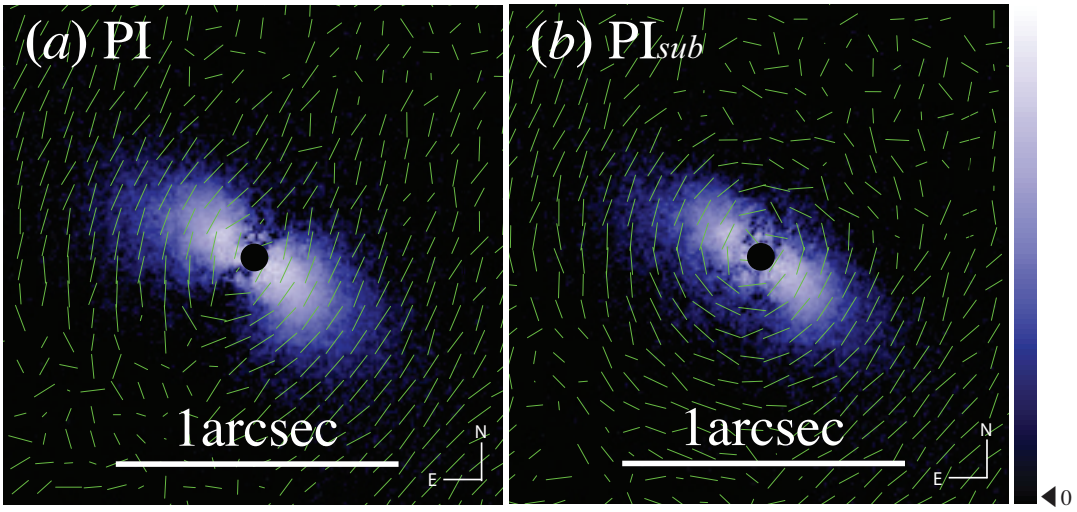

FIGURE 5.2: PI and overlapped polarization vector map images (2.0″×2.0″) before (*a*) and after (*b*) halo subtraction. The saturated region is occulted by a software mask (r = 5 pixel ∼ 0.05″), the vectors are binned with spatial resolution, and the lengths are arbitrary for presentation purposes. (*a*): The effect of a polarized halo appears to have a tendency toward the minor axis of the disk. (*b*): The polarization tendency to the minor axis was removed, and the disk-origin polarization along the disk surface was revealed.

The results show inconsistent results with sub-mm observation regarding the hole radius, and this morphologic inconsistency at different wavelengths may be interpreted to a result of the physical interaction between disk and an unseen (proto-)planet.

5.2 Observation and Data Reduction

Near-infrared (1.6μm) linear polarimetric differential images (PDI) of GM Aur disk were obtained using the HiCIAO on the Subaru Telescope on the night of 2010 December 2. We used a double Wollaston prism to split incident light into four 5″×5″ channels, two each of o- and e-rays sets (qPDI) to reduce the saturated radius under the expected inner hole size (r∼0.14 arcsec, 20 AU at 140 pc). The imaging scale of HiCIAO in qPDI mode is 9.5 mas per pixel. We obtained 21 data sets (four angular positions of the half-wave plate; 0°, 45°, 22.5° and 67.5° for one data set to obtain full polarization coverage with minimal artifacts) with 8 s exposure for each frame. We strictly removed low quality data from among them to obtain the best quality. The total integration time of the resultant polarization intensity image was 576 s using 18 data sets. This observation was a part of the program of the SEEDS (Strategic Explorations of Exoplanets and Disks with Subaru; Tamura, 2009) project.

The Image Reduction and Analysis Facility (IRAF)[1] software with the custom script pipeline designed by Hashimoto et al. (2011) was used for the polarimetric data reduction in the standard manner of infrared image reduction. After bias subtraction and bad pixel correction, we obtained $+Q$, $-Q$, $+U$, and $-U$ images by subtracting two images of e- and o-ray images at each angular position of the half-wave plate, then $2Q$ and $2U$ images were made by $(+Q) - (-Q)$ and $(+U) - (-U)$ (Hinkley et al., 2009). The polarized intensity (PI) was given by PI $= \sqrt{Q^2 + U^2}$.

Although a disk-like elliptical structure is visible in PI image, the polarization vectors shows a tendency to align toward the minor axis of the disk (See Figure 5.2), not a circular symmetry as expected from the Fresnel reflection. This is considered as a residual stellar halo in the obtained images, because the standard polarimetry reduction procedure cannot perfectly remove the convolved stellar PSF. To obtain more authentic disk-origin PI, we first compute the polarization halo by calculating the average polarization strength P (1.27±0.05%) and the average polarization angle θ (150.5±0.5°) from the unsaturated Stokes I, Q, and U images. By subtracting polarization halo model from the Stokes Q and U images, we obtained the halo-subtracted Stokes parameters, $Q_{\rm sub}$ and $U_{\rm sub}$. The final halo-subtracted polarized intensity ($\rm PI_{sub}$) is computed via $\rm PI_{sub}$=$\sqrt{Q_{\rm sub}^2 + U_{\rm sub}^2}$. Figure 5.2b is the resultant $\rm PI_{sub}$ image with polarization vectors which show circular symmetric tendency.

We also computed the radial Stokes parameters which are given as $Q_{\rm r} = +Q\cos 2\phi + U\sin 2\phi$ and $U_{\rm r} = -Q\sin 2\phi + U\cos 2\phi$. Where ϕ is the position angle of the line from the star to the location of certain point. Q_r is represents the polarization in tangential direction, thus it must show a similar image with $\rm PI_{sub}$ image. Besides, U_r is represent the polarization in radial direction, and thus it should contain less or no polarized light from the disk surface (Avenhaus et al., 2014, Schmid et al., 2006). Therefore, we can use the radial Stokes Q_r and U_r images for verifying our resultant image. Q_r image (Figure 5.3a) shows the elliptical disk structure just as $\rm PI_{sub}$ image, whereas U_r contains no elliptical our circular structure, but faint and noisy signals. Accordingly, we concluded that the final $\rm PI_{\mathit{sub}}$ image is robust.

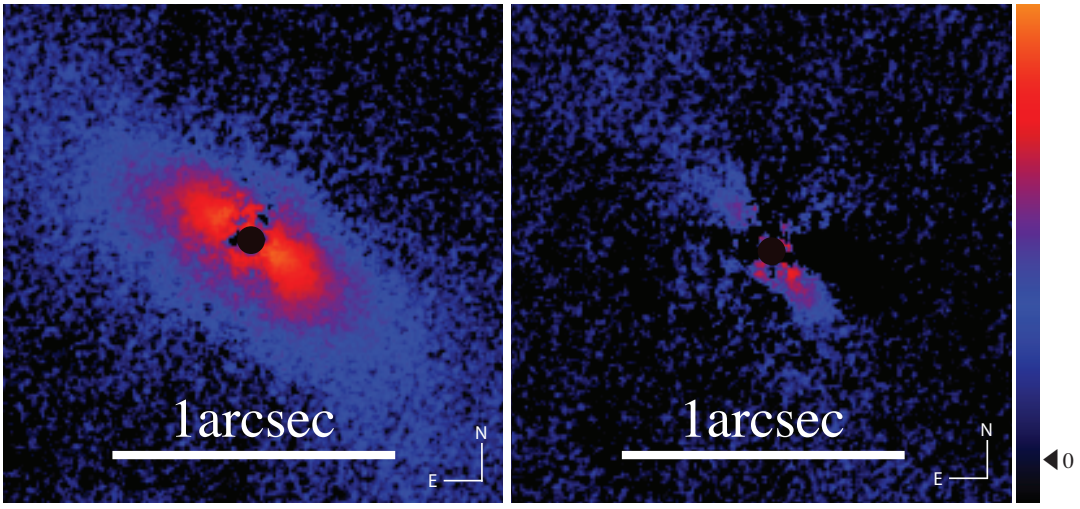

FIGURE 5.3: The radial Stokes Q_r (*left*) and U_r (*right*) images of LkCa 15 disk. The saturated region is occulted by a software mask (r$\sim$0.1°). In the Q_r image, both the outer and inner disks are significantly detected as expected from the PI image. On the other hand, the U_r image shows no disk-like component.

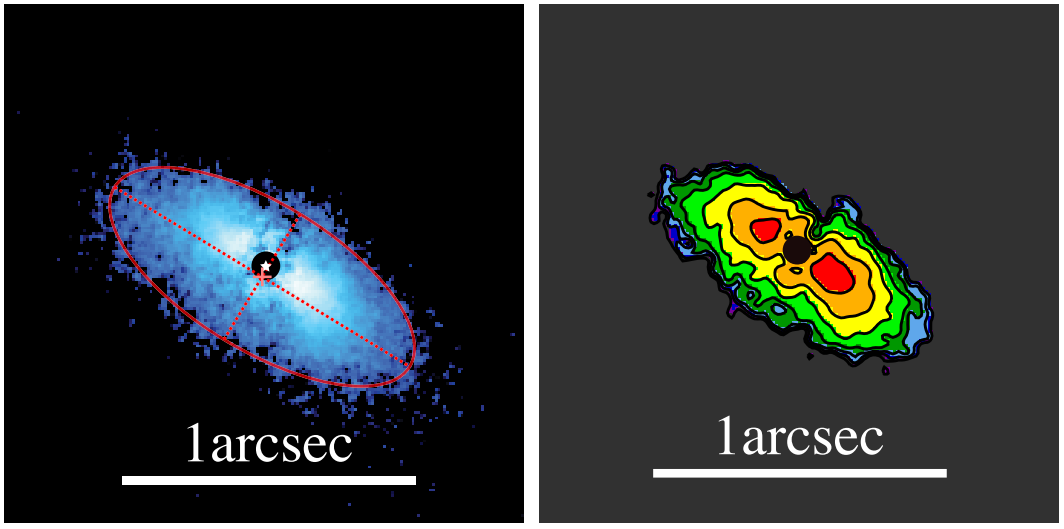

FIGURE 5.4: *left*: Elliptical fitting results of the outer edge of the disk. The image has been smoothed by a gaussian with r=2 pixels to reduce the effects of speckles on the inferred structure of the disk. *right*: The inner peaks of the disk (*red regions*) and the central inner hole (between *red regions* and software mask) are more clear in contour map of the disk. The image has been smoothed by a gaussian with r=3 pixels and the contrast is adjusted to emphasis contour edges.

5.3 Results

The final *H*-band PI image of the GM Aur disk with a software mask (r∼40 mas) is shown in Figure 5.2b. The symmetric and elliptical disk structure is resolved. The elliptical shape of the disk could be due to the systems. Thus, we fitted elliptical isophotes on a resulting images in order to measure the inclinations and position angles (PAs) of the disk. The elliptical fitting results are shown in Table 5.1, and overlaid on Figure 5.4.

We found significant offset between the disk center and the location of central star as ∼0.37 mas at position angle of 252°, which is roughly along the minor axis. This offset indicates that the southeast side is inclined toward us (i.e., Dong et al., 2012b).

Figure 5.5 show the radial surface brightness profiles along the major and minor axes. We fitted a power-law at each slope, and found possible inner hole with the radius of 18±2AU. This is the first detection of the hole at NIR wavelengths, and the hole radius is smaller than the results of observations at sub-mm wavelengths (28AU; Andrews et al., 2011b). Generally, disk shows symmetric surface profiles in the range of the error.

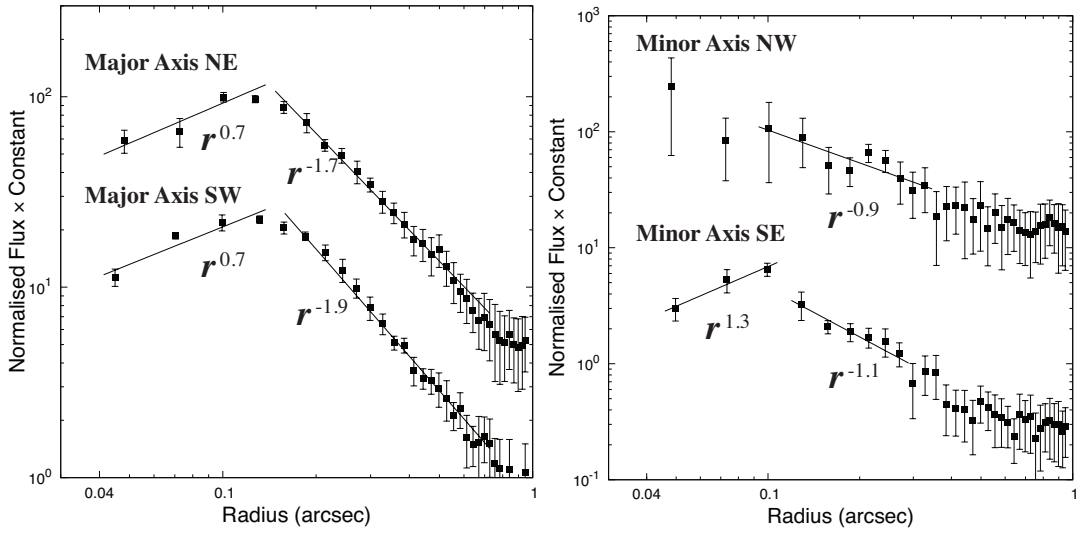

FIGURE 5.5: Radial surface brightness profiles with 1σ error bars at major and minor axes. The values were measured at each axis within the range of ±10°, and were binned with a width of dr=4 pixels. The typical error of of power index is ∼0.05. The gap and inner disk slopes are confirmable along the major axis (*left panel*).

[1]The IRAF software is distributed by the National Optical Astronomy Observatory, which is operated by the Association of Universities for Research in Astronomy (AURA) under a cooperative agreement with the National Science Foundation.

TABLE 5.1: Geometric Measurements of GM Aur disk

Parameter	Outer edge[a]	Inner edge[b]
Radius of semi-major axis (AU)	70±4	18±2
Position angle of semi-major axis (°)[c]	59±2	53±2
Inclination (°)[d]	64±2	.
Geometric center offset (mas)[e]	(-12±5,-36±6)	(-8±1,-4±1)

[a] The positions where flux becomes noise level were obtained first from the radial profiles at postion angles every 10°. Then the least-squares estimation elliptical fitting with five free geometric parameters was conducted using IRAF package stsdas.analysis.
[b] On the basis of flux peaks in radial profiles. The elliptical fitting was not available at inner edge because the number of peak points was not enough to fit with small error.
[c] Counterclockwise from north axis.
[d] Derived from the ellipticity. The inclination of a face-on disk is 0°, and that of an edge-on disk is 90°.
[e] (ΔR.A., ΔDec.). The origin of the coordinate corresponds to the position of the central star.

5.4 Discussion

5.4.1 Different Brightness Slope: Polarization and Non-polarization

The radial polarized intensity (PI) profiles of the outer disk along the two major axes (Figure 5.5) are well fitted to a power law with power indices of -1.7 and -1.9 for northeast and southwest axes, respectively, which indicate flared disk surface. We found that the power indices of minor axis, ∼-1.0 is not consistent with that of the radial intensity (I) profiles from HST/NICMOS observations (Schneider et al., 2003), power index of -3.5 for F160W band filter. Since wavelengths difference between HiCIAO *H*-band filter (1.3-1.9 μm) and NICMOS F160W band filter (1.4-1.8 μm) is negligible in surface brightness comparison, the power index difference between PI and I profiles may indicate the change of polarization efficiency at different radii. The ratio of polarized light to entire scattered light is expected to be of the order of 50% in ideal situation, 100% scattering of zero-polarized light by spherical grains (Follette et al., 2013). However, in real, polarization efficiency is determined by many variables such as composition of particle shape and size, multiple scattering, and scattering angle change by flared surface (e.g., Perrin et al., 2009, Simpson et al., 2009, Whitney and Wolff, 2002). Therefore, some of physical parameters mentioned above make polarization efficiency higher as radius increases. We are concentrating on polarization efficiency change on overall disk surface, and thus multiple scattering effect by local topology is not considered at here. One explanation is highly flared disk, as indicated by the major axis profiles. However, if scattering

angle of flared surface significantly changes polarization efficiency, the brightness slope near and far side of minor axis should be asymmetric, which is not reconciled with almost symmetric brightness slope of northwest and southeast minor axis (r= -0.9 and -1.1, respectively). Furthermore, a steep brightness decreasing slope seen in I profile ($\propto r^{-3.5}$, Schneider et al., 2003) suggests that outer disk is not highly flared, thus the effect of scattering angle change by flared surface may be small. Another explanation is the change of dust particle structure, such as size, porosity and oblateness. Therefore, the power index difference between PI and I profiles may be a sign of various grain growth progresses at different radii. Multiple radio wavelengths analysis must be done to reveal detailed dust grain properties (e.g., Pérez et al., 2012, 2015).

5.4.2 Imaging diagnostics: Cavity radius and planet mass

Recent imaging observations on disks have revealed the presence of spatial differentiation of the grain sizes in transitional disks, since observations at different wavelengths trace different grain sizes, showing different spatial structures of the disks (e.g., missing cavity at near-infrared imaging; Dong et al., 2012a). Zhu et al. (2012) and Pinilla et al. (2012a) suggested that the dust filtration effect by planet-induced cavity edge may allow dust particles at different radii to have different grain sizes. de Juan Ovelar et al. (2013a) performed 2-dimensional hydrodynamical and dust evolution models combined with instrument simulations, and provided the predictions on on emitted/scattered light spatial images at different wavelengths with several cases of planet masses/locations (See Figure 5.6).

To estimate possible planet mass in GM Aur disk by using $f(M_{\rm p})$ fitting results (See Figure 5.6 bottom panel and de Juan Ovelar et al., 2013a) with hole sizes at near-infrared (this work) and sub-millimeter wavelengths (28AU; Andrews et al., 2011b), we assumed that (1) a 18 AU radius hole seen in HiCIAO infrared polarized intensity image is induced by a planet at 20 AU separation from the central star, and that (2) hole size seen in ZIMPOL can be replaced with that seen in HiCIAO, since ZIMPOL and HiCIAO polarized intensity images trace similar dust particle sizes (1-10μm in general) and their main differences are resolution and sharpness. Thus it should be noted that this is only a rough estimation. Consequently, we obtained 3-4 $M_{\rm Jup}$ as the mass of possible planet at 20 AU separation.

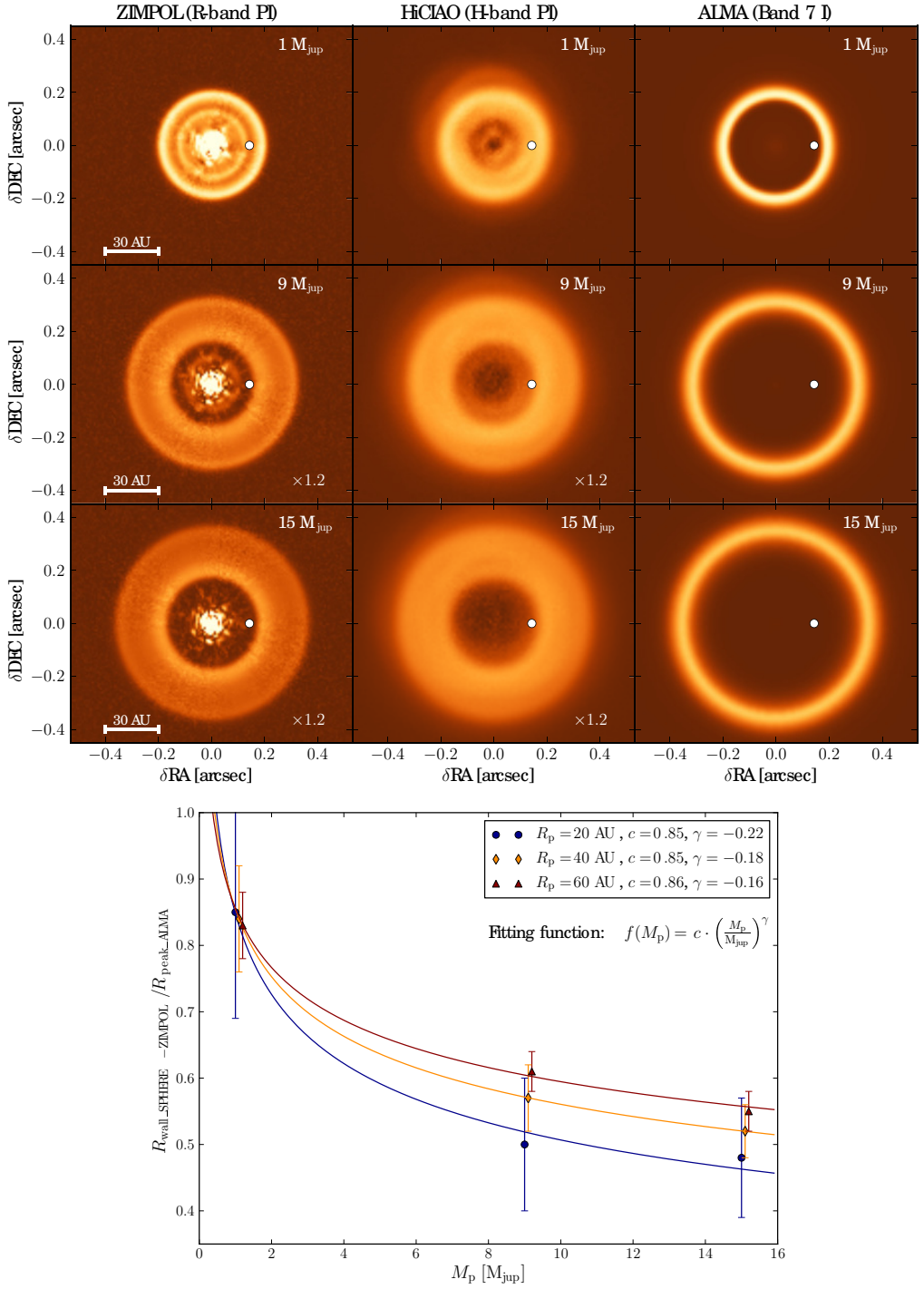

FIGURE 5.6: Adapted from de Juan Ovelar et al. (2013a). *top*: Simulated images of the disc-planet models at different wavelengths instruments, in the case of an embedded planet at 20 AU separation (*white dot*). The cases of 9 and 15 $M_{\rm Jup}$ in R and H polarised-intensity have been multiplied by a small factor to enhance the contrast. *bottom*: SPHERE ZIMPOL R-band cavity edge to ALMA Band 7 peak ratio ($f(M_{\rm p}) = R_{\rm wall\_SPHERE-ZIMPOL}/R_{\rm peak\_ALMA}$) versus planet mass ($M_{\rm p}$) for the three planet orbit radii ($R_{\rm p}$).

5.4.3 The origin of the inner hole

To explain formation of sub-mm inner cavities transitional disks, a number of physical mechanisms have been suggested, such as photoevaporation, grain growth, disk wind by magnetorotational instability (MRI), and gravitational interaction between disk and planet(s). However, unfortunately at present, none of suggested mechanisms has clearly explained the formation of an infrared inner hole in transitional disks, including GM Aur disk.

Photoevaporation plays a dominant role when the mass accretion rate is sufficiently low. However the high mass accretion rate of GM Aur disk (4×10^{-9}-$1\times10^{-8} M_{\odot}$; Espaillat et al., 2007a, Ingleby et al., 2015) requires a substantial supply of material from massive outer disk ($\sim0.16 M_{\odot}$; Hughes et al., 2009). *Grain growth models* (e.g., Dullemond and Dominik, 2005, Strom et al., 1989, Tanaka et al., 2005) should mainly affect the large dust grains and proceed without reducing the gas density. However, the observations of CO emission lines indicate the presence of inner gas hole in GM Aur disk (Dutrey et al., 2008, Salyk et al., 2007). *Protoplanetary disk winds model* (Chiang and Murray-Clay, 2007, Suzuki et al., 2010b) is not reconciled with the silicate emission at 10μm in the IRS spectrum of GM Aur (Calvet et al., 2005), which indicates the existence of micron-size interstellar medium grains in wall atmosphere. *Disk-planet interaction* produces only a wide gap in the disk even with a system of 4 our more planets (Dodson-Robinson and Salyk, 2011, Zhu et al., 2011). More recently, Rosenfeld et al. (2014) proposed that radial flow of gas with near free-fall velocity can explain both the dust depletion at inner cavities that survive even in the relatively high mass accretion rate from outer disk (*fast radial flows model*). However, at present, this scenario needs more observational verifications such as twisted velocity isophotes and hot H_2 that is induced by shocks from fast accretion flows.

In previous studies, *dust filtration effect* by planet-induced gap had been the most conceivable mechanism to explain the inner hole in GM Aur transitional disk (Hughes et al., 2009). However, dust filtration effect may not be reconciled with a near-infrared inner hole we discovered in this work, because a near-infrared inner hole indicates the absence of micron-size particles in the inner region, while dust filtration effect works on only sub-mm size particles and can not prevent infalling of micron-size paticles which easily couples and flow with accreting gas. (Rice et al., 2006, Zhu et al., 2012). In other

words, dust filtration effect can explain sub-mm hole, but has difficulty in make near-infrared hole in the disk. Dong et al. (2012a) also reported about cavity-less near-infrared polarized scattered light images of several transitional disks which have sub-mm emission cavities. Therefore, even though dust filtration may play a key role in inner disk clearing, to produce near-infrared holes in transitional disks, there must be additional process such as grain growth (Zhu et al., 2012). Consequently, the newly discovered near-infrared inner hole makes the GM Aur disk more mysterious than before. If other transitional disks with sub-mm emission cavities have a similar near-infrared hole, the presence of the near-infrared central cavities in transitional disks will become an important issue in the future studies of disk evolution.

5.5 Conclusion

We have presented a spatially resolved image of a transitional disk associated with young T Tauri star GM Aur at near-infrared wavelengths, obtained using Subaru/HiCIAO, and have revealed a large inner hole, which is seen for the first time at this wavelengths. The measured hole radius (18 AU) is significantly smaller than that from the latest measurement at sub-millimeter wavelengths (28 AU, Andrews et al., 2011b). This inconsistency in hole sizes may be induced by a possible few $M_{\rm Jup}$ planet embedded in the hole; an estimated mass is 3-4 $M_{\rm Jup}$ with some assumptions (See Section 5.4.2).

The physical mechanisms of a large inner hole surrounded by massive outer disk are still not well understood. Especially clearing mechanism of a near-infrared hole in a transitional disk is not yet unveiled. With submillimeter inner hole, dust filtration mechanism is the most conceivable hypothesis. However our discovery of the near-infrared inner hole suggests that the dust filtration effect should be combined with some additional disk clearing processes, or that micron-size particles should not be coupled well with accreting gas for some reason. The future high resolution imaging observations by ALMA (the Atacama Large Millimeter Array) will play an important role in verification of the dust filtration scenario by tracing the gas flow in the near-infrared hole in the GM Aur disk.

The known physical characters of the GM Aur transitional disk is very similar to those of the LkCa 15 pre-transitional disk in; possible planet(s) and a large cavity (this work); high accretion rates ($2.4\times10^{-9}M_{\odot}$ for LkCa 15, $4\times10^{-9}\sim1\times10^{-8}M_{\odot}$ for GM Aur; Espaillat et al., 2007a, Ingleby et al., 2015, respecively); surface density and temperature

of the disk (Hughes et al., 2009). The difference is mainly the presence of inner disk in the LkCa 15 system. Therefore, these two (pre-)transitional disks of GM Aur and LkCa 15 may be on the similar evolutionary path in different phases, before and after inner disk clearing process. To directly observe the evidence of multiple planetary system and to reveal the location in evolutionary timeline toward a mature planetary system, future ground-based observations with the Extreme Adaptive Optics (ExAO) system such as the Subaru Coronagraphic ExAO (SCExAO, Jovanovic et al., 2015) are required.

Chapter 6

Summary and Overview of DoAr 25, LkCa 15, and GM Aur disks

6.1 Summary of DoAr 25, LkCa 15, and GM Aur disks

In previous chapters, we reported and discussed the structures of three different disks around young T Tauri stars, DoAr 25 , LkCa 15, and GM Aur (Chapter 3, 4, and 5, respectively). We discovered different characteristic structures from each of disks; disk wing as dust shell remnant, warped inner disk from LkCa 15, and inner cavity from GM Aur. As part of the project SEEDS, which is one of the largest near-infrared polarimetry disk surveys around T Tauri stars to date and have revealed various disk structures (e.g., Follette et al., 2015, Hashimoto et al., 2011, Mayama et al., 2012, Muto et al., 2012), those characteristic strucutres show that the circumstellar disk morphology has wider diversity than we thought.

DoAr 25 full disk in early inner-clearing process? — No cavity was resolved in high resolution imaging polarimetry. The disk wing, which is a possible outflow-entrained dust shell remnant (e.g., Sako et al., 2005, Schneider et al., 2003), may be a sign of the extreme youth of circumstellar system of DoAr 25. It is also predictable that there is no massive planet in the DoAr 25 disk within radius of 18 AU, because massive planets embedded in the disk will produce large cavity in very short timescale, only a few orbital-period (Kley and Nelson, 2012).

LkCa 15 pre-transitional disk with warped inner disk — Consistency in large gap size between infrared ($\sim$ 48 AU) and sub-millimeter observations (Piétu et al., 2006) proposes the presence of multiple planets less massive than 1 $M_{\rm Jup}$ carving and filtrating the disk edges (de Juan Ovelar et al., 2013a, Zhu et al., 2011). A bright inner disk with a misaligned position angle respect to that of the outer disk can be interpreted as warped inner disk, which can be caused by the gravitational perturbation from planets (e.g., Mouillet et al., 1997).

GM Aur transitional disk with near-infrared inner hole — The inner hole is resolved first for the first time at near-infrared wavelengths, and the radius of near-infrared hole ($\sim$ 18 AU) is significantly smaller than that of sub-millimeter hole ($\sim$ 28 AU; Andrews et al., 2011b). This cavity radius inconsistency between two different wavelengths observations has been expected to be caused by a planet massive than 1 $M_{\rm Jup}$ (de Juan Ovelar et al., 2013a). With considering high mass accretion rate, the feasible history of the disk is as follow; there was planet-induced gap between inner and outer disk, then inner disk diminished by *some* inside-out clearing mechanism. However, dust filtration effect by outer gap edge only work on large dust particles, and thus planet-induced gap cannot

TABLE 6.1: Summary of studies on three targets.

Host star	DoAr 25	LkCa 15	GM Aur
M_* ($M_\odot$)[a]	$\sim$ 0.64	$\sim$ 0.97	$\sim$ 0.84
Sp.T[a]	K5	K5	K3
Age (Myr)[a]	$\sim$ 1	$\sim$ 2 - 3	$\sim$ 2 - 3
Distance (pc)	$\sim$ 123	$\sim$ 140	$\sim$ 140
Association	ρ Ophiuchus	Taurus-Auriga	Taurus-Auriga
Disk	Full disk	Pre-transitional Disk	Transitional Disk
Cavity	Cavity-less	Gap (r=47 AU)	Hole (r=18AU)
Flared Disk (p[1])	Yes (-1.8$\pm$0.1)	No (-3.4$\pm$0.3)	Yes (-2.0$\pm$0.1)
M_d ($M_\odot$)[a]	$\sim$ 0.2	$\sim$ 0.2	$\sim$ 0.2
$\dot{M}$ ($M_\odot$/yr)[a]	10^{-10} - 10^{-9}	2.4×10^{-9}	4×10^{-9} - 1×10^{-8}
Note	Dust shell remnant	Warped inner disk	Sub-mm hole (r=28 AU)[b]
Companion	DoAr 25 b	LkCa 15 b, c	(Not discovered)
Mass ($M_{\rm Jup}$)	$\sim$13[c]	$<$0.5[d]	.

[1] Power indices of power law fit on the radial profile slopes.
[a] Calvet et al. (2005), Espaillat et al. (2007a), Greene and Lada (1996), Ingleby et al. (2015), Kraus and Hillenbrand (2009), Luhman and Rieke (1999), Najita et al. (2015), Natta et al. (2006), Simon et al. (2000), Wilking et al. (2005); [b] Andrews et al. (2011b); [c] Part III in this thesis; [d] Sallum et al. (2015).

prevent resupply of gas and small dust. At present, it is still unknown what kind of inside-out clearing mechanism can disrupt both gas and small dust of inner region.

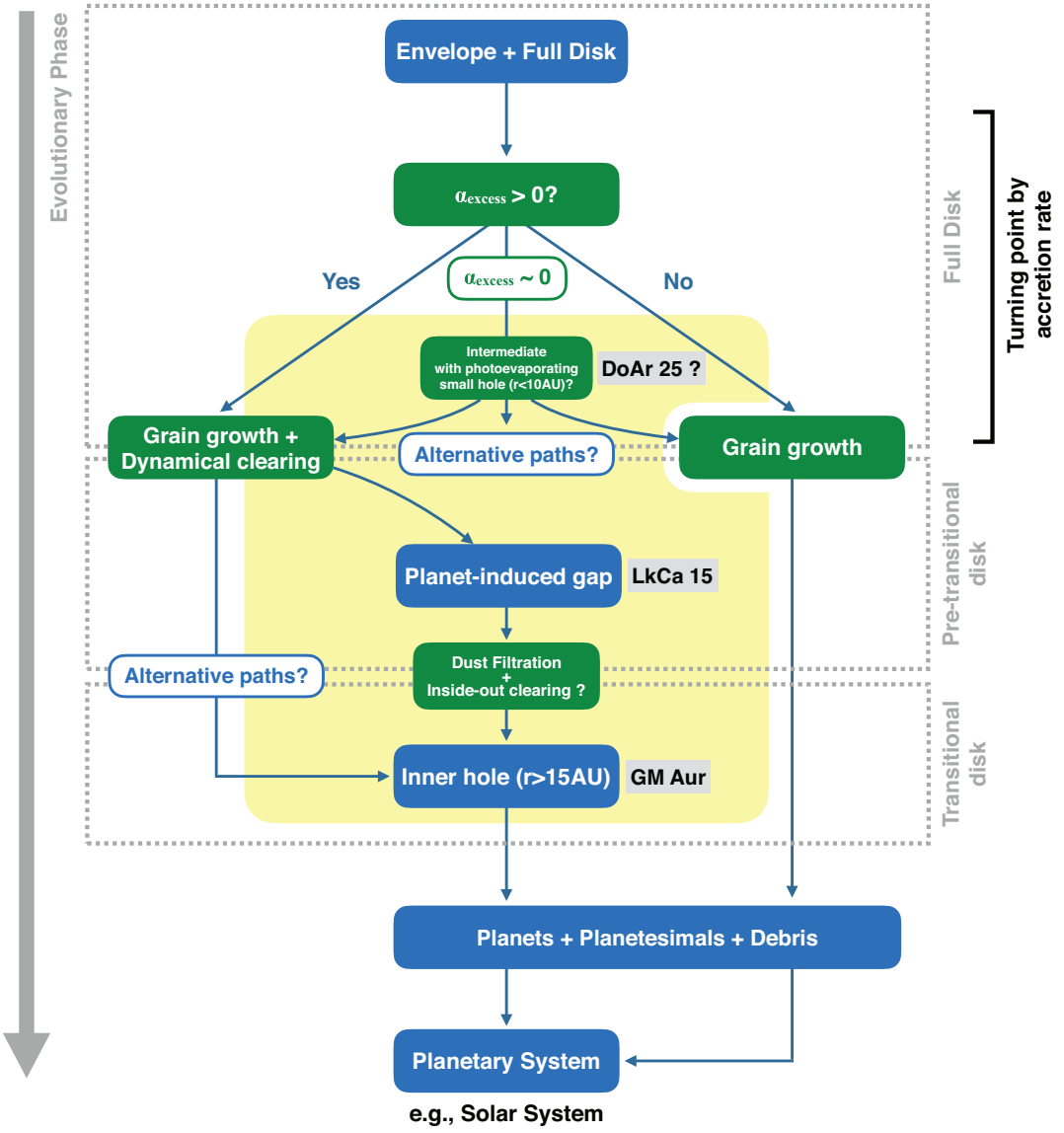

FIGURE 6.1: Morphologic evolutionary pathways of accretion disks. Blue represents disk structures, and green represents physical process in the disk. Yellow region indicates where we discussed in our studies of DoAr 25, LkCa 15, and GM Aur disks. LkCa 15 and GM Aur disks are possibly in similar pathway at different phases. Beside, DoAr 25 disk is different with other two disks, and could be in different pathway at more earlier phase. The peculiar structures in DoAr 25 disk such as disk wing and tilted secondary disk is not dominantly considered in the diagram because they have no counterparts in other observations.

6.2 Morphologic Evolutionary Pathways

It has been reported that GM Aur and LkCa 15 have similar physical parameters, such as high mass accretion rates, surface densities, and the effective temperature of the disks (Espaillat et al., 2007a, Hughes et al., 2009, Ingleby et al., 2015), and our work revealed that LKCa 15 has planet-induced large gap with warped inner disk and that GM Aur has large inner hole which is the possible result of dust filtration by planet-induced gap. Thus we can assume that GM Aur disk is in the earlier phase than LkCa 15 disk in the similar evolutionary pathway.

While the LkCa 15 and GM Aur disks can be categorized into pre-transitional disk and transitional disks, respectively, it is difficult to apply usual disk categorization to the DoAr 25 disk. It doesn't have overall infrared excess from near to far infrared wavelengths which represents full disk, and its mid-infrared deficit is not enough to make deep valley in SED which represents (pre-)transitional disk. However, it is expected that inner disk clearing and grain growth are in early/intermediate phase, on the basis of SED and radial brightness profiles. As mentioned above, massive enough planets can make clear cavity within timescale of a few orbital-period, thus it is more conceivable to assume that photoevaporating is dominant mechanism, instead of planet-disk interaction, on the possible inner clearing in Doar 25 disk. Therefore, DoAr 25 disk may be following a different evolutionary sequences from that of other young disks such as LkCa 15 and GM Aur disks. Three disks have similar massive disk ($\sim 0.2\ M_{\odot}$; Andrews and Williams, 2007a, Andrews et al., 2011b, Najita et al., 2015), hence, at present, the one of the possible physical quantities that separate point of LkCa-15-like/GM-Aur-like disk and DoAr-25-like disk is mass accretion rate. Figure 6.1 is present the morphologic evolutionary diagram as discussed at here.

6.3 Finding Evolutionary Indices

Figure 6.2 shows schematic history of three disks. Although the estimated ages of GM Aur and LkCa 15 is similar (2-3 Myr, Kraus and Ireland, 2012, Simon et al., 2000), their evolutionary phases are different; *large inner hole* for GM Aur and *planet-induced gap* for LkCa 15. Moreover, even though GM Aur disk may have had a planet-induced gap in the past, current highly flared disk (power index of $r \sim -2$, Section 5 and Table 6.1) indicates that more highly flared outer disk may have been existed with the gap.

Besides, the outer disk of LkCa 15 is almost flat with a constant opening angle (power index of $r \lesssim -3.4$, Section 4 and Table 6.1; also see Dong et al., 2012a, for review of flat and flared disks). In general, more-evolved disks have less flaring angle than less-evolved disks due to dust settling (Dullemond and Dominik, 2004). This significant flaring angle difference between GM Aur disk and LkCa 15 disk may indicate that a possible gap with flared disk of GM Aur in the previous phase should be distinguished from a gap with less-flared disk of current LkCa 15 disk. Considering estimated ages in the literature, the inner disk of GM Aur had already been cleared while that of LkCa 15 is still optically thick. Thus the different speed of evolution may be connected with flaring angles of outer disks. Or alternatively, highly flared disk with large inner hole similar to GM Aur may have different inner hole clearing mechanism other than planet-induced gap.

Interestingly, the mass accretion rate of GM Aur disk is also higher than that of LkCa 15 in an order of magnitude ($2.4\times10^{-9}M_{\odot}$ for LkCa 15, 4×10^{-9}-$1\times10^{-8}M_{\odot}$ for GM Aur; Espaillat et al., 2007a, Ingleby et al., 2015, respecively). This is not reconcile with expectation, because, typically, mass accretion rate onto the star are known to decrease as evolution progresses (Espaillat et al., 2012, Najita et al., 2007, Williams and

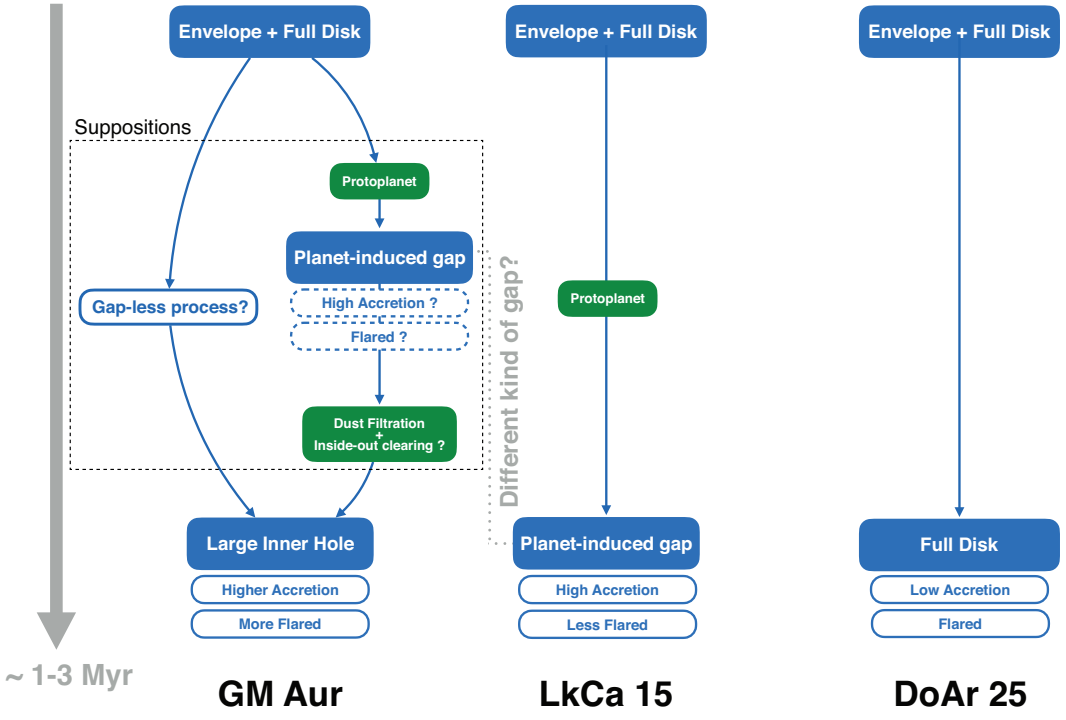

FIGURE 6.2: Schematic history of three disks. Blue represents disk structures, and green represents physical processes or factors in the disk.

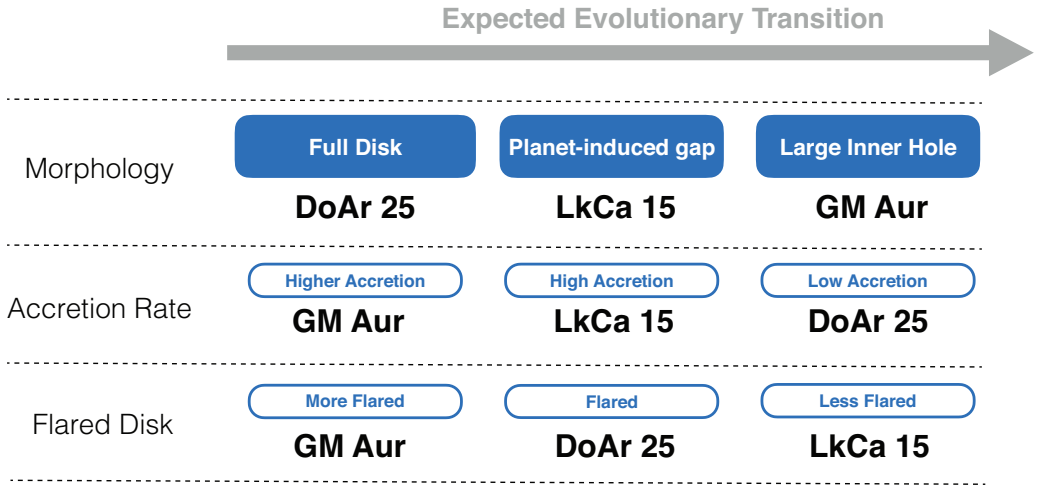

FIGURE 6.3: Expected evolutionary transitions based on different disk features. Orders of disks based on expected physical transition are not consistent with each other.

Cieza, 2011). Moreover, DoAr 25 disk has very low mass accretion rate even though it is less evolved than the others and has very young estimated age less then 1 Myr (Wilking et al., 2005). This may indicate that DoAr 25 disk has have low mass accretion rate since its initial stage. Najita et al. (2007) and Espaillat et al. (2012) assumed that more-evolved disks have less mass accretion rates than less-evolved disks if they have similar disk masses, and proposed evolutionary order as full disk—pre-transitional disk—transitional disk.

Figure 6.3 shows expected evolutionary transitions based on different disk properties; morphology (Espaillat et al., 2007a, 2010, 2012, 2014a), mass accretion rate (Espaillat et al., 2012, Najita et al., 2007), and flared disk (e.g., Dullemond and Dominik, 2004, Williams and Cieza, 2011). Although these three disks have similar disk masses, differences in physical properties does not represent evolutionary stage only. From our morphologic studies, we propose the evolutionary order of three target objects as DoAr 25 (full disk)–LkCa 15 (pre-transitional disk)–GM Aur (transitional disk). However, as mentioned above, the mass accretion rate is does not decrease in this order as expected in previous works (See $\dot{M}$ in Table 6.1); descending order of mass accretion rate is GM Aur (transitional disk)–LkCa 15 (pre-transitional disk)–DoAr 25 (full disk). Moreover, the order of power indices of radial scattered light brightness profile slopes is not reconciled with the other orders (See *Flared Disk* in Table 6.1); descending order of power index is GM Aur (transitional disk)–DoAr 25 (full disk)–LkCa 15 (pre-transitional disk).

Consequently, the evolution of protoplanetary disk—from full disk to transitional disk—may have more various pathways than current expectations, and may experience more various physical transitions. A certain physical property, such as mass accretion rate or flaring angle, may serve as a key parameter in evolutionary pathway, but they can not be a dominant index for tracing the evolutionary pathway.

The alternative suggestion is as follow: each different kind of protoplanetary disks—full disk, pre-transitional disk, and transitional disk—has a different dynamical formation history, and therefore they represent not a certain stage in a common evolutionary history, but different evolutionary histories for each of disks. In this case, large inner hole in transitional disks such as the GM Aur disk may have to be explained without dust filtration effect by planet-induced gap edge. In other words, the observed diversity of protoplanetary disks may be dominantly influenced by different clearing processes, more than evolutionary phases.

6.4 Expected Advanced Studies

Although high resolution imaging observations have revealed many various structures in transitional disks, our theoretical understanding on morphologic evolution of transitional disk is still far from perfect. To approach better understanding, both of gas and various-size dust distributions have to be resolved in same high resolution image to trace morphologic changes of protoplnaetary disks. Especially, newly discovered large μm-size dust deficit (near-infrared hole) in GM Aur disk is not completely explained by dust filtration which had been the most convincible mechanism in previous studies, and it is necessary to trace detailed gas distribution in the hole for advanced understanding. However, currently, technical gap between different wavelengths observations is still large, especially in resolution. Therefore, the future ground-based imaging observations with higher resolution, such as ALMA (the Atacama Large Millimeter Array) may lead us to promising insight, because ALMA will provide higher resolution than that of current near-infrared observations, and will resolve detailed distribution and flow of gas in the disk. Moreover, also in near-infrared observations, the next generation ExAO (the Extreme Adaptive Optics), such as SCExAO (the Subaru Coronagraphic ExAO, Jovanovic et al., 2015) will present more detailed structure of the disks.

Many disk diagnostic studies, including this work, simplify disk structures, and mainly discuss gapped, holed, or warped disks. However, there are many kind of characteristic structures like thin debris ring (e.g., Thalmann et al., 2011), asymmetric spiral arms (e.g., Muto et al., 2012), and arc structure in the cavity (Mayama et al., 2012). For advanced discussion on morphologic evolution including these structures, detailed structural categorization must be conducted in the first place. However, at present, most of high resolution direct imaging of circumstellar disks is obtained from the project SEEDS dominantly, and current resolved disk catalogue is not big enough to statistically discuss all complex disk structures. More additional disk observations are required in the future.

Part III

Non-disk-origin Planetary-Mass Companions on Wide Orbit

Chapter 7

Planetary-Mass Companions on Wide Orbit Around Disk-host Star

Abstract

We report the discovery of a planetary-mass companion with a wide separation of $\sim 11.6''$ ($\sim$1430 AU at 123 pc distance) from its primary, young T Tauri star DoAr 25. We initially detected two companion candidates from multi-epoch imaging observations using three different instruments (IRCS and HiCIAO on Subaru Telescope, and NICMOS2 on Hubble Space Telescope), then we ruled out one of companion candidates by using multiple companionship verifications; common proper motions, photometric model comparisons, and statistical probabilities. The confirmed companion has registered in VizieR database as BKLT J162623-244308, but has not been discussed for its properties yet. Follow-up IRCS near-infrared spectroscopy observation on the companion shows peculiar continuum, which may be indicative of an edge-on disk associated with the companion. We also constrained the upper mass limit of a possible darker unseen planet by conducting high contrast imaging reduction techniques, such as ADI and LOCI. DoAr 25 has a young cavity-less protoplanetary disk, and thus it is clear that this wide-orbit planetary mass companion is not originated from the protoplanetary disk associated with DoAr 25. Its formation process is may

be different with typical planets originated from a protoplanetary disk, even though it has similar masses of massive planets.

7.1 Introduction

7.1.1 Background

Over the past two decades, nearly two thousands of extrasolar planets have been discovered. About five dozens of those objects were detected through the direct imaging method, about a dozen of them has very wide orbital separations over 100 AU[1]. Recent discoveries of wide orbit planetary-mass companions (PMCs, e.g., GU Psc b, HD106906 b, SR 12 C, FW Tau b; Bailey et al., 2014, Kraus et al., 2014, Kuzuhara et al., 2011, Naud et al., 2014, respectively.) around young stars are a significant challenge to conventional planet formation models.

The conventional models for planet formation are *the core-accretion model* (e.g., Ida and Lin, 2004a, Kokubo and Ida, 2002) and *the disk gravitational instability model* (e.g., Boss, 1997, Cameron, 1978). However, the core accretion model requires a very steep increase in the planet formation timescale with increasing distance from the host star; even Neptune, separated ∼30 AU from the sun, is regarded as a difficult planet to form in the age of the solar system (Pollack et al., 1996). In the gravitational instability model, the disk needs massive surface density to be Toomre unstable at the planet forming location (Safronov, 1960, Toomre, 1964), but the disks around young Class II stars (Andrews and Williams, 2005, 2007b, Andrews et al., 2009) have not enough surface density to be Toomre unstable at a large separation beyond 100 AU (e.g., Dodson-Robinson et al., 2009, Meru and Bate, 2010).

The origin of wide orbit PMCs is still not well understood, although several formation scenarios have been proposed so far. The first plausible scenario is that wide orbit PMCs initially formed in a protoplanetary disk, then ejected to outer orbit due to a dynamical interaction with other massive companions such as binary stars (e.g., Reipurth and Clarke, 2001). However most of wide orbit PMCs are orbiting around single stars and do not have any other reported nearby massive objects. Thereby, the ejection scenario would be ruled out. The second one is that wide orbit PMCs and their primary stars were both formed via molecular cloud core fragmentation (e.g., Bate, 2009, Bate et al.,

[1]The Extrasolar Planets Encyclopedia:http://exoplanet.eu/ ;Schneider et al. (2011)

2003). In this scenario, wide orbit PMCs are formed as the case of the extreme mass-ratio between a primary star and a secondary, or moreover. However, the obvious observational evidence of this scenario has not been reported yet. This non-disk-origin scenario may expand the spatial scale of protoplanetary system into a thousand au, beyond the typical protoplanetary disk.

7.1.2 Wide orbit PMCs around disk-host stars: DoAr 25, LkCa 15, and GM Aur

T Tauri stars have very young ages, typically less than 10 Myr, thus even planetary-mass companions could be bright enough to be detected by sky surveys. From the infrared sky surveys (UKIDSS, 2MASS, and WISE; Lawrence et al., 2007, Skrutskie et al., 2006, Wright et al., 2010, respectively), we searched the nearest possible stellar objects in the separation of 15″, and it was found that only DoAr 25 has on dark object at $\sim$ 10″ separation. There has been no published detailed studies on this object, thus in this part, the companionship and the physical properties of companion candidate will be discussed.

7.1.3 In This Work

In this work, we had conducted multiple observations on around DoAr 25 using 8.2m Subaru Telescope and appropriate instruments on each target. We present the results of the direct imaging of two wide orbit PMC candidates around the T Tauri star DoAr 25 (K5V, 0.64 $M_{\odot}$, $\sim$0.93 Myr-old, Wilking et al., 2005), in L1688 cloud of the ρ Ophiuchi star-forming region(ρ Oph). One of the companion candidates is in fact confirmed as a planetary-mass companion associated with DoAr 25, while the other is considered as a background object in L1688 cloud (hereafter, the former is DoAr 25 b and the latter is DoAr 25 PC. PC stands for pseudo-companion). We also report the result of the high-contrast imaging survey around DoAr 25. We effectively removed the effect of stellar halo, and revealed closer region from DoAr 25 where ordinary imaging observations are not available. Finally, we discuss the origin of wide orbit PMCs around young stars while referring to the study of DoAr 25 disk from Chapter 3

TABLE 7.1: Observations Summary of DoAr 25

Date	Instrument	Mode	Band	Exposure Time	Field of View	Pixel Scale (mas/pixel)
2005 May 8	HST/NICMOS2	Imaging	H	6s×54	19.2″×19.2″	x:75.948±0.047 y:75.355±0.026
2009 Oct 12	Subaru/IRCS	Imaging	K	15s×17	21″×21″	20.0
2012 May 16	Subaru/HiCIAO	qPDI[a]	H	20s×100	5″×5″	9.5
2013 May 11	Subaru/IRCS	Imaging	J&K	6s×54	21″×21″	20.6
2014 May 16	Subaru/HiCIAO	DI[b]	H	10s×15	20″×20″	9.5
2014 Jun 21	Subaru/HiCIAO	Spectroscopy	J&H	240s×8	.	.

[a] Quad-Polarized Differential Imaging for disk detection.
[b] Direct Imaging for companion detection.

7.2 Observation and Data Reduction

7.2.1 Near-Infrared Imaging

We observed DoAr 25 b and DoAr 25 PC, with the Infrared Camera and Spectrograph (IRCS; Kobayashi et al., 2000, Tokunaga et al., 1998), and the high-contrast imaging instrument HiCIAO (Tamura et al., 2006) mounted on the 8.2 m Subaru Telescope with the adaptive optics system AO188 (Hayano et al., 2008, 2010). The first observations were operated with IRCS on 2009 October 12 in K band, and the exposure time was 15s $\times$ 7. The second observations were carried out also with IRCS on 2013 May 11 in J and K band with 6 s $\times$ 54 exposures. The third observations carried out with HiCIAO on 2014 Jun 7 in H-band with 10s $\times$ 15 exposures in DI (Direct Imaging) Mode. FS140 (Hawarden et al., 2001) was observed in each band as the photometric standard star during the same nights. IRCS data were reduced in standard procedures with the Imaging Reduction and Analysis Facility (IRAF). The Hubble Space Telescope (HST) archive data were also obtained. DoAr 25 b and DoAr 25 PC were imaged by the NICMOS Camera 2 with F160W filter in 2005 May 8, but they have not been discussed as substellars object yet. To obtain infrared CIT system magnitude, we used a bandpass averaged flux density for the F160W filter using a model reference spectra of Vega (Bohlin, 2007) from the photometric keyword tables in NICMOS Data Handbook, Version 8.0.

The distortions of IRCS and HiCIAO installed on the Subaru Telescope are very small and stable, but the change of the internal environments such as a replacement of cold or mirrors could affect the the optical alignment between AO188 and instruments. For precise astrometry, we corrected distortions on each imaging datum. To make distortion maps for IRCS and HiCIAO data, we additionally observed the globular cluster M15, and compared the astrometric results to distortion-corrected images taken from the HST with the Advanced Camera for Surveys (ACS). The pixel scales are changed after distortion corrections. The calibrated pixel scales are 20.0, 20.6, and 9.5 mas/pixel for the first, second IRCS observations, and HiCIAO observation, respectively. All measurements were operated on sky-subtracted, flat-normalized and uncombined images separately, then averaged. The geometric distortions of the NICMOS data were corrected with the NICMOS geometric distortion coefficients and equations described in the NICMOS Data Handbook, and calibrated science frames were used.

7.2.2 *JH*-band Spectroscopy

J and *H*-band spectra of DoAr 25 b were obtained on 2014 June 21 with 240s × 8 exposures. The spectroscopic observations were taken in ABBA sequence, where A and B stand for the first and second positions on the slit. The slit width was 0.15″, and the resolutions were about 955λ at *J*-band and 764λ at *H*-band. The spectra were extracted by using APALL task in IRAF, and reduced in standard procedures. Cosmic rays in raw data were removed by using IRAF task L.A.Cosmic which was created by van Dokkum (2001). Wavelength calibrations were carried out by Argon emission lines. The effect of the telluric absorption was removed by dividing by the spectra of nearby G9 star FS140, and multiplying by a blackbody spectrum of the effective temperature of G9 star. The intrinsic absorption lines from G9 star were removed manually beforehand by using SPLOT task in IRAF.

7.2.3 High contrast *H*-band imaging Reduction

The qPDI (Quad-polarized differential imaging) with Angular Differential Imaging (ADI, see Section 7.2.3.1) observations of DoAr 25 were done in the *H*-band on 2012 May 16 with HiCIAO on the Subaru Telescope combined with AO188.

In qPDI+ADI mode, we used a double Wollaston prism to split incident light into four images, two o- and e-rays sets, to reduce the saturated radius. Each of split images has a 5″×5″ field of view with a pixel scale of 9.5 mas/pixel. The half-waveplate was rotated to four different angular positions for the polarization measurements. We obtained 100 data sets with 20 s exposure per half-waveplate position each cycle. The total integration time of the polarization intensity image was 2000 s. Although this polarimetric observation is basically purposed to detect polarized scattered light from the disk associated with DoAr 25 (See Chapter 3), we converted polarization images into non-polarization images by combining different polarization angle images, and reduced as ordinary ADI data.

We used LOCI (Locally Optimized Combination of Images, see Section 7.2.3.2) method for data reduction to obtain high contrast and to suppress stellar halo and speckle noise. Each of initial images are divided into concentric ring subsection, then the optimized background reference is calculated for each subsection separately based on the counterpart subsection of the other images. The individual reference image is

constructed from these locally optimized data for each individual initial image. By subtracting the series of locally optimized reference images from the series of initial images, instead of subtracting single median reference image from that, the the final combined image obtains better contrast and higher signal-to-noise ratio than the result of classical ADI data reduction described in Marois et al. (2006).

7.2.3.1 Angular Differential Imaging

For most large telescopes using azimuthal mount, the top of pupil always remains toward zenith due to its platform construction. Thus, in the conventional observations, the field orientation on the camera is fixed to be kept constant by camera rotation. However, in Angular Differential Imaging (ADI; Marois et al., 2006) observations, the pupil orientation is kept constant instead by turning off camera rotator or by additional rotation, thus the field will rotate around the image center where the target star is located.

Figure 7.1 illustrates how the images taken in ADI are then processed. In the series of initial images (A_i), although the stellar halo and speckle noise appear almost consistently throughout the series of images, the separated faint point source P moves around the central star. Thus, the median combined image (B) contains only the stellar halo and speckle noise, and no significant signal of moving point source. Then image B is subtracted from each initial image, leaving a series of halo-speckle subtracted images (C_i) containing only the point source P and some time-variable noise. The C_i images are then derotated into the coordinate system of the sky field (D_i) and median-combined into the final image (E) which will contain more significant point source signal and less background noise.

7.2.3.2 Locally Optimized Combination of Images

The above reduction method, hereafter classic ADI, is the simplest way to handling ADI data, and the time-variable noise that changes shot-by-shot is not completely removed. The fundamental idea of Locally Optimized Combination of Images (LOCI; Lafrenière et al., 2007) resembles that of classic ADI method, but is more advanced and sophisticated method to perform the angular differential data reduction. In LOCI methods, each of initial images are divided into concentric ring subsection (See Figure 7.2), then the optimized background reference is calculated for each subsection separately based

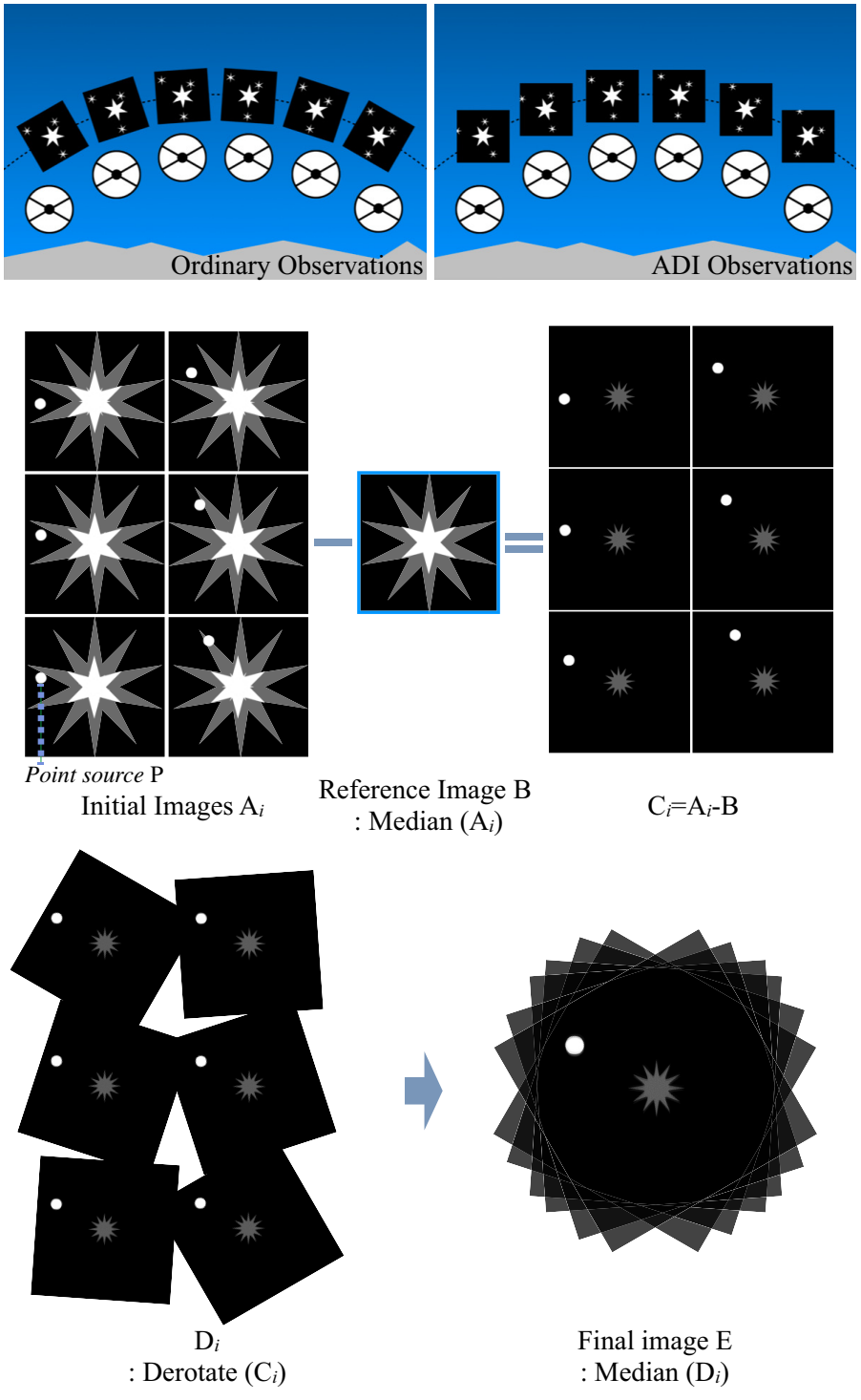

FIGURE 7.1: Schematic of ADI data reduction procedure. Top figures are showing difference between ordinary observation and ADI observations. Middle and bottom figures are showing schematic of ADI data reduction procedure

on the counterpart subsection of the other images. The individual reference image is constructed from these locally optimized data for each individual initial image.

By subtracting the series of locally optimized reference images from the series of initial images, instead of subtracting single median reference image from that, the the final combined image obtain better contrast and higher signal-to-noise ratio than the result of classic ADI method.

7.3 Results and Discussion

The resultant images of companion candidates are shown in Figure 7.3.

7.3.1 Common Proper Motion

To distinguish DoAr 25 b and DoAr 25 PC from background objects on similar line-of-sight, we investigated the separations from DoAr 25 A with four-epoch astrometry. Young stellar objects(YSOs) in a star-forming region have large proper motions, thus if a nearby object is a background object, it would have a negligible proper motion and changes in separation due to the large proper motion of DoAr25. There are three individual measurements of the proper motion of DoAr25 (Ducourant et al., 2005, Roeser et al.,

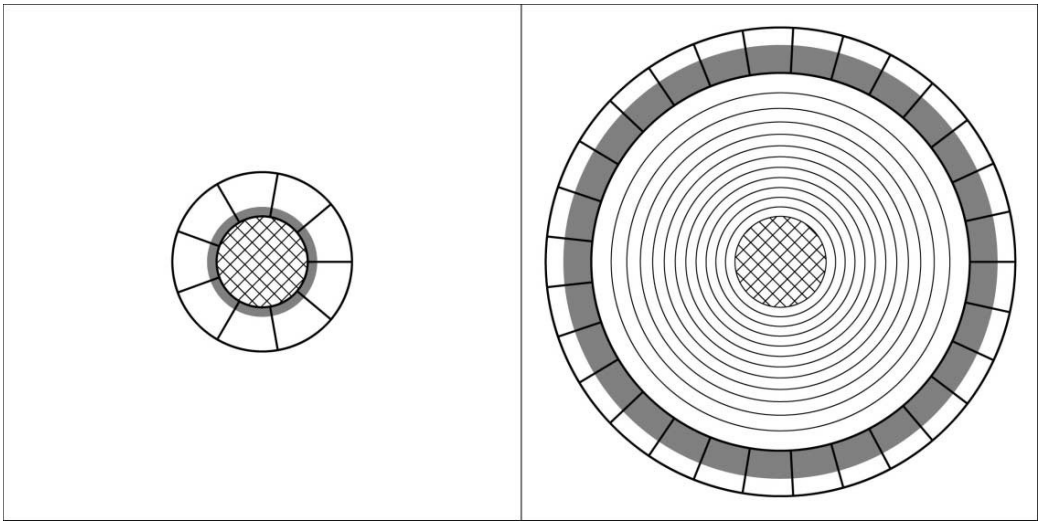

FIGURE 7.2: Example of concentric ring division (the 1st and 13th subtraction annuli, respectively) in LOCI method. Subtraction subsection is shaded in gray, and optimization subsection is delimited by thick lines. The cross-hatched region in central circle represents the saturated region. (Figure adapted from Lafrenière et al., 2007).

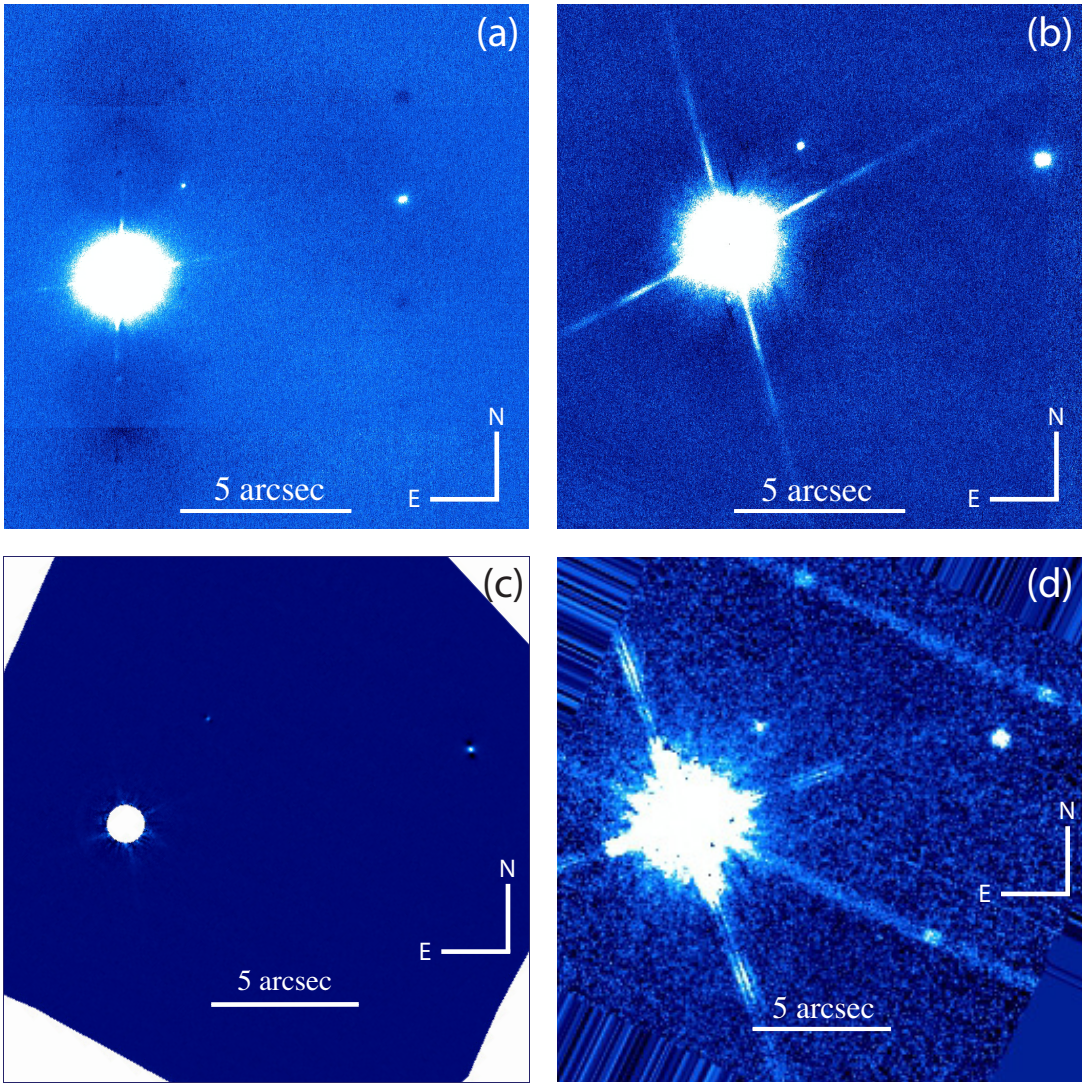

FIGURE 7.3: NIR imaging results of DoAr25. (*a*): *J*-band image by Subaru/IRCS. (*b*): *K*-band image by Subaru/IRCS. (*c*): *H*-band image by Subaru/HiCIAO in DI mode. (*d*): *H*-band image by HST/NICMOS2.

2010, Zacharias et al., 2013, see Table 7.2). At first, we adopted all three measurements, then compared the results.

Figure 7.4 shows the measured separations of DoAR 25 b and PC from DoAR 25 at each epoch, with three expected background trajectories based on Table 7.2. DoAR 25 b is keeping the almost same location in 9 years, we can easily confirmed that they have common proper motion. On the other hand, DoAr 25 PC shows unexpected movement. Interestingly, it dose not even follow any of three expected background trajectories. To verify the association of DoAr 25 PC, we considered the third case; an isolated member in ρ Oph. Combining the average proper motion of ρ Oph members (-5.53 $\pm$ 0.89 mas/yr

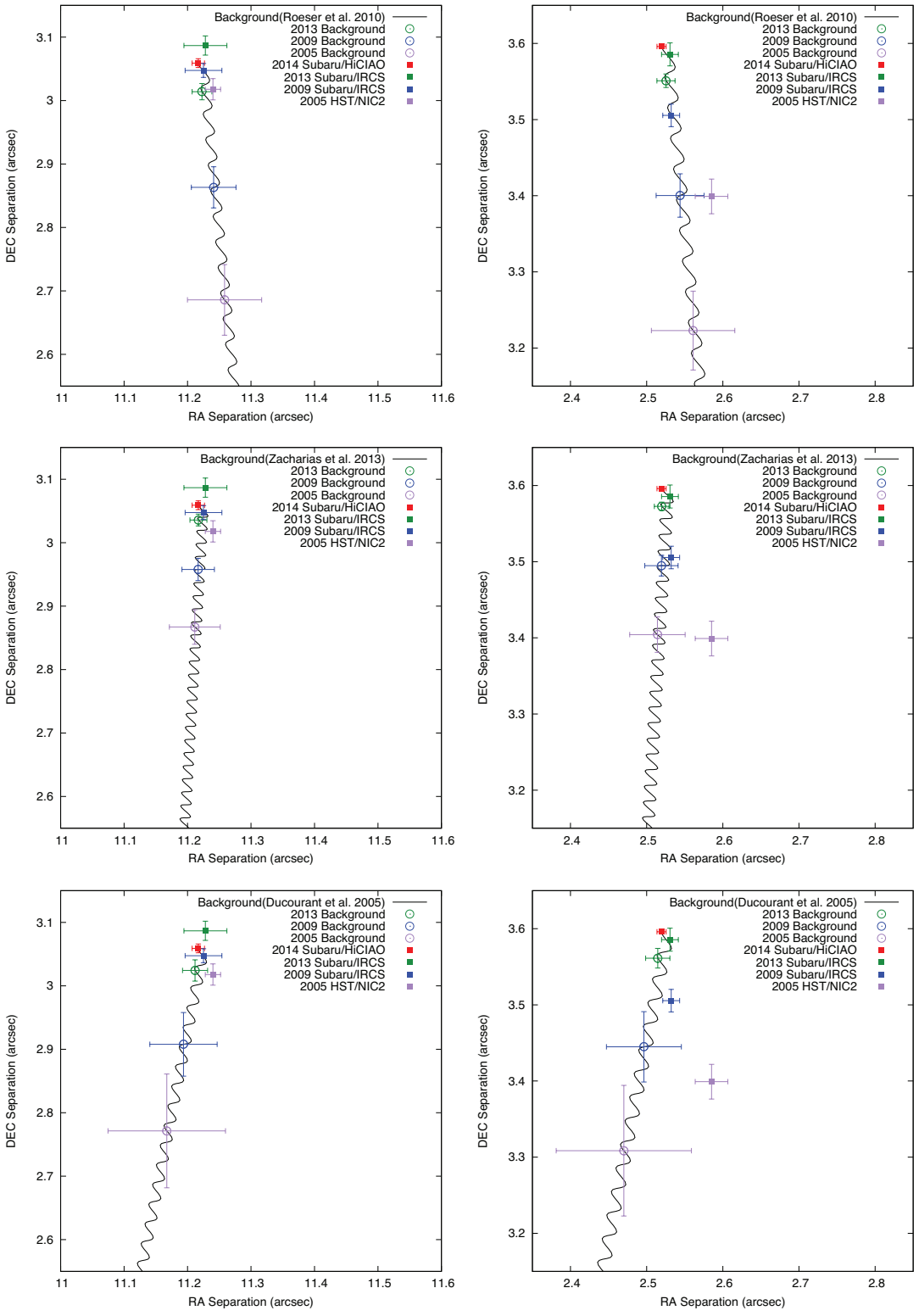

FIGURE 7.4: The relative astrometry of the DoAr 25 b (*left*) and PC (*right*) to DoAr 25. DoAr 25 b stays at almost same place in 9 years, and thus it shares the same proper motion of DoAr 25. DoAr 25 PC shows unexpected movement, and thus it is necessary to consider it is not associated with DoAr 25 (See Section 7.3.1).

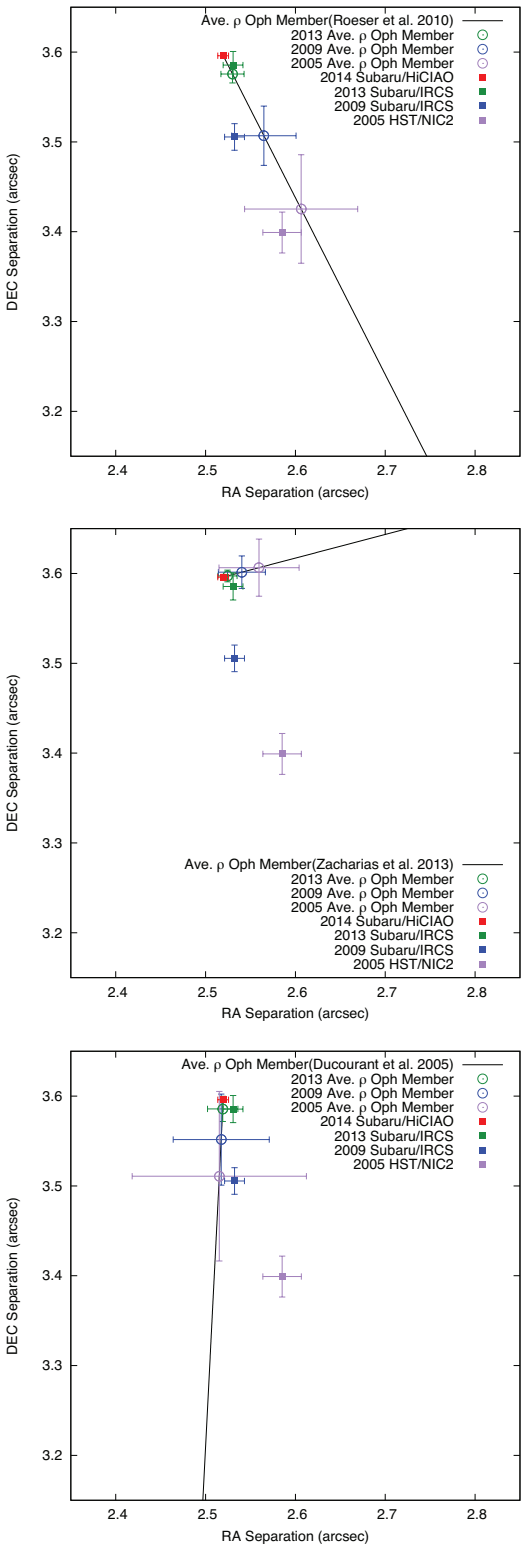

FIGURE 7.5: The relative astrometry of the DoAr 25 PC to the average motion of ρ Oph members. (See Section 7.3.1)

in RA, -21.74 ± 0.93 mas/yr in DEC; van Leeuwen, 2007) with the proper motions of DoAr 25, we estimated the trajectories of the average movement of ρ Oph member relative to DoAr 25 (Figure 7.5). When PPMXL (Roeser et al., 2010) is adopted as the proper motion of DoAr25, DoAr 25 PC falls in to the trajectory of average movement of ρ Oph member with good agreement at all four epochs (*Top* of Figure 7.5). Beside, other trajectories are not match at all, both of speed and direction. If we adopt PPMXL as the proper motion of DoAr 25, the movement of DoAr 25 PC is explained as individual low-mass object in ρ Oph region with less contradictions. However, consequently, the association of DoAr 25 PC is not clearly decidable at here.

7.3.2 Photometry

Table 7.3 shows the summary of photometry of DoAr 25 b and DoAr 25 PC. The estimated spectral types based on the evolutionary model (See below) are also shown in the same table. We adopted the stellar extinction value of DoAr 25 (A_V=2.9 mag, Wilking et al., 2005) for calculating the dereddened luminosities of DoAR 25 b and PC. The full extinction value of L1688 cloud on this line-of-sight is A_V = 8.1 mag (COMPLETEteam, 2012), the low stellar extinction indicates that DoAR 25 is lies at the surface of the cloud (Wilking et al., 2005). A_V = 0 and 8.1 are also used for comparison.

Mass Estimation

TABLE 7.2: The proper motions of DoAr 25 from individual catalogues.

	Roeser et al. (2010) (PPMXL)	Zacharias et al. (2013) (UCAC3)	Ducourant et al. (2005)
RA	3.9 ± 5.3mas/yr	-1.2 ± 3.3 mas/yr	-6 ± 9 mas/yr
DEC	-40.3 ± 5.3 mas/yr	-20.6 ± 2.2 mas/yr	-31 ± 9 mas/yr

TABLE 7.3: Photometry Results of DoAr 25 b and PC.

Object	$J_{\rm mag}$	$H_{\rm mag}$[a]	$K_{\rm mag}$	$J_{\rm SpT}$	$H_{\rm SpT}$	$K_{\rm SpT}$
DoAr25 b	16.8 ± 0.5	15.7 ± 0.1	14.7 ± 0.2	L3±1	L3±1	L2±1
DoAr25 PC	18.3 ± 0.9	17.0 ± 0.9	16.1 ± 0.3	L5±2	L5±2	L5±2

[a] F150W magnitude was converted to CIT system *H*-band magnitude.

We have estimated the masses of DoAR 25 b and PC by using two evolutionary models for brown dwarfs, DUSTY model (dusty atmosphere; Chabrier et al., 2000) and COND model (dust-free atmosphere; Baraffe et al., 2003). DUSTY model takes into account the effects of scattering and absorption occurring by dust in atmosphere. On the other hand, COND model neglects dust opacity since all grains are gravitationally settled down bellow the photosphere with a very-low effective temperature $T_{\rm eff} < 1300$ K, such as T-dwarfs (e.g., Baraffe et al., 2003). The both models estimate the effective temperatures higher than 1300K for DoAR 25 b and PC, thus we adopted DUSTY model for our final decisions. The distance to the L1688 cloud has a range of estimates, but is most likely between 120 pc and 145 pc (Wilking et al., 2008). As mentioned above, DoAr 25 lies on the surface of the cloud, we adopted 123 $\pm$ 11 pc (The average of three recent measurements; 131 $\pm$ 3 pc, 119 $\pm$ 6 pc, and $120^{+4.5}_{-4.2}$ pc; respectively Loinard et al., 2008, Lombardi et al., 2008, Mamajek, 2008) as the distance to DoAr25. Only 1-10 Myr assumption we can obtain consistent mass estimates for observed *JHK* luminosities. Besides, for 100 Myr - 1 Gyr, we cannot obtain consistent results from *JHK* luminosities. This supports a similar youth with central star DoAr 25 (1 Myr). Consequently, from DUSTY model, we obtained 13^{+2}_{-8} $M_{\rm Jup}$ for DoAr 25 b with the age of 1-10 Myr (See below). The properties of DoAR 25 PC strongly depend on its age (1-100 Myr) and stellar extinction; 12$\sim$39 $M_{\rm Jup}$ with A_V=2.9 mag, 15-100 $M_{\rm Jup}$ with A_V=8.1 mag.

Luminosity-Age Diagram

DoAr 25 is a very young stellar object, and thus it is reasonable to assume that its companion would share a similar age with the primary star. We estimated the ages of DoAR 25 b and PC on the basis of DUSTY model. Figure 7.6, a luminosity-age diagram, shows evolutionary tracks with *JHK* photometries in absolute magnitudes. If the age and the distance are convincible, the estimated masses from the absolute luminosity on each photometric band should be consistent with each other. Both of DoAR 25 b and PC shows good agreements in younger evolutionary tracks. Considering large model uncertainties in young age, we adopted 1-10 Myr and 1-100 Myr as the ages of DoAR 25 b and PC, respectively.

(H-K_s)-(J-H) and (J-K)-J Diagrams

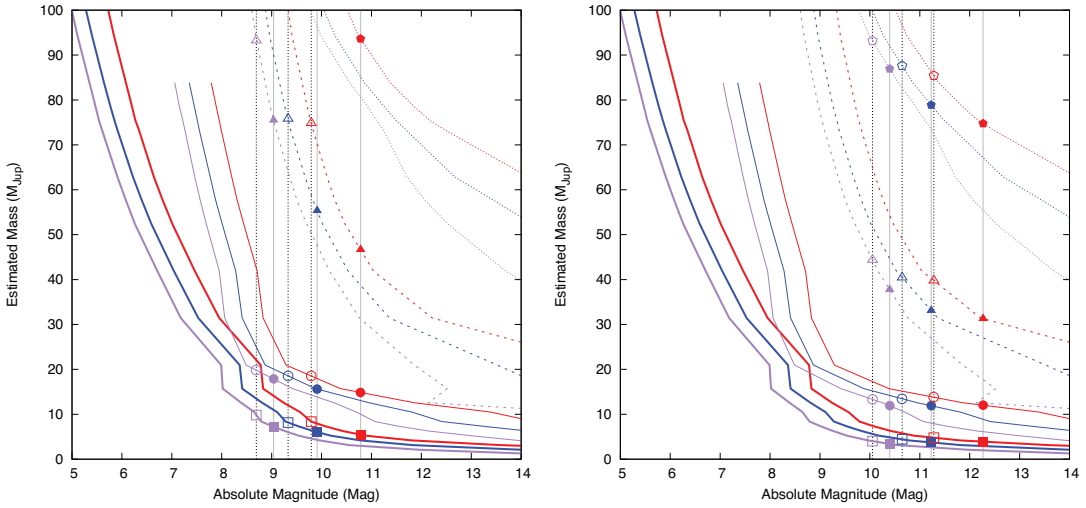

FIGURE 7.6: The luminosity-age diagrams of DoAr 25 b (*right*) and PC (*left*) based on the evolutionary model. *red* : *J*-band, *blue* : *H*-band, *purple* : *K*-band. *bold solid line* : 1 Myr, *solid line* : 10 Myr, *broken line* : 100 Myr, *dotted line* : 1 Gyr. *filled* : dereddened with $A_V = 2.9$, *opened* : dereddened with $A_V = 8.1$.

Figure 7.7 shows the color-color and color-magnitude diagrams. For context, DUSTY and COND evolutionary tracks and reference populations of dereddened young brown dwarfs [2] [3] and FW Tau b (will be discussed in Section 7.3.4) are also plotted.

On (*H*-K_s)-(*J*-*H*) diagram, DoAR 25 b falls in younger(< 1 Myr) and later sequence than late-M type dwarfs of ρ Oph (blue pentagon), and roughly lies on the line of very young dwarfs ($\lesssim$1 Myr). Especially, similar peculiar object FW Tau b (open green circle) is close to DoAr 25 b with the extinction correction of $A_V = 2.9$ mag. On the other hand, DoAR 25 PC lies on the 1 Myr DUSTY track. On the (*J*-*K*)-*J* diagram, DoAr 25 b shows similar trend, younger, late, and close to FW Tau b at $A_V = 2.9$ mag. Besides, DoAr 25 PC lies on the 10 Myr DUSTY track.

7.3.3 Statistical Probabilities

Since many objects in star-forming regions share their proper motions, the co-moving confirmation may be not enough to conclude that DA25 b is a gravitationally bounded companion to DoAR 25 on the basis of co-moving only. Therefore, we carried out additional confirmation to rule out chance of coincidence.

[2] Late-M and early-L dwarfs from ρ Oph (de Oliveira et al., 2012), late-M dwarfs from USco (Lodieu et al., 2008), early-L dwarfs from ONC (Weights et al., 2009), and field dwarfs (McLean et al., 2003), and references therein.

[3] de Oliveira et al. (2012) photometries are *K*s-band, which is typically ∼0.1 mag less bright than *K*-band for low-mass objects

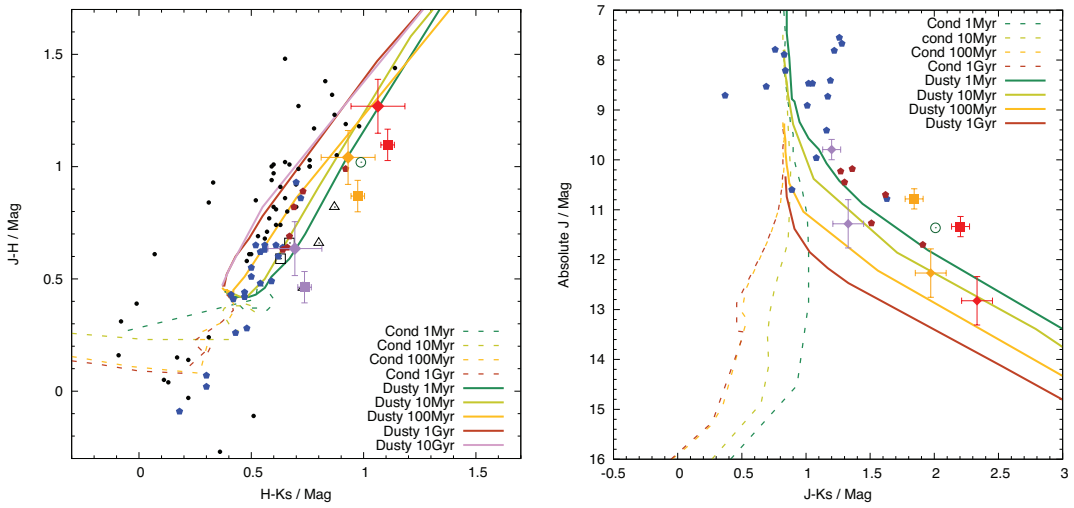

FIGURE 7.7: (H-K_s)-(J-H) and (J-K)-J diagrams. *filled square* : DoAr 25 b, *filled rhombus* : DoAr 25 PC, *red points* : reddened, *yellow points* : dereddened with $A_V = 2.9$, *purple points* : dereddened with $A_V = 8.1$, *open circle* : FW Tau b, *open triangles* : <1Myr-old L-dwarfs in ONC, *open squares* : ∼5Myr-old M-dwarfs in USCO, *blue filled pentagons* : young M-dwarfs in ρ Oph, *brown filled pentagons* : young L-dwarfs in ρ Oph, *black circles* : field dwarfs.

Using following procedure (based on description in Kuzuhara et al., 2011), we computed the probability that isolated late-type dwarfs fall in a field-of-view of our observations. The ratio $R = N(0.02 \lesssim M/M_\odot \lesssim 0.08)/N(0.08 < M/M_\odot \lesssim 10)$, meaning the relative numbers of late-type dwarfs (later than M6) to normal YSOs in ρ Oph, was estimated to be $0.20^{+0.04}_{-0.03}$ (de Oliveira et al., 2012), which agrees with general Rs of other star-forming regions, Taurus(0.18 ± 0.04), IC348(0.12 ± 0.12) and Trapezium(0.26 ± 0.04) derived by (Luhman et al., 2007). The number of ordinary YSOs in L1688 was estimated to be 12 Class Is, 33 flat types, 100 class IIs, and 2 class IIIs by the Spitzer C2D survey results (Evans et al., 2003, Padgett et al., 2008). Since the Spitzer is insensitive to Class III objects, we adopted the abundance ratio of Class III/Class II ~ 0.91 based on X-ray survey combined with IR study of ρ Oph (Grosso et al., 2000). Thus, we can estimate the number of late-type YSOs to be 44 in L1688 region ($3600'' \times 4597.5''$), and the probability that late-type dwarfs fall in a IRCS field of view around DoAR 25 ($21'' \times 21''$) by chance is less than 0.13%. Our observations detected two late-type dwarfs, and the probability that both of them are chance alignment is even lower, $\sim 1.4 \times 10^{-4}$%. The next closest confirmed ρ Oph member to DoAR 25 is GY92 3 (M8; Alves de Oliveira and Casali, 2008) 89 arcsec away from DoAR 25, and the above probability in this area is ~ 9.3%, which is close to general Rs in star-forming region.

Therefore, comprehensively, we concluded that DoAr 25 b is a physically associated companion to its primary star DoAr25. The true character of DoAr 25 PC is still in debate, but it is clear that DoAr 25 PC is associated with DoAr 25, thus it is out of the scope of this study.

7.3.4 Spectral Type of DoAr 25 b

From follow-up spectroscopic observations, we have found that DoAr 25 has weird spectral continuum. Figures 7.8 and 7.9 show comparisons of DoAr 25 b's spectra and other known late-type dwarfs' spectra. The *J*-band continuum is close to that of late-M dwarfs, while *H*-band continuum is mostly weaken and no significant features expected from a late-M or later dwarf. Although the smooth decreasing at *H*-band resembles that of early-M, the luminosity of DoAr 25 b is too faint as that earlier type at this distance (∼123 pc). This *J*-*H* spectral continuum of DoAr 25 b is somewhat irregular, it is difficult to figure out the spectral type by typical comparative method. To ensure this results, we verified our data procedure by applying the same procedure to the data of the well-known late-type object KPNO-Tau 4 observed by same telescope and instrument. As a result, we obtained a clear triangle shape in *H*-band continuum as expected from a young M9 dwarf, hence, we concluded that the peculiar spectra of DoAr 25 b is an intrinsic feature of the object, or at least, of the circumstellar environment.

Current feasible explanations for peculiar spectra are a brown dwarf or massive planet with an edge-on disk, or with infrared veiling effect from a warm inner disk (e.g., FW Tau b in Bowler et al., 2014, Kraus et al., 2014, 2015). An edge-on disk can cause the strong extinction that make stellar luminosity decrease noticeably, and can make the color of objects become redder than that of ordinary objects due to the additional emission from the disk at longer wavelengths. Infrared veiling around young Class I object makes the absorption weaker than expectation due to the stellar continuum is superimposed by the components of warm-inner-disk continuum (Basri and Batalha, 1990, Batalha and Basri, 1993, Hartigan et al., 1990). If the disk behaves like a blackbody of $T_{\rm eff} \lesssim 1000$ K (e.g., Liu et al., 2003, Shu et al., 1994), the disk emission superimposing the stellar emission would have the peak around *K*-band, and would have relatively weak emission at *J*-band. Thus, we first conducted reduced χ^2 fitting between dereddened *J*-band spectra of DoAR 25 b, late-M YSOs in ρ Ophiuchi (from Muzic et al., 2012) and field M dwarfs (from The IRTF Spectral Library) with the range of extinction level $A_{\rm V}$=0-12

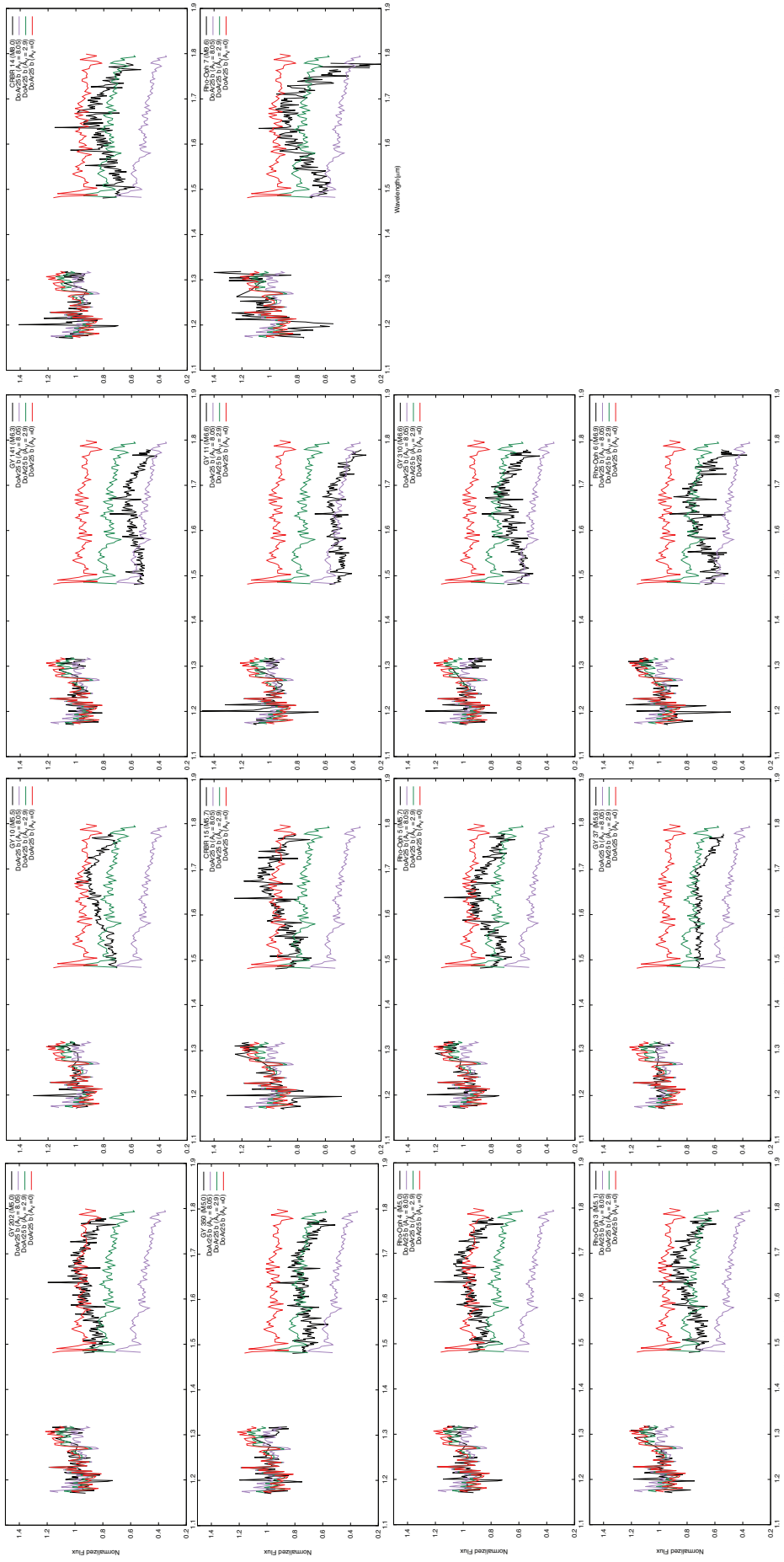

FIGURE 7.8: The spectra comparisons with young late-type objects from Muzic et al. (2012). *Black lines* represent the spectra of young late-type objects. *Red, green, and purple lines* represents the spectra of DoAr 25 b with different extinction level. *Red*: no extinction correction, A_v=0; *green*: measured extinction level of DoAr 25 b, A_v=2.9; *purple*: maximum extinction level of the same region, A_v=8.05.

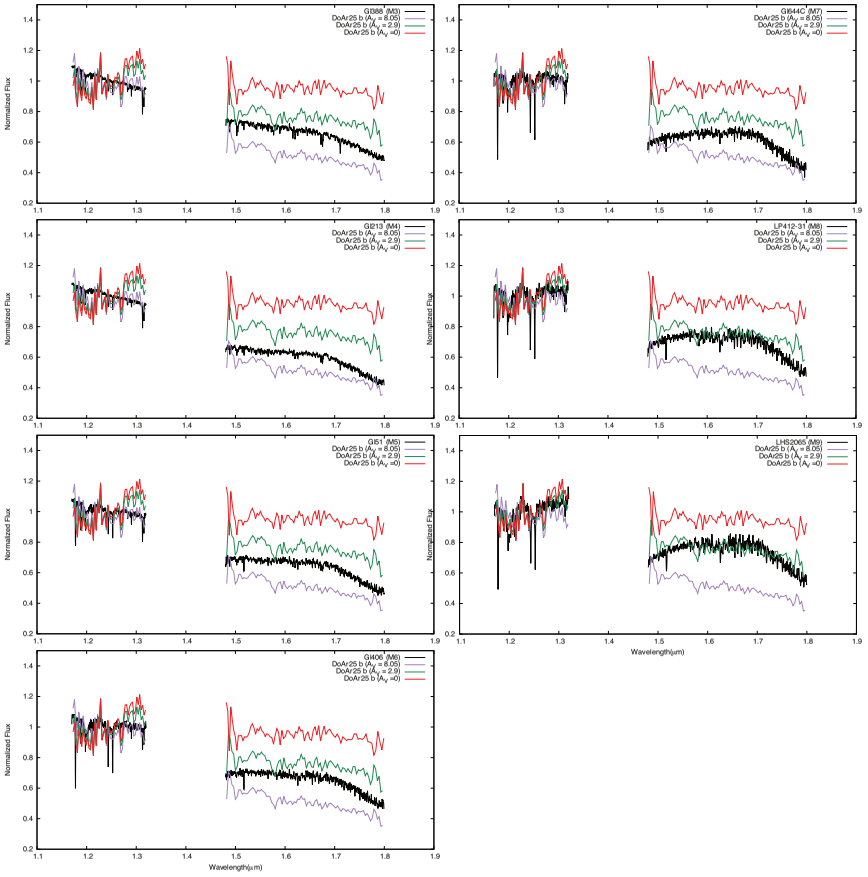

FIGURE 7.9: The spectra comparisons with field late-type objects from The IRTF Spectral Library. *Black lines* represent the spectra of field late-type objects. *Red, green, and purple lines* represents the spectra of DoAr 25 b with different extinction level. *Red*: no extinction correction, A_V=0; *green*: measured extinction level of DoAr 25 b, A_V=2.9; *purple*: maximum extinction level of the same region, A_V=8.05.

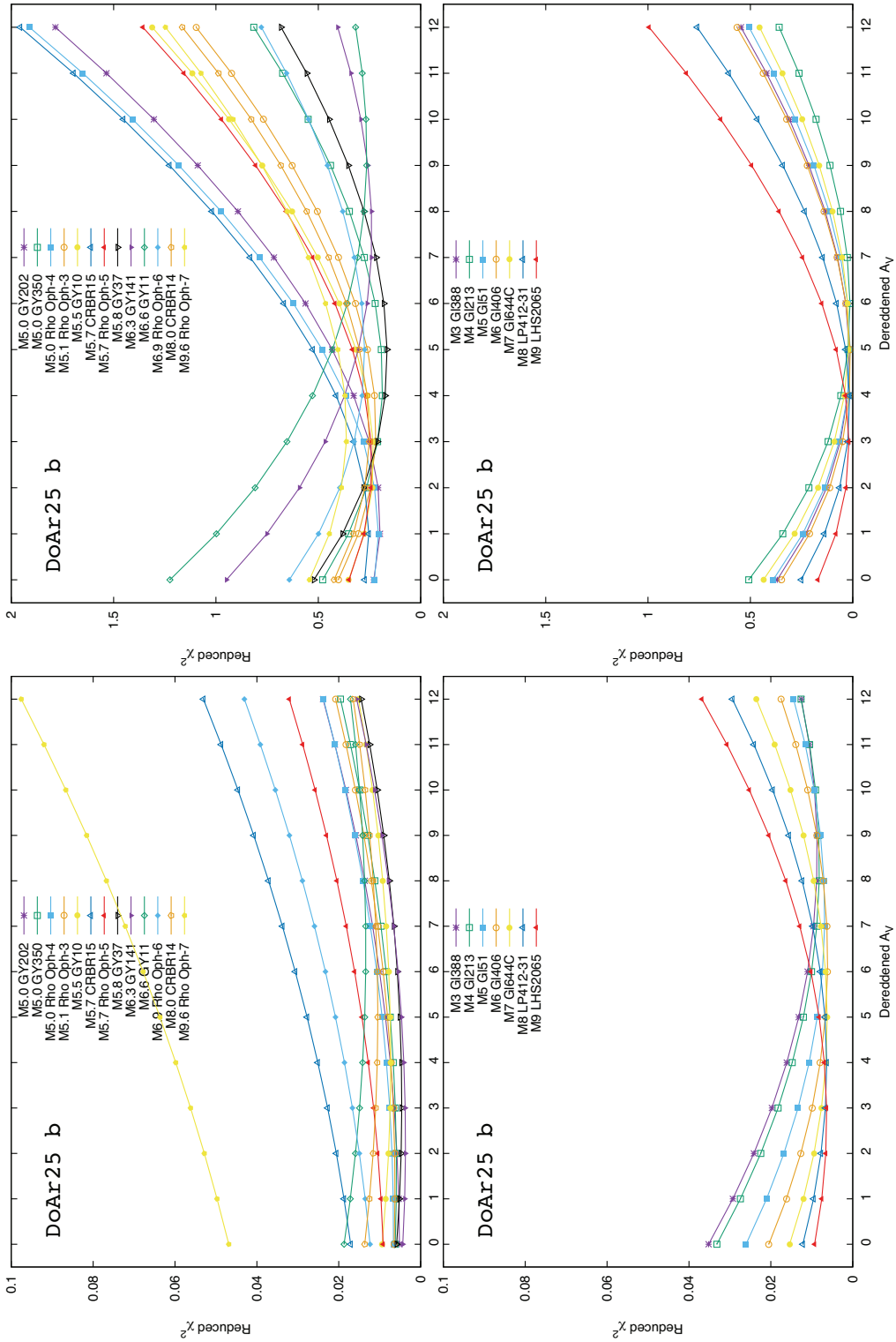

FIGURE 7.10: The reduced χ^2 fitting results of DoAr 25 b at *J*-band. *top left* : at J-band only with late-M dwarfs in ρ Oph, *bottom left* : at J-band only with field dwarfs, *top right* : at J-H band with late-M dwarfs in ρ Oph, *bottom right* : at J-H band with field dwarfs.

mag (Figure 7.10). The best fitting results are GY141 (M6.3) with A_V=2 mag from late-M YSOs, and Gl406 (M6) with A_V=6 mag from field dwarfs.

Figure 7.11 shows comparison between dereddend DoAR 25 b spectra and the best-fit reference spectra. In the case of the young brown dwarf GY141 (M6.3) with A_V=2, the *H*-band flux of DoAR 25 b is significantly higher then that of GY141. On the contrary, in the case of the field brown dwarf Gl406 (M6) with A_V=6 mag, the *H*-band flux of DoAr 25 b is weaker then that of Gl406. As mentioned above, the blackbody emission from the disk contribute to the flux of *H*-band where disk emission is more dominant. Therefore, the spectra of DoAR 25 b is more reconciled with being a young late-M (∼M6) brown dwarf than being a field brown dwarf, if there is an effect of the edge-on disk.

The actual extinction value of the edge-on disk is unmeasurable at the moment, and unknown stellar environments could influence on spectra since DoAR 25 b is located in ongoing star forming region. The intrinsic spectral type of DoAR 25 b is still controversial, edge-on disk and infrared veiling are the most conceivable scenarios for peculiar spectra at the present.

7.3.5 Constraints On Inner-orbit Planets

In LOCI algorithm, a planet FWHM parameter must be decided for best subsection dividing to prevent partial self-subtraction effect (See Section 7.2.3.2 and Lafrenière et al., 2007). Typically, we start with FWHM of a central star for initial LOCI image, then update it with FWHM of a detected point-like source to obtain best resultant image. Unfortunately, no significant point source was confirmed in the initial LOCI image (left panel of Figure 7.12). While not described here in detail, we had conducted classical ADI analysis (See Chapter 7.2.3.1 and Marois et al., 2006), and had found a point-like source around central star (right top panel of Figure 7.12). We measured and used FWHM of this point-like source, conducted additional LOCI analysis (right panel of Figure 7.12), consequently, no statistically significant signal was detected, including point-like source seen in the resultant image of classical ADI analysis.

The HiCIAO result image using the LOCI algorithm has variable contrasts as a function of separation from image center since partial self-subtraction effects in the algorithm (See Figure 7.13a, b and Lafrenière et al., 2007). To constraint possible

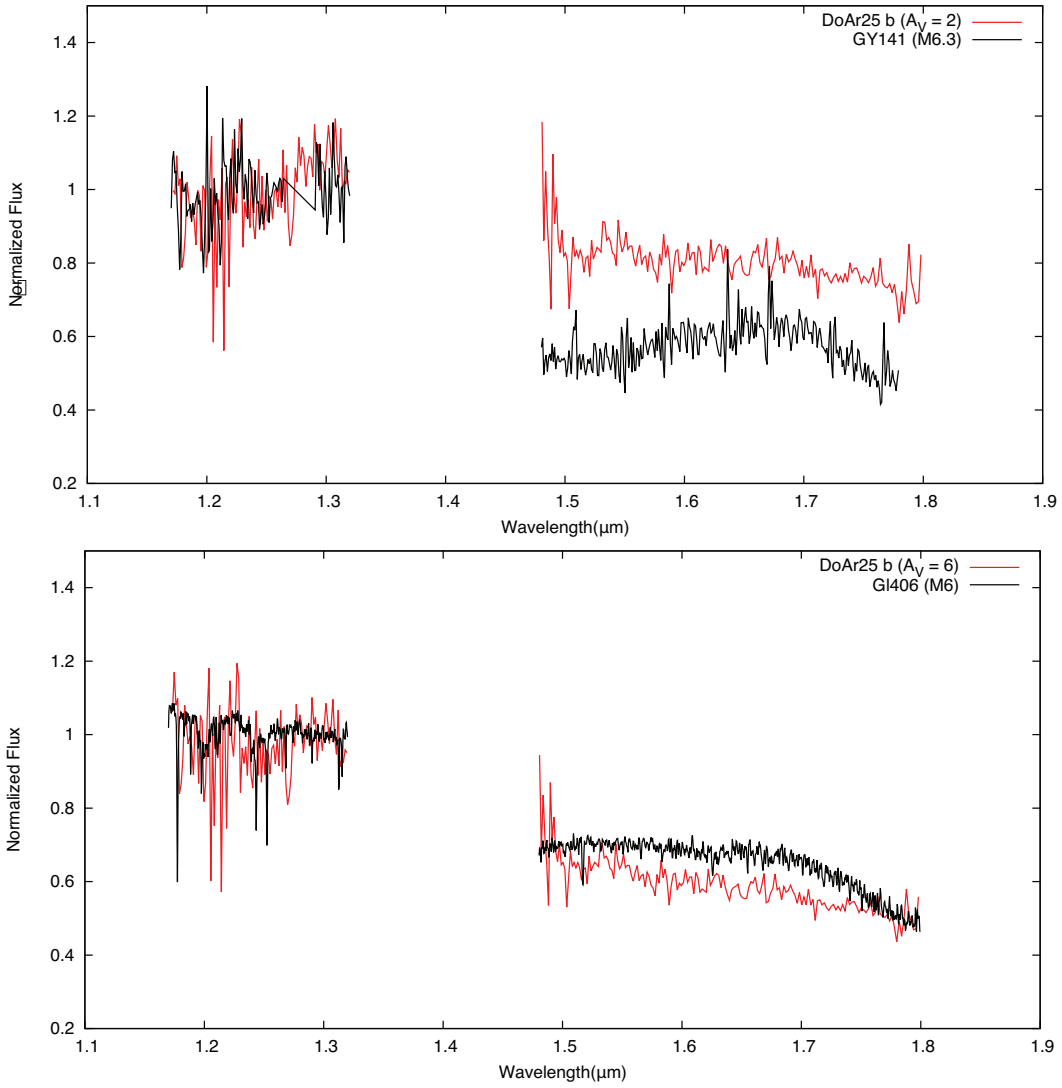

FIGURE 7.11: The spectra comparisons with the best fitting results, ρ Oph M6.3 with A_V=2 (*top*) and field M6 with A_V=6 (*bottom*). The edge-on disk may be explainable the *H*-band excess in *top* panel (See Section 7.3.4).

planet mass around the central star, we first calculated 5 sigma contrast and magnitude as follow;

$$\begin{aligned} \text{Contrast} =& \frac{5\sigma \times \pi(\text{FWHM}/2)^2}{\int_S F_* dS}, \\ \text{Magnitude} =& m_* - 2.5\log(\text{Contrast}). \end{aligned} \tag{7.1}$$

Where F_* is flux of the central star, S is radius over FWHM, and M_* is magnitude of the central star. After self-subtraction correction, we converted this to mass by using

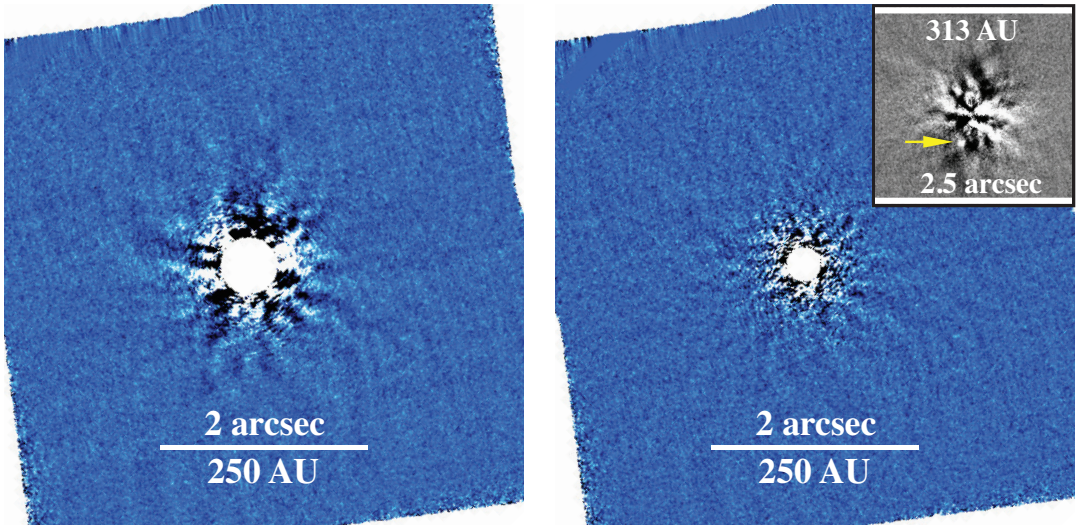

FIGURE 7.12: The resultant LOCI images. *left*: Using stellar FWHM (∼10 pixel) as possible planet FWHM. *right*: Using point-like signal FWHM (∼5 pixel) as possible planet FWHM parameter. *top left* panel shows the resultant image of classical ADI method which planet-like signal was found (*yellow arrow*).

DUSTY model as the detectable companion mass limit. The result is shown in Figure 7.13c. We concluded that there is no planet with more massive than 10 $M_{\rm Jup}$ in the vicinity of DoAr 25 and its disk(r = 2.5″ ∼ 313 AU). On the region over 2.5″ distance from the central star, IRCS observations achieves the better detection limit ∼2$M_{\rm Jup}$.

7.4 General Discussion

7.4.1 DoAr 25 b : a wide orbit PMC with peculiar NIR spectrum

From the multiple verifications, we concluded that DoAR 25 b is a planetary-mass companion orbiting >1400 AU away from DoAr 25. Its peculiar NIR spectrum is an unsolved problem at the moment, but its NIR colors resemble a extremely young and late-type dwarfs, including the similar peculiar object FW Tau b. FW Tau b is also wide orbit PMC (r∼ 330 ± 30 AU; Kraus et al., 2014). If this peculiarity is a common or more frequent feature of wide orbit PMCs, it could be one of the key clues to understand their formation and evolution.

7.4.2 Non-disk-origin of wide orbit PMCs

The category of wide-orbit planetary-mass objects is growing rapidly, and DoAR 25 b is one of the extremely separated and lightest objects in the category (See Figure 7.14

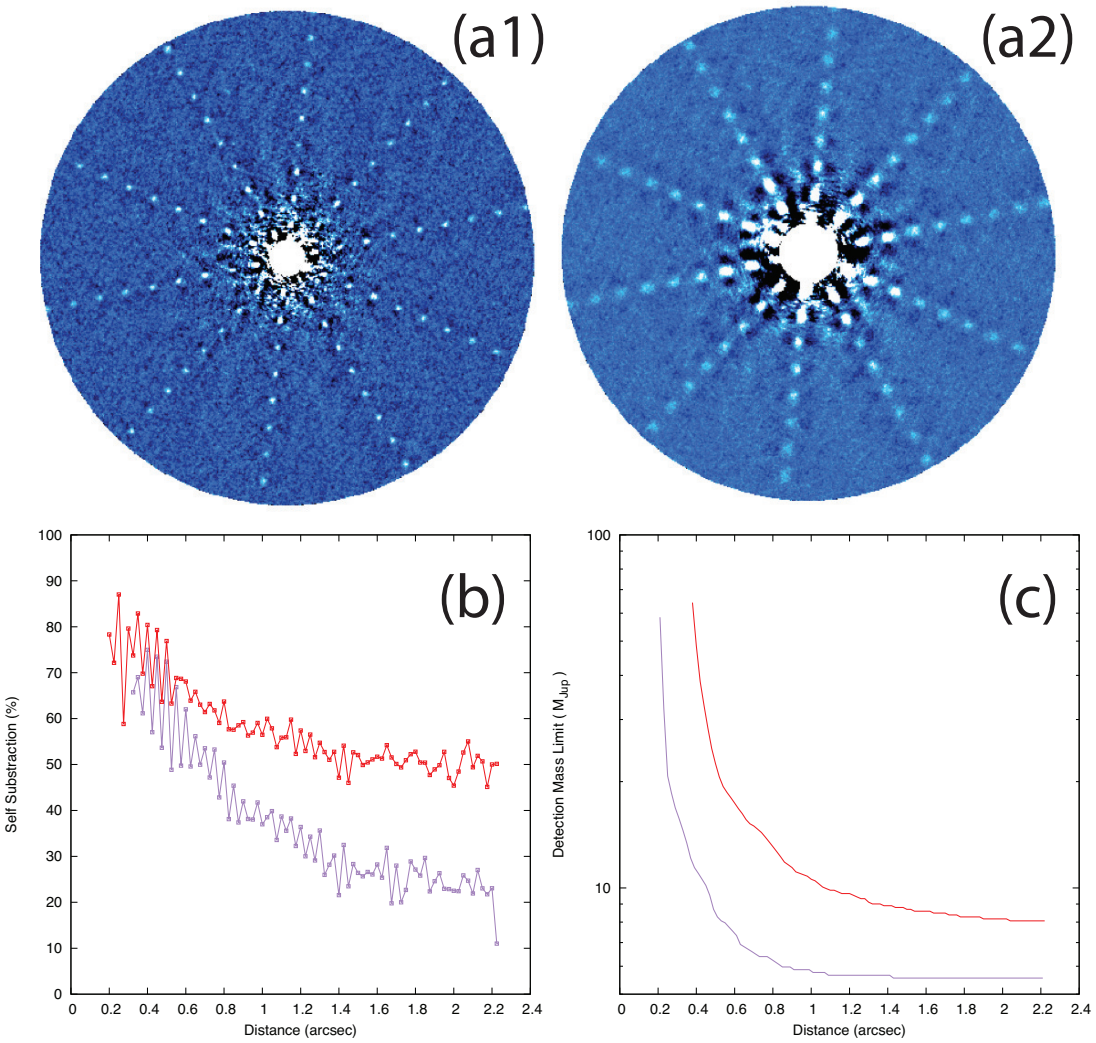

FIGURE 7.13: (a1) and (a2) show partial self-subtraction effect in our LOCI analysis with stellar FWHM and point like signal FWHM as possible planet FWHM parameter, respectively, by implanted artificial point sources. (b) and (c) present self-subtraction rates and detectable mass limit at 5σ, with using stellar FWHM (*red*) and point-like source FWHM (*purple*) as possible planet FWHM parameter.

and Table 7.4). The formation mechanisms are poorly understood. There are trials to explain the formation of wide-orbit planets with the gravitational instability model (e.g., Dodson-Robinson et al., 2009, Meru and Bate, 2010), but the origin of PMCs over 100 AU separations are still not well explained.

Planet formation is expected to make characteristic disk structures such as gaps, spiral arms and holes (e.g., Follette et al., 2015, Hashimoto et al., 2011, 2012, 2015) and the planet-scattering from the initial location within a disk also causes the disk disrupting effect (Jilkova and Zwart, 2015, Raymond et al., 2012). Thus if DoAr 25 b were originated from the protoplanetary disk associated with DoAr 25 and subsequently

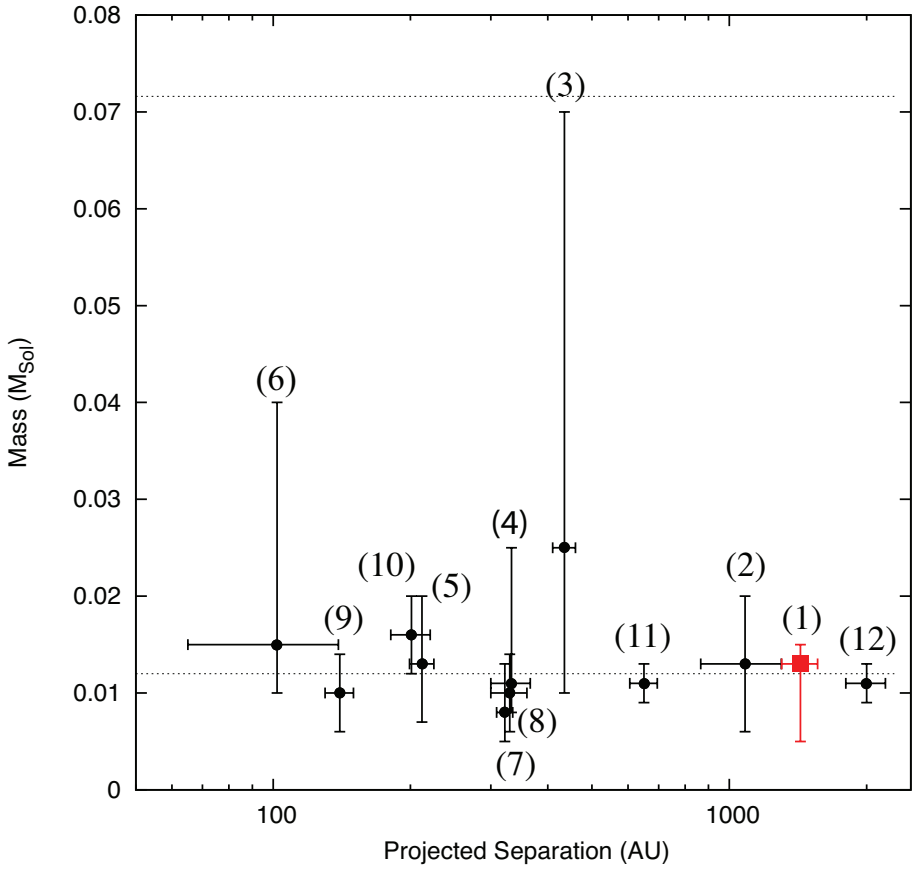

FIGURE 7.14: The separation-mass distributions of young wide orbit PMCs in Table 7.4. *lower dashed line* : the mass boundary between massive gas planets and low-mass brown dwarfs, *upper dashed line* : the mass boundary between massive brown dwarfs and normal stars.

TABLE 7.4: Masses and Separations of wide orbit PMCs around young primary stars ($<$ 10Myr).

Object	Mass ($M_{\rm Jup}$)	Separation (AU)	Reference
DoAr 25 b	13^{+2}_{-8}	1433±130	(1) This Work
SR 12 C	13±7	1083±217	(2) Kuzuhara et al. (2011)
CT Cha B	25^{+45}_{-15}	435±25	(3) Schmidt and Neuhäuser (2008)
DH Tau B	11^{+14}_{-3}	333±33	(4) Itoh et al. (2005)
CHXR73 B	13^{+7}_{-6}	212±13	(5) Luhman et al. (2006)
GQ Lup B	15^{+25}_{-5}	102±37	(6) McElwain et al. (2007)
1RXSJ160089 B	8^{+5}_{-3}	322±13	(7) Lafrenière et al. (2008)
FW Tau b	10±4	330±30	(8) Kraus et al. (2014)
ROXs 12 b	16±4	201±20	(9) Kraus et al. (2014)
ROXs 42B b	10±4	140±10	(10) Kraus et al. (2014)
HD 106906 b	13±2	∼650	(11) Bailey et al. (2014)
GU Psc b	9-13	∼2000	(12) Naud et al. (2014)

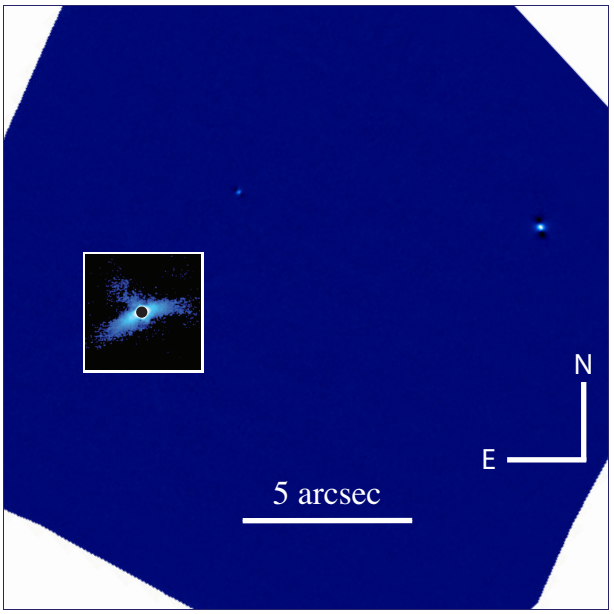

FIGURE 7.15: DoAr 25 system; Protoplanetary disk and DoAr 25 b associated with DoAr 25. Polarized intensity image of disk and LOCI image of DoAr 25 b are combined in same scale and coordinate (HiCIAO at *H*-band).

migrated outward, the disk would be disrupted or would have complex structures. In other words, a young cavity-less symmetric disk around DoAr 25 can be indicative of the non-protoplanetary-disk origin of DoAr 25 b. If wide orbit PMCs such as DoAr 25 b have a non-disk-origin and their evolutionary process is different from ordinary inner-orbit planets, the most plausible formation mechanism for wide-orbit PMCs is the cloud core fragmentation model. The largest numerical simulations of star formation with cloud core fragmentation, carried out by Bate (2009), Bate et al. (2003), show that the extreme mass ratio system(1:<0.05) with wide separation(>1000 AU) can be formed. This means that a very wide-orbit PMCs and ordinary near-orbit planets could have different origins (disk-origin and non-disk-origin), and they must distinguished from each other even though they have similar mass. The presence of non-disk-origin PMCs at outside of the disk is also indicative of a wide expansion of our view on the scale of a planetary system.

The number of currently known wide-orbit PMCs is only a few 10s, and their general properties are still not well revealed. Furthermore precise and robust measurement of masses of planetary-mass objects (PMOs) is very difficult at the present, because many uncertainties exist in the evolutionary models for substellar objects. In order to understand their detailed features, the statistically enough number of direct detections of young wide-orbit PMC system and floating PMOs is necessary to compare with the

theoretical predictions. Moreover, comprehensive observations on systems consisting of young protoplanetary disk and wide orbit PMCs such as DoAr 25 system (See Figure 7.15) are required for tracing simultaneous evolution of various circumstellar components.

Thesis Summary

Chapter 8

Thesis Summary

In this thesis, I have attempted to reveal the diversity of protoplanetary systems in two points of view; protoplanetary disk and planetary mass companions beyond the disk, especially, disk structures and non-disk-origin planetary objects. The observational results and discussions are provided in the previous chapters. In this chapter I wish summarise previous parts and propose future works.

In Chapter 3-6, I conducted the morphologic studies on protoplanetary disks, from full disk to transitional disk, on the basis of the results of high-resolution direct imaging observations. Consequently, I suggested that the disk diversity is not showing a certain phase in a common disk evolutionary path, but an individual clearing process by different dynamical environments such as physical properties of planets in the disks. In Chapter 7, I reported the discovery and the physical verification of DoAr 25 b, which is a possible disk-host planetary mass object orbiting DoAr 25. Based on the results of imaging observation on DoAr 25 disk from Chapter 3, I proposed that DoAr 25 b is not originated from the protoplanetary disk around DoAr 25 even it has a planetary mass.

These results and discussions commonly suggest that it is necessary to expand our traditional understanding on the planetary systems. Pre-transitional disks may be not a former phase of transitional disks. Planetary objects around stars may have various origins from protoplanetary disks to interstellar molecular clouds, and have more wider orbital ranges, from < 1 au to $> 1,000$ au. Planetary systems have more various histories and more larger scales than our current understanding. To probe into the actual scales and details of the planetary systems, a large number of samples of highly resolved protoplanetary disks and high-contrast planet surveys are strongly required.

Furthermore, disk radiation transfer models (e.g., HOCHUNK3D; Whitney et al., 2013) also have to be conduct to understanding observed radiation features from the disks.

ALMA recently starts to provide the sub-mm interferometry imaging results of disks in unprecedented high spatial resolution (ALMA Partnership et al., 2015) and opened the advanced field of observational studies on protoplanetary disks. SCExAO, the Subaru Coronagraphic Extreme Adaptive Optics, is expected to find out unseen planets around young stars and to resolve the details of the disks in infrared wavelengths in future ground based observations. The high resolution imaging diagnostics using infrared direct imaging by Subaru Telescope with SCExAO and sub-mm interferometry by ALMA will allow us trace various-size dust distribution in detail. With resolving the details of LkCa 15 and GM Aur disks, the verification of the presence of planets in disk cavities of LkCa 15 and GM Aur may provide essential hints for studying the disk-planet interaction.

Bibliography

Mirza Ahmic, Bryce Croll, and Pawel Artymowicz. Dust distribution in the β pictoris circumstellar disks. *The Astrophysical Journal*, 705(1):529–542, October 2009.

R L Akeson, R Millan-Gabet, D R Ciardi, A F Boden, A I Sargent, J D Monnier, H McAlister, T ten Brummelaar, J Sturmann, L Sturmann, and N Turner. Radial structure in the tw hya circumstellar disk. *The Astrophysical Journal*, 728(2):96, February 2011.

E Akiyama, T Muto, N Kusakabe, A Kataoka, J Hashimoto, T Tsukagoshi, J Kwon, T Kudo, R Kandori, C A Grady, M Takami, M Janson, M Kuzuhara, T Henning, M L Sitko, J C Carson, S Mayama, T Currie, C Thalmann, J Wisniewski, M Momose, N Ohashi, L Abe, W Brandner, T D Brandt, S Egner, M Feldt, M Goto, O Guyon, Y Hayano, M Hayashi, S Hayashi, K W Hodapp, M Ishi, M Iye, G R Knapp, T Matsuo, M W McElwain, S Miyama, J I Morino, A Moro-Martin, T Nishimura, T S Pyo, G Serabyn, T Suenaga, H Suto, R Suzuki, Y H Takahashi, N Takato, H Terada, D Tomono, E L Turner, M Watanabe, T Yamada, H Takami, T Usuda, and M Tamura. Discovery of a disk gap candidate at 20 au in tw hydrae. *The Astrophysical Journal*, 802(2):L17, April 2015.

R D Alexander and P J Armitage. Dust dynamics during protoplanetary disc clearing. *Monthly Notices of the Royal Astronomical Society*, 375(2):500–512, February 2007.

R D Alexander, C J Clarke, and J E Pringle. Photoevaporation of protoplanetary discs - i. hydrodynamic models. *Monthly Notices of the Royal Astronomical Society*, 369(1):216–228, June 2006a.

R D Alexander, C J Clarke, and J E Pringle. Photoevaporation of protoplanetary discs - ii. evolutionary models and observable properties. *Monthly Notices of the Royal Astronomical Society*, 369(1):229–239, June 2006b.

ALMA Partnership, C L Brogan, L M Pérez, T R Hunter, W R F Dent, A S Hales, R E Hills, S Corder, E B Fomalont, C Vlahakis, Y Asaki, D Barkats, A Hirota, J A Hodge, C M V Impellizzeri, R Kneissl, E Liuzzo, R Lucas, N Marcelino, S Matsushita, K Nakanishi, N Phillips, A M S Richards, I Toledo, R Aladro, D Broguiere, J R Cortes, Cortes, P. C., D Espada, F Galarza, D Garcia-Appadoo, L Guzman-Ramirez, E M Humphreys, T Jung, S Kameno, R A Laing, S Leon, G Marconi, A Mignano, B Nikolic, L A Nyman, M Radiszcz, A Remijan, J A Rodón, T Sawada, S Takahashi, R P J Tilanus, B Vila Vilaro, L C Watson, T Wiklind, E Akiyama, E Chapillon, I De Gregorio-Monsalvo, J Di Francesco, F Gueth, A Kawamura, C F Lee, Q Nguyen Luong, J Mangum, V Piétu, P Sanhueza, K Saigo, S Takakuwa, C Ubach, T van Kempen, A Wootten, A Castro-Carrizo, H Francke, J Gallardo, J Garcia, S Gonzalez, T Hill, T Kaminski, Y Kurono, H Y Liu, C Lopez, F Morales, K Plarre, G Schieven, L Testi, L Videla, E Villard, P Andreani, J E Hibbard, and K Tatematsu. The 2014 alma long baseline campaign: First results from high angular resolution observations toward the hl tau region. *The Astrophysical Journal Letters*, 808(1):L3, July 2015.

C Alves de Oliveira and M Casali. Deep near-ir variability survey of pre-main-sequence stars in ρ ophiuchi. *Astronomy and Astrophysics*, 485(1):155–166, July 2008.

Sean M Andrews and Jonathan P Williams. Circumstellar dust disks in taurus-auriga: The submillimeter perspective. *The Astrophysical Journal*, 631(2):1134–1160, October 2005.

Sean M Andrews and Jonathan P Williams. High-resolution submillimeter constraints on circumstellar disk structure. *The Astrophysical Journal*, 659(1):705–728, April 2007a.

Sean M Andrews and Jonathan P Williams. A submillimeter view of circumstellar dust disks in ρ ophiuchi. *The Astrophysical Journal*, 671(2):1800–1812, December 2007b.

Sean M Andrews, A M Hughes, D J Wilner, and Chunhua Qi. The structure of the doar 25 circumstellar disk. *The Astrophysical Journal*, 678(2):L133–L136, May 2008.

Sean M Andrews, D J Wilner, A M Hughes, Chunhua Qi, and C P Dullemond. Protoplanetary disk structures in ophiuchus. *The Astrophysical Journal*, 700(2):1502–1523, August 2009.

Sean M Andrews, D J Wilner, A M Hughes, Chunhua Qi, and C P Dullemond. Protoplanetary disk structures in ophiuchus. ii. extension to fainter sources. *The Astrophysical Journal*, 723(2):1241–1254, November 2010.

Sean M Andrews, Katherine A Rosenfeld, David J Wilner, and Michael Bremer. A closer look at the lkca 15 protoplanetary disk. *The Astrophysical Journal Letters*, 742(1):L5, November 2011a.

Sean M Andrews, David J Wilner, Catherine Espaillat, A M Hughes, C P Dullemond, M K McClure, Chunhua Qi, and J M Brown. Resolved images of large cavities in protoplanetary transition disks. *The Astrophysical Journal*, 732(1):42, May 2011b.

D Apai, I Pascucci, W Brandner, Th Henning, R Lenzen, D E Potter, A M Lagrange, and G Rousset. Naco polarimetric differential imaging of tw hya. a sharp look at the closest t tauri disk. *Astronomy and Astrophysics*, 415:671–676, February 2004.

Philip J Armitage. Dynamics of protoplanetary disks. *Annual Review of Astronomy and Astrophysics*, 49(1):195–236, September 2011.

P Artymowicz. Self-regulating protoplanet growth. *Icarus (ISSN 0019-1035)*, 70(2):303–318, May 1987.

Henning Avenhaus, Sascha P Quanz, Hans Martin Schmid, Michael R Meyer, Antonio Garufi, Sebastian Wolf, and Carsten Dominik. Structures in the protoplanetary disk of hd142527 seen in polarized scattered light. *The Astrophysical Journal*, 781(2):87, February 2014.

Vanessa Bailey, Tiffany Meshkat, Megan Reiter, Katie Morzinski, Jared Males, Kate Y L Su, Philip M Hinz, Matthew Kenworthy, Daniel Stark, Eric Mamajek, Runa Briguglio, Laird M Close, Katherine B Follette, Alfio Puglisi, Timothy Rodigas, Alycia J Weinberger, and Marco Xompero. Hd 106906 b: A planetary-mass companion outside a massive debris disk. *The Astrophysical Journal*, 780(1):L4, January 2014.

I Baraffe, G Chabrier, T S Barman, F Allard, and P H Hauschildt. Evolutionary models for cool brown dwarfs and extrasolar giant planets. the case of hd 209458. *Astronomy and Astrophysics*, 402:701–712, May 2003.

Gibor Basri and Celso Batalha. Hamilton echelle spectra of young stars. i - optical veiling. *Astrophysical Journal*, 363:654–669, November 1990.

C C Batalha and Gibor Basri. The atmospheres of t tauri stars. ii - chromospheric line fluxes and veiling. *Astrophysical Journal*, 412:363–374, July 1993.

Matthew R Bate. Stellar, brown dwarf and multiple star properties from hydrodynamical simulations of star cluster formation. *Monthly Notices of the Royal Astronomical Society*, 392(2):590–616, January 2009.

Matthew R Bate, Ian A Bonnell, and Volker Bromm. The formation of a star cluster: predicting the properties of stars and brown dwarfs. *Monthly Notice of the Royal Astronomical Society*, 339(3): 577–599, March 2003.

Edwin Bergin, Nuria Calvet, Michael L Sitko, Herve Abgrall, Paola D'Alessio, Gregory J Herczeg, Evelyne Roueff, Chunhua Qi, David K Lynch, Ray W Russell, Suellen M Brafford, and R Brad Perry. A new probe of the planet-forming region in t tauri disks. *The Astrophysical Journal*, 614(2): L133–L136, October 2004.

T Birnstiel, S M Andrews, and B Ercolano. Can grain growth explain transition disks? *Astronomy and Astrophysics*, 544:A79, August 2012.

T Birnstiel, C P Dullemond, and P Pinilla. Lopsided dust rings in transition disks. *Astronomy and Astrophysics*, 550:L8, February 2013a.

T Birnstiel, P Pinilla, S M Andrews, M Benisty, and B Ercolano. Transition disks - grain growth, planets, or photoevaporation? *Instabilities and Structures in Proto-Planetary Disks*, 46:02001, April 2013b.

R C Bohlin. Hst stellar standards with 1 *The Future of Photometric*, 364:315, April 2007.

A P Boss. Giant planet formation by gravitational instability. *Science*, 276(5320):1836–1839, 1997.

Alan P Boss, R Paul Butler, William B Hubbard, Philip A Ianna, Martin Kürster, Jack J Lissauer, Michel Mayor, Karen J Meech, Francois Mignard, Alan J Penny, Andreas Quirrenbach, Jill C Tarter, and Alfred Vidal-Madjar. Working group on extrasolar planets. *IAU Transactions*, 26(T26A):183–186, March 2007.

J Bouwman, A de Koter, C Dominik, and L B F M Waters. The origin of crystalline silicates in the herbig be star hd 100546 and in comet hale-bopp. *Astronomy and Astrophysics*, 401:577–592, April 2003.

Brendan P Bowler, Michael C Liu, Adam L Kraus, and Andrew W Mann. Spectroscopic confirmation of young planetary-mass companions on wide orbits. *The Astrophysical Journal*, 784(1):65, March 2014.

Timothy D Brandt, Masayuki Kuzuhara, Michael W McElwain, Joshua E Schlieder, John P Wisniewski, Edwin L Turner, J Carson, T Matsuo, B Biller, M Bonnefoy, C Dressing, M Janson, G R Knapp, A Moro-Martin, C Thalmann, T Kudo, N Kusakabe, J Hashimoto, L Abe, W Brandner, T Currie, S Egner, M Feldt, T Golota, M Goto, C A Grady, O Guyon, Y Hayano, M Hayashi, S Hayashi, T Henning, K W Hodapp, M Ishii, M Iye, R Kandori, J Kwon, K Mede, S Miyama, J I Morino, T Nishimura, T S Pyo, E Serabyn, T Suenaga, H Suto, R Suzuki, M Takami, Y Takahashi, N Takato, H Terada, D Tomono, M Watanabe, T Yamada, H Takami, T Usuda, and M Tamura. The moving group targets of the seeds high-contrast imaging survey of exoplanets and disks: Results and observations from the first three years. *The Astrophysical Journal*, 786(1):1, May 2014a.

Timothy D Brandt, Michael W McElwain, Edwin L Turner, Kyle Mede, David S Spiegel, Masayuki Kuzuhara, Joshua E Schlieder, John P Wisniewski, L Abe, B Biller, W Brandner, J Carson, T Currie, S Egner, M Feldt, T Golota, M Goto, C A Grady, O Guyon, J Hashimoto, Y Hayano, M Hayashi, S Hayashi, T Henning, K W Hodapp, S Inutsuka, M Ishii, M Iye, M Janson, R Kandori, G R Knapp, T Kudo, N Kusakabe, J Kwon, T Matsuo, S Miyama, J I Morino, A Moro-Martin, T Nishimura, T S Pyo, E Serabyn, H Suto, R Suzuki, M Takami, N Takato, H Terada, C Thalmann, D Tomono, M Watanabe, T Yamada, H Takami, T Usuda, and M Tamura. A statistical analysis of seeds and other high-contrast exoplanet surveys: Massive planets or low-mass brown dwarfs? *The Astrophysical Journal*, 794(2):159, October 2014b.

J M Brown, G A Blake, C P Dullemond, B Merín, J C Augereau, A C A Boogert, N J II Evans, V C Geers, F Lahuis, J E Kessler-Silacci, K M Pontoppidan, and E F van Dishoeck. Cold disks: Spitzer spectroscopy of disks around young stars with large gaps. *The Astrophysical Journal*, 664(2): L107–L110, August 2007.

G Bryden, Xingming Chen, D N C Lin, Richard P Nelson, and John C B Papaloizou. Tidally induced gap formation in protostellar disks: Gap clearing and suppression of protoplanetary growth. *The Astrophysical Journal*, 514(1):344–367, March 1999.

R Paul Butler, Steven S Vogt, Geoffrey W Marcy, Debra A Fischer, Jason T Wright, Gregory W Henry, Greg Laughlin, and Jack J Lissauer. A neptune-mass planet orbiting the nearby m dwarf gj 436. *The Astrophysical Journal*, 617(1):580–588, December 2004.

N Calvet, P D'Alessio, D M Watson, R Franco-Hernández, E Furlan, J Green, P M Sutter, W J Forrest, L Hartmann, K I Uchida, L D Keller, B Sargent, J Najita, T L Herter, D J Barry, and P Hall. Disks in transition in the taurus population: Spitzer irs spectra of gm aurigae and dm tauri. *The Astrophysical Journal*, 630(2):L185–L188, September 2005.

Nuria Calvet, Paola D'Alessio, Lee Hartmann, David Wilner, Andrew Walsh, and Michael Sitko. Evidence for a developing gap in a 10 myr old protoplanetary disk. *The Astrophysical Journal*, 568(2): 1008–1016, April 2002.

A G W Cameron. Physics of the primitive solar accretion disk. *Moon and the Planets*, 18(1):5–40, February 1978.

H Canovas, F Ménard, J de Boer, C Pinte, H Avenhaus, and M R Schreiber. Nonazimuthal linear polarization in protoplanetary disks. *Astronomy and Astrophysics*, 582:L7, October 2015.

S Casassus, S Perez M, A Jordán, F Ménard, J Cuadra, M R Schreiber, A S Hales, and B Ercolano. The dynamically disrupted gap in hd 142527. *The Astrophysical Journal Letters*, 754(2):L31, August 2012.

G Chabrier, I Baraffe, F Allard, and P Hauschildt. Evolutionary models for very low-mass stars and brown dwarfs with dusty atmospheres. *The Astrophysical Journal*, 542(1):464–472, October 2000.

G Chauvin, A M Lagrange, H Beust, M Bonnefoy, A Boccaletti, D Apai, F Allard, D Ehrenreich, J H V Girard, D Mouillet, and D Rouan. Orbital characterization of the β pictoris b giant planet. *Astronomy and Astrophysics*, 542:A41, June 2012.

E I Chiang and P Goldreich. Spectral energy distributions of passive t tauri disks: Inclination. *The Astrophysical Journal*, 519(1):279–284, July 1999.

Eugene Chiang and Ruth Murray-Clay. Inside-out evacuation of transitional protoplanetary discs by the magneto-rotational instability. *Nature Physics*, 3(9):604–608, September 2007.

Lucas Cieza, Deborah L Padgett, Karl R Stapelfeldt, Jean-Charles Augereau, Paul Harvey, Neal J II Evans, Bruno Merin, David Koerner, Anneila Sargent, Ewine F van Dishoeck, Lori Allen, Geoffrey Blake, Timothy Brooke, Nicholas Chapman, Tracy Huard, Shih-Ping Lai, Lee Mundy, Philip C Myers, William Spiesman, and Zahed Wahhaj. The spitzer c2d survey of weak-line t tauri stars. ii. new constraints on the timescale for planet building. *The Astrophysical Journal*, 667(1):308–328, September 2007.

Lucas A Cieza, Jonathan J Swift, Geoffrey S Mathews, and Jonathan P Williams. The masses of transition circumstellar disks: Observational support for photoevaporation models. *The Astrophysical Journal*, 686(2):L115–L118, October 2008.

Lucas A Cieza, Matthias R Schreiber, Gisela A Romero, Marcelo D Mora, Bruno Merin, Jonathan J Swift, Mariana Orellana, Jonathan P Williams, Paul M Harvey, and Neal J II Evans. The nature of transition circumstellar disks. i. the ophiuchus molecular cloud. *The Astrophysical Journal*, 712(2): 925–941, April 2010.

Lucas A Cieza, Matthias R Schreiber, Gisela A Romero, Jonathan P Williams, Alberto Rebassa-Mansergas, and Bruno Merin. The nature of transition circumstellar disks. iii. perseus, taurus, and auriga. *The Astrophysical Journal*, 750(2):157–24, April 2012.

C J Clarke, A Gendrin, and M Sotomayor. The dispersal of circumstellar discs: the role of the ultraviolet switch. *Monthly Notices of the Royal Astronomical Society*, 328(2):485–491, December 2001.

COMPLETEteam. 2mass final ophiuchus extinction map. 2012.

Thayne Currie, Takayuki Muto, Tomoyuki Kudo, Mitsuhiko Honda, Timothy D Brandt, Carol Grady, Misato Fukagawa, Adam Burrows, Markus Janson, Masayuki Kuzuhara, Michael W McElwain, Katherine Follette, Jun Hashimoto, Thomas Henning, Ryo Kandori, Nobuhiko Kusakabe, Jungmi Kwon, Kyle Mede, Jun-Ichi Morino, Jun Nishikawa, Tae-Soo Pyo, Gene Serabyn, Takuya Suenaga, Yasuhiro Takahashi, John Wisniewski, and Motohide Tamura. Recovery of the candidate protoplanet hd 100546 b with gemini/nici and detection of additional (planet-induced?) disk structure at small separations. *The Astrophysical Journal Letters*, 796(2):L30, December 2014.

Paola D'Alessio, Lee Hartmann, Nuria Calvet, Ramiro Franco-Hernandez, William J Forrest, Ben Sargent, Elise Furlan, Keven Uchida, Joel D Green, Dan M Watson, Christine H Chen, F Kemper, G C Sloan, and Joan Najita. The truncated disk of coku tau/4. *The Astrophysical Journal*, 621(1): 461–472, March 2005.

Nicolas Dauphas and Marc Chaussidon. A perspective from extinct radionuclides on a young stellar object: The sun and its accretion disk. *Annual Review of Earth and Planetary Sciences*, 39(1): 351–386, May 2011.

Rebekah I Dawson, Ruth A Murray-Clay, and Daniel C Fabrycky. On the misalignment of the directly imaged planet β pictoris b with the system's warped inner disk. *The Astrophysical Journal Letters*, 743(1):L17, December 2011.

M de Juan Ovelar, M Min, C Dominik, C Thalmann, P Pinilla, M Benisty, and T Birnstiel. Imaging diagnostics for transitional discs. *Astronomy and Astrophysics*, 560:A111, December 2013a.

Maria de Juan Ovelar, Michiel Min, Carsten Dominik, Christian Thalmann, Paola Pinilla, Benisty Myriam, and Til Birnstiel. Imaging diagnostics for transitional discs. *Protostars and Planets VI*, July 2013b.

Jerome de Leon, Michihiro Takami, Jennifer L Karr, Jun Hashimoto, Tomoyuki Kudo, Michael Sitko, Satoshi Mayama, Nobuyuki Kusakabe, Eiji Akiyama, Hauyu Baobab Liu, Tomonori Usuda, Lyu Abe, Wolfgang Brandner, Timothy D Brandt, Joseph Carson, Thayne Currie, Sebastian E Egner, Markus Feldt, Katherine Follette, Carol A Grady, Miwa Goto, Olivier Guyon, Yutaka Hayano, Masahiko Hayashi, Saeko Hayashi, Thomas Henning, Klaus W Hodapp, Miki Ishii, Masanori Iye, Markus Janson, Ryo Kandori, Gillian R Knapp, Masayuki Kuzuhara, Jungmi Kwon, Taro Matsuo, Michael W McElwain, Shoken Miyama, Jun-Ichi Morino, Amaya Moro-Martin, Tetsuo Nishimura, Tae-Soo Pyo, Eugene Serabyn, Takuya Suenaga, Hiroshi Suto, Ryuji Suzuki, Yasuhiro Takahashi, Naruhisa Takato, Hiroshi Terada, Christian Thalmann, Daigo Tomono, Edwin L Turner, Makoto Watanabe, John P Wisniewski, Toru Yamada, Hideki Takami, and Motohide Tamura. Near-ir high-resolution imaging polarimetry of the su aur disk: Clues for tidal tails? *The Astrophysical Journal Letters*, 2015.

C Alves de Oliveira, C Alves de Oliveira, E Moraux, J Bouvier, and H Bouy. Spectroscopy of new brown dwarf members of ρ ophiuchi and an updated initial mass function. *Astronomy and Astrophysics*, 539:A151, March 2012.

Sarah E Dodson-Robinson and Colette Salyk. Transitional disks as signposts of young, multiplanet systems. *The Astrophysical Journal*, 738(2):131, September 2011.

Sarah E Dodson-Robinson, Dimitri Veras, Eric B Ford, and C A Beichman. The formation mechanism of gas giants on wide orbits. *The Astrophysical Journal*, 707(1):79–88, December 2009.

R Dong, R Rafikov, Z Zhu, L Hartmann, B Whitney, T Brandt, T Muto, J Hashimoto, C Grady, K Follette, M Kuzuhara, R Tanii, Y Itoh, C Thalmann, J Wisniewski, S Mayama, M Janson, L Abe, W Brandner, J Carson, S Egner, M Feldt, M Goto, O Guyon, Y Hayano, M Hayashi, S Hayashi, T Henning, K W Hodapp, M Honda, S Inutsuka, M Ishii, M Iye, R Kandori, G R Knapp, T Kudo, N Kusakabe, T Matsuo, M W McElwain, S Miyama, J I Morino, A Moro-Martin, T Nishimura, T S Pyo, H Suto, R Suzuki, M Takami, N Takato, H Terada, D Tomono, E L Turner, M Watanabe, T Yamada, H Takami, T Usuda, and M Tamura. The missing cavities in the seeds polarized scattered light images of transitional protoplanetary disks: A generic disk model. *The Astrophysical Journal*, 750(2):161, May 2012a.

Ruobing Dong, Jun Hashimoto, Roman Rafikov, Zhaohuan Zhu, Barbara Whitney, Tomoyuki Kudo, Takayuki Muto, Timothy Brandt, Melissa K McClure, John Wisniewski, L Abe, W Brandner, J Carson, S Egner, M Feldt, M Goto, C Grady, O Guyon, Y Hayano, M Hayashi, S Hayashi, T Henning, K W Hodapp, M Ishii, M Iye, M Janson, R Kandori, G R Knapp, N Kusakabe, M Kuzuhara, J Kwon, T Matsuo, M McElwain, S Miyama, J I Morino, A Moro-Martin, T Nishimura, T S Pyo, E Serabyn, H Suto, R Suzuki, M Takami, N Takato, H Terada, C Thalmann, D Tomono, E Turner, M Watanabe, T Yamada, H Takami, T Usuda, and M Tamura. The structure of pre-transitional protoplanetary disks. i. radiative transfer modeling of the disk+cavity in the pds 70 system. *The Astrophysical Journal*, 760(2):111, December 2012b.

Ruobing Dong, Zhaohuan Zhu, and Barbara Whitney. Observational signatures of planets in protoplanetary disks i. gaps opened by single and multiple young planets in disks. *The Astrophysical Journal*, 809(1):93, August 2015.

C Ducourant, R Teixeira, J P Perie, J F Lecampion, J Guibert, and M J Sartori. Pre-main sequence star proper motion catalogue. *Astronomy and Astrophysics*, 438(2):769–778, August 2005.

C P Dullemond and C Dominik. The effect of dust settling on the appearance of protoplanetary disks. *Astronomy and Astrophysics*, 421(3):1075–1086, July 2004.

C P Dullemond and C Dominik. Dust coagulation in protoplanetary disks: A rapid depletion of small grains. *Astronomy and Astrophysics*, 434(3):971–986, May 2005.

R H Durisen, A P Boss, L Mayer, A F Nelson, T Quinn, and W K M Rice. Gravitational instabilities in gaseous protoplanetary disks and implications for giant planet formation. *Protostars and Planets V*, pages 607–622, 2007.

A Dutrey, S Guilloteau, V Piétu, E Chapillon, F Gueth, T Henning, R Launhardt, Y Pavlyuchenkov, K Schreyer, and D Semenov. Cavities in inner disks: the gm aurigae case. *Astronomy and Astrophysics*, 490(2):L15–L18, November 2008.

C Espaillat, N Calvet, P D'Alessio, J Hernández, C Qi, L Hartmann, E Furlan, and D M Watson. On the diversity of the taurus transitional disks: Ux tauri a and lkca 15. *The Astrophysical Journal*, 670 (2):L135–L138, December 2007a.

C Espaillat, J Muzerolle, J Hernández, C Briceño, N Calvet, P D'Alessio, M McClure, D M Watson, L Hartmann, and B Sargent. A slowly accreting ˜10 myr-old transitional disk in orion ob1a. *The Astrophysical Journal*, 689(2):L145–L148, December 2008a.

C Espaillat, P D'Alessio, J Hernández, E Nagel, K L Luhman, D M Watson, N Calvet, J Muzerolle, and M McClure. Unveiling the structure of pre-transitional disks. *The Astrophysical Journal*, 717(1): 441–457, July 2010.

C Espaillat, L Ingleby, J Hernández, E Furlan, P D'Alessio, N Calvet, S Andrews, J Muzerolle, C Qi, and D Wilner. On the transitional disk class: Linking observations of t tauri stars and physical disk models. *The Astrophysical Journal*, 747(2):103, March 2012.

C Espaillat, J Muzerolle, J Najita, S Andrews, Z Zhu, N Calvet, S Kraus, J Hashimoto, A Kraus, and P D'Alessio. An observational perspective of transitional disks. *Protostars and Planets VI*, pages 497–520, 2014a.

Catherine Espaillat. A herschel view of dust evolution in protoplanetary disks. *Proceedings of the International Astronomical Union*, 8(S299):140–144, June 2013.

Catherine Espaillat, Nuria Calvet, Paola D'Alessio, Edwin Bergin, Lee Hartmann, Dan Watson, Elise Furlan, Joan Najita, William Forrest, Melissa McClure, Ben Sargent, Chris Bohac, and Samuel T Harrold. Probing the dust and gas in the transitional disk of cs cha with spitzer. *The Astrophysical Journal*, 664(2):L111–L114, August 2007b.

Catherine Espaillat, Nuria Calvet, Kevin L Luhman, James Muzerolle, and Paola D'Alessio. Confirmation of a gapped primordial disk around lkca 15. *The Astrophysical Journal*, 682(2):L125–L128, August 2008b.

Catherine Espaillat, Laura Ingleby, Jesus Hernandez, and Nuria Calvet. Exploring the dust-gas connection in the protoplanetary disk of gm aur. *Spitzer Proposal*, -1:11071, December 2014b.

Neal J II Evans, Lori E Allen, Geoffrey A Blake, A C A Boogert, Tyler Bourke, Paul M Harvey, J E Kessler, David W Koerner, Chang Won Lee, Lee G Mundy, Philip C Myers, Deborah L Padgett, K Pontoppidan, Anneila I Sargent, Karl R Stapelfeldt, Ewine F van Dishoeck, Chadwick H Young, and Kaisa E Young. From molecular cores to planet-forming disks: An sirtf legacy program. *The Publications of the Astronomical Society of the Pacific*, 115(8):965–980, August 2003.

T M Evans, M J Ireland, A L Kraus, F Martinache, P Stewart, P G Tuthill, S Lacour, J M Carpenter, and L A Hillenbrand. Mapping the shores of the brown dwarf desert. iii. young moving groups. *The Astrophysical Journal*, 744(2):120, January 2012.

exoplanet.eu. The extrasolar planets encyclopaedia. URL http://exoplanet.eu/.

Katherine B Follette, Motohide Tamura, Jun Hashimoto, Barbara Whitney, Carol Grady, Laird Close, Sean M Andrews, Jungmi Kwon, John Wisniewski, Timothy D Brandt, Satoshi Mayama, Ryo Kandori, Ruobing Dong, Lyu Abe, Wolfgang Brandner, Joseph Carson, Thayne Currie, Sebastian E Egner, Markus Feldt, Miwa Goto, Olivier Guyon, Yutaka Hayano, Masahiko Hayashi, Saeko Hayashi, Thomas Henning, Klaus Hodapp, Miki Ishii, Masanori Iye, Markus Janson, Gillian R Knapp, Tomoyuki Kudo, Nobuhiko Kusakabe, Masayuki Kuzuhara, Michael W McElwain, Taro Matsuo, Shoken Miyama, Jun-Ichi Morino, Amaya Moro-Martin, Tetsuo Nishimura, Tae-Soo Pyo, Eugene Serabyn, Hiroshi Suto, Ryuji Suzuki, Michihiro Takami, Naruhisa Takato, Hiroshi Terada, Christian Thalmann, Daigo Tomono, Edwin L Turner, Makoto Watanabe, Toru Yamada, Hideki Takami, and Tomonori Usuda. Mapping h-band scattered light emission in the mysterious sr21 transitional disk. *The Astrophysical Journal*, 767(1):10, April 2013.

Katherine B Follette, Carol A Grady, Jeremy R Swearingen, Michael L Sitko, Elizabeth H Champney, Nienke van der Marel, Michihiro Takami, Marc J Kuchner, Laird M Close, Takayuki Muto, Satoshi Mayama, Michael W McElwain, Misato Fukagawa, Koen Maaskant, Michiel Min, Ray W Russell, Tomoyuki Kudo, Nobuhiko Kusakabe, Jun Hashimoto, Lyu Abe, Eiji Akiyama, Wolfgang Brandner, Timothy D Brandt, Joseph Carson, Thayne Currie, Sebastian E Egner, Markus Feldt, Miwa Goto, Olivier Guyon, Yutaka Hayano, Masahiko Hayashi, Saeko Hayashi, Thomas Henning, Klaus Hodapp, Miki Ishii, Masanori Iye, Markus Janson, Ryo Kandori, Gillian R Knapp, Masayuki Kuzuhara, Jungmi Kwon, Taro Matsuo, Shoken Miyama, Jun-Ichi Morino, Amaya Moro-Martin, Tetsuo Nishimura, Tae-Soo Pyo, Eugene Serabyn, Takuya Suenaga, Hiroshi Suto, Ryuji Suzuki, Yasuhiro Takahashi, Naruhisa Takato, Hiroshi Terada, Christian Thalmann, Daigo Tomono, Edwin L Turner, Makoto Watanabe, John P Wisniewski, Toru Yamada, Hideki Takami, Tomonori Usuda, and Motohide Tamura. Seeds adaptive optics imaging of the asymmetric transition disk oph irs 48 in scattered light. *The Astrophysical Journal*, 798(2):132, January 2015.

Misato Fukagawa, Masahiko Hayashi, Motohide Tamura, Yoichi Itoh, Saeko S Hayashi, Yumiko Oasa, Taku Takeuchi, Jun-Ichi Morino, Koji Murakawa, Shin Oya, Takuya Yamashita, Hiroshi Suto, Satoshi Mayama, Takahiro Naoi, Miki Ishii, Tae-Soo Pyo, Takayuki Nishikawa, Naruhisa Takato, Tomonori Usuda, Hiroyasu Ando, Masanori Iye, Shoken M Miyama, and Norio Kaifu. Spiral structure in the circumstellar disk around ab aurigae. *The Astrophysical Journal*, 605(1):L53–L56, April 2004.

Misato Fukagawa, Motohide Tamura, Yoichi Itoh, Tomoyuki Kudo, Yusuke Imaeda, Yumiko Oasa, Saeko S Hayashi, and Masahiko Hayashi. Near-infrared images of protoplanetary disk surrounding hd 142527. *The Astrophysical Journal*, 636(2):L153–L156, January 2006.

E Furlan, Dan M Watson, M K McClure, P Manoj, C Espaillat, P D'Alessio, N Calvet, K H Kim, B A Sargent, W J Forrest, and L Hartmann. Disk evolution in the three nearby star-forming regions of taurus, chamaeleon, and ophiuchus. *The Astrophysical Journal*, 703(2):1964–1983, October 2009.

D A Golimowski, D R Ardila, J E Krist, M Clampin, H C Ford, G D Illingworth, F Bartko, N Benítez, J P Blakeslee, R J Bouwens, L D Bradley, T J Broadhurst, R A Brown, C J Burrows, E S Cheng, N J G Cross, R Demarco, P D Feldman, M Franx, T Goto, C Gronwall, G F Hartig, B P Holden, N L Homeier, L Infante, M J Jee, R A Kimble, M P Lesser, A R Martel, S Mei, F Menanteau, G R Meurer, G K Miley, V Motta, M Postman, P Rosati, M Sirianni, W B Sparks, H D Tran, Z I Tsvetanov, R L White, W Zheng, and A W Zirm. Hubble space telescope acs multiband coronagraphic imaging of the debris disk around β pictoris. *The Astronomical Journal*, 131(6):3109–3130, June 2006.

C Gräfe, S Wolf, V Roccatagliata, J Sauter, and S Ertel. Mid-infrared observations of the transitional disks around dh tauri, dm tauri, and gm aurigae. *Astronomy and Astrophysics*, 533:A89, September 2011.

Thomas P Greene and Charles J Lada. Near-infrared spectra and the evolutionary status of young stellar objects: Results of a 1.1-2.4 micron survey. *Astronomical Journal v.112*, 112:2184, November 1996.

Thomas P Greene, Bruce A Wilking, Philippe Andre, Erick T Young, and Charles J Lada. Further mid-infrared study of the rho ophiuchi cloud young stellar population: Luminosities and masses of pre-main-sequence stars. *Astrophysical Journal*, 434:614–626, October 1994.

N Grosso, T Montmerle, S Bontemps, P André, and E D Feigelson. X-rays and regions of star formation: a combined rosat-hri/near-to-mid ir study of the rho oph dark cloud. *Astronomy and Astrophysics*, 359:113–130, July 2000.

Patrick Hartigan, Lee Hartmann, Scott J Kenyon, Stephen E Strom, and Michael F Skrutskie. Correlations of optical and infrared excesses in t tauri stars. *Astrophysical Journal*, 354:L25–L28, May 1990.

Lee Hartmann. Comments on inferences of star formation histories and birth lines. *The Astrophysical Journal*, 585(1):398–405, March 2003.

J Hashimoto, M Tamura, T Muto, T Kudo, M Fukagawa, T Fukue, M Goto, C A Grady, T Henning, K Hodapp, M Honda, S Inutsuka, E Kokubo, G Knapp, M W McElwain, M Momose, N Ohashi, Y K Okamoto, M Takami, E L Turner, J Wisniewski, M Janson, L Abe, W Brandner, J Carson, S Egner, M Feldt, T Golota, O Guyon, Y Hayano, M Hayashi, S Hayashi, M Ishii, R Kandori, N Kusakabe, T Matsuo, S Mayama, S Miyama, J I Morino, A Moro-Martin, T Nishimura, T S Pyo, H Suto, R Suzuki, N Takato, H Terada, C Thalmann, D Tomono, M Watanabe, T Yamada, H Takami, and T Usuda. Direct imaging of fine structures in giant planet-forming regions of the protoplanetary disk around ab aurigae. *The Astrophysical Journal Letters*, 729(2):L17, March 2011.

J Hashimoto, R Dong, T Kudo, M Honda, M K McClure, Z Zhu, T Muto, J Wisniewski, L Abe, W Brandner, T Brandt, J Carson, S Egner, M Feldt, M Fukagawa, M Goto, C A Grady, O Guyon, Y Hayano, M Hayashi, S Hayashi, T Henning, K Hodapp, M Ishii, M Iye, M Janson, R Kandori, G Knapp, N Kusakabe, M Kuzuhara, J Kwon, T Matsuo, S Mayama, M W McElwain, S Miyama, J I Morino, A Moro-Martin, T Nishimura, T S Pyo, G Serabyn, T Suenaga, H Suto, R Suzuki, Y Takahashi, M Takami, N Takato, H Terada, C Thalmann, D Tomono, E L Turner, M Watanabe, T Yamada, H Takami, T Usuda, and M Tamura. Polarimetric imaging of large cavity structures in the pre-transitional protoplanetary disk around pds 70: Observations of the disk. *The Astrophysical Journal*, 758(1):L19, September 2012.

J Hashimoto, T Tsukagoshi, J M Brown, R Dong, T Muto, Z Zhu, J Wisniewski, N Ohashi, T Kudo, N Kusakabe, L Abe, E Akiyama, W Brandner, T Brandt, J Carson, T Currie, S Egner, M Feldt, C A Grady, O Guyon, Y Hayano, M Hayashi, S Hayashi, T Henning, K Hodapp, M Ishii, M Iye, M Janson, R Kandori, G Knapp, M Kuzuhara, J Kwon, T Matsuo, M W McElwain, S Mayama, K Mede, S Miyama, J I Morino, A Moro-Martin, T Nishimura, T S Pyo, G Serabyn, T Suenaga, H Suto, R Suzuki, Y Takahashi, M Takami, N Takato, H Terada, C Thalmann, D Tomono, E L Turner, M Watanabe, T Yamada, H Takami, T Usuda, and M Tamura. The structure of pre-transitional protoplanetary disks. ii. azimuthal asymmetries, different radial distributions of large and small dust grains in pds 70based on data collected at the subaru telescope, which is operated by the national astronomical observatory of japan. , the submillimeter array is a joint project between the smithsonian astrophysical observatory and the academia sinica institute of astronomy and astrophysics and is funded by the smithsonian institution and the academia sinica. *The Astrophysical Journal*, 799 (1):43, January 2015.

Timothy G Hawarden, S K Leggett, Michael B Letawsky, David R Ballantyne, and Mark M Casali. Jhk standard stars for large telescopes: the ukirt fundamental and extended lists. *Monthly Notices of the Royal Astronomical Society*, 325(2):563–574, August 2001.

Yutaka Hayano, Hideki Takami, Olivier Guyon, Shin Oya, Masayuki Hattori, Yoshihiko Saito, Makoto Watanabe, Naoshi Murakami, Yosuke Minowa, Meguru Ito, Stephen Colley, Michael Eldred, Taras Golota, Matthew Dinkins, Nobunari Kashikawa, and Masanori Iye. Current status of the laser guide star adaptive optics system for subaru telescope. *Adaptive Optics Systems. Edited by Hubin*, 7015: 701510–701510–8, July 2008.

Yutaka Hayano, Hideki Takami, Shin Oya, Masayuki Hattori, Yoshihiko Saito, Makoto Watanabe, Olivier Guyon, Yosuke Minowa, Sebastian E Egner, Meguru Ito, Vincent Garrel, Stephen Colley, Taras Golota, and Masanori Iye. Commissioning status of subaru laser guide star adaptive optics system. In Brent L Ellerbroek, Michael Hart, Norbert Hubin, and Peter L Wizinowich, editors, *Proceedings of the SPIE*, pages 77360N–77360N–8. Subaru Telescope, National Astronomical Observatory of Japan, United States, SPIE, July 2010.

C Hayashi and T Nakano. Evolution of stars of small masses in the pre-main-sequence stages. *Progress of Theoretical Physics*, 30(4):460–474, October 1963.

C Hayashi, K Nakazawa, and Y Nakagawa. Formation of the solar system. *IN: Protostars and planets II (A86-12626 03-90). Tucson*, pages 1100–1153, 1985.

Sasha Hinkley, Ben R Oppenheimer, Rémi Soummer, Douglas Brenner, James R Graham, Marshall D Perrin, Anand Sivaramakrishnan, James P Lloyd, Lewis C Jr Roberts, and Jeffrey Kuhn. Speckle suppression through dual imaging polarimetry, and a ground-based image of the hr 4796a circumstellar disk. *The Astrophysical Journal*, 701(1):804–810, August 2009.

Wayne S Holland, Jane S Greaves, B Zuckerman, R A Webb, Chris McCarthy, Iain M Coulson, D M Walther, William R F Dent, Walter K Gear, and Ian Robson. Submillimetre images of dusty debris around nearby stars. *Nature*, 392(6):788–791, April 1998.

J R Houck, T L Roellig, J van Cleve, W J Forrest, T Herter, C R Lawrence, K Matthews, H J Reitsema, B T Soifer, D M Watson, D Weedman, M Huisjen, J Troeltzsch, D J Barry, J Bernard-Salas, C E Blacken, B R Brandl, V Charmandaris, D Devost, G E Gull, P Hall, C P Henderson, S J U Higdon, B E Pirger, J Schoenwald, G C Sloan, K I Uchida, P N Appleton, L Armus, M J Burgdorf, S B Fajardo-Acosta, C J Grillmair, J G Ingalls, P W Morris, and H I Teplitz. The infrared spectrograph (irs) on the spitzer space telescope. *The Astrophysical Journal Supplement Series*, 154(1):18–24, September 2004.

R Hueso and T Guillot. Evolution of protoplanetary disks: constraints from dm tauri and gm aurigae. *Astronomy and Astrophysics*, 442(2):703–725, November 2005.

A Meredith Hughes, Sean M Andrews, Catherine Espaillat, David J Wilner, Nuria Calvet, Paola D'Alessio, Chunhua Qi, Jonathan P Williams, and Michiel R Hogerheijde. A spatially resolved inner hole in the disk around gm aurigae. *The Astrophysical Journal*, 698(1):131–142, June 2009.

A Meredith Hughes, Charles L H Hull, David J Wilner, and Richard L Plambeck. Interferometric upper limits on millimeter polarization of the disks around dg tau, gm aur, and mwc 480. *The Astronomical Journal*, 145(4):115, April 2013.

S Ida and D N C Lin. Toward a deterministic model of planetary formation. i. a desert in the mass and semimajor axis distributions of extrasolar planets. *The Astrophysical Journal*, 604(1):388–413, March 2004a.

Shigeru Ida and D N C Lin. Toward a deterministic model of planetary formation. ii. the formation and retention of gas giant planets around stars with a range of metallicities. *The Astrophysical Journal*, 616(1):567–572, November 2004b.

Laura Ingleby, Catherine Espaillat, Nuria Calvet, Michael Sitko, Ray Russell, and Elizabeth Champney. Using fuv to ir variability to probe the star-disk connection in the transitional disk of gm aur. *The Astrophysical Journal*, 805(2):149, June 2015.

Shu-ichiro Inutsuka, Masahiro N Machida, and Tomoaki Matsumoto. Emergence of protoplanetary disks and successive formation of gaseous planets by gravitational instability. *The Astrophysical Journal Letters*, 718(2):L58–L62, August 2010.

M J Ireland and A L Kraus. The disk around coku tauri/4: Circumbinary, not transitionaldata presented herein were obtained at the w. m. keck observatory, which is operated as a scientific partnership among the california institute of technology, the university of california, and the national aeronautics and space administration. the observatory was made possible by the generous financial support of the w. m. keck foundation. *The Astrophysical Journal*, 678(1):L59, May 2008.

Yoichi Itoh, Masahiko Hayashi, Motohide Tamura, Takashi Tsuji, Yumiko Oasa, Misato Fukagawa, Saeko S Hayashi, Takahiro Naoi, Miki Ishii, Satoshi Mayama, Jun-Ichi Morino, Takuya Yamashita, Tae-Soo Pyo, Takayuki Nishikawa, Tomonori Usuda, Koji Murakawa, Hiroshi Suto, Shin Oya, Naruhisa Takato, Hiroyasu Ando, Shoken M Miyama, Naoto Kobayashi, and Norio Kaifu. A young brown dwarf companion to dh tauri. *The Astrophysical Journal*, 620(2):984–993, February 2005.

Brian Jackson, Richard Greenberg, and Rory Barnes. Tidal heating of extrasolar planets. *The Astrophysical Journal*, 681(2):1631–1638, July 2008.

Lucie Jilkova and Simon Portegies Zwart. A debris disc under the influence of a wide planetary-mass companion: the system of hd 106906. *Monthly Notices of the Royal Astronomical Society*, 451(1): 5323–5331, July 2015.

N Jovanovic, F Martinache, O Guyon, C Clergeon, G Singh, T Kudo, V Garrel, K Newman, D Doughty, J Lozi, J Males, Y Minowa, Y Hayano, N Takato, J Morino, J Kuhn, E Serabyn, B Norris, P Tuthill, G Schworer, P Stewart, L Close, E Huby, G Perrin, S Lacour, L Gauchet, S Vievard, N Murakami, F Oshiyama, N Baba, T Matsuo, J Nishikawa, M Tamura, O Lai, F Marchis, G Duchêne, T Kotani, and J Woillez. The subaru coronagraphic extreme adaptive optics system: Enabling high-contrast imaging on solar-system scales. *Publications of the Astronomical Society of the Pacific*, 127(955): 890–910, September 2015.

Paul Kalas, James R Graham, Eugene Chiang, Michael P Fitzgerald, Mark Clampin, Edwin S Kite, Karl Stapelfeldt, Christian Marois, and John Krist. Optical images of an exosolar planet 25 light-years from earth. *Science*, 322(5):1345–1348, November 2008.

M F Kessler, J A Steinz, M E Anderegg, J Clavel, G Drechsel, P Estaria, J Faelker, J R Riedinger, A Robson, B G Taylor, and S Ximénez de Ferrán. The infrared space observatory (iso) mission. *Astronomy and Astrophysics*, 315:L27–L31, November 1996.

P D Klaassen, A Juhasz, G S Mathews, J C Mottram, I De Gregorio-Monsalvo, E F van Dishoeck, S Takahashi, E Akiyama, E Chapillon, D Espada, A Hales, M R Hogerheijde, M Rawlings, M Schmalzl, and L Testi. Alma detection of the rotating molecular disk wind from the young star hd 163296. *Astronomy and Astrophysics*, 555:A73, July 2013.

W Kley and G Dirksen. Disk eccentricity and embedded planets. *Astronomy and Astrophysics*, 447(1): 369–377, February 2006.

W Kley and R P Nelson. Planet-disk interaction and orbital evolution. *Annual Review of Astronomy and Astrophysics*, 50(1):211–249, September 2012.

Naoto Kobayashi, Alan T Tokunaga, Hiroshi Terada, Miwa Goto, Mark Weber, Robert Potter, Peter M Onaka, Gregory K Ching, Tony T Young, Kent Fletcher, Douglas Neil, Louis Robertson, Daniel Cook, Masatoshi Imanishi, and David W Warren. Ircs: infrared camera and spectrograph for the subaru telescope. *Proc. SPIE Vol. 4008*, 4008:1056–1066, August 2000.

C M Koepferl, B Ercolano, J Dale, P S Teixeira, T Ratzka, and L Spezzi. Disc clearing of young stellar objects: evidence for fast inside-out dispersal. *Monthly Notices of the Royal Astronomical Society*, 428(4):3327–3354, February 2013.

D W Koerner, A I Sargent, and S V W Beckwith. A rotating gaseous disk around the t tauri star gm aurigae. *Icarus*, 106(1):2–10, November 1993.

Eiichiro Kokubo and Shigeru Ida. Formation of protoplanet systems and diversity of planetary systems. *The Astrophysical Journal*, 581(1):666–680, December 2002.

Adam L Kraus and Lynne A Hillenbrand. Unusually wide binaries: Are they wide or unusual? *The Astrophysical Journal*, 703(2):1511–1530, October 2009.

Adam L Kraus and Michael J Ireland. Lkca 15: A young exoplanet caught at formation? *The Astrophysical Journal*, 745(1):5, January 2012.

Adam L Kraus, Michael J Ireland, Frantz Martinache, and James P Lloyd. Mapping the shores of the brown dwarf desert. i. upper scorpius. *The Astrophysical Journal*, 679(1):762–782, May 2008.

Adam L Kraus, Michael J Ireland, Frantz Martinache, and James P Lloyd. Searching for young planets with sparse aperture masking. *COOL STARS*, 1094(1):453–456, February 2009.

Adam L Kraus, Michael J Ireland, Frantz Martinache, and Lynne A Hillenbrand. Mapping the shores of the brown dwarf desert. ii. multiple star formation in taurus-auriga. *The Astrophysical Journal*, 731(1):8, April 2011.

Adam L Kraus, Michael J Ireland, Lucas A Cieza, Sasha Hinkley, Trent J Dupuy, Brendan P Bowler, and Michael C Liu. Three wide planetary-mass companions to fw tau, roxs 12, and roxs 42b. *The Astrophysical Journal*, 781(1):20, January 2014.

Adam L Kraus, Sean M Andrews, Brendan P Bowler, Gregory Herczeg, Michael J Ireland, Michael C Liu, Stanimir Metchev, and Kelle L Cruz. An alma disk mass for the candidate protoplanetary companion to fw tau. *The Astrophysical Journal Letters*, 798(1):L23, January 2015.

O Krauss and G Wurm. Photophoresis and the pile-up of dust in young circumstellar disks. *The Astrophysical Journal*, 630(2):1088–1092, September 2005.

John E Krist, Karl R Stapelfeldt, Francois Ménard, Deborah L Padgett, and Christopher J Burrows. Wfpc2 images of a face-on disk surrounding tw hydrae. *The Astrophysical Journal*, 538(2):793–800, August 2000.

Shiv S Kumar. The structure of stars of very low mass. *Astrophysical Journal*, 137:1121, May 1963a.

Shiv S Kumar. The helmholtz-kelvin time scale for stars of very low mass. *Astrophysical Journal*, 137: 1126, May 1963b.

M Kuzuhara, M Tamura, M Ishii, T Kudo, S Nishiyama, and R Kandori. The widest-separation substellar companion candidate to a binary t tauri star. *The Astronomical Journal*, 141(4):119, March 2011.

M Kuzuhara, M Tamura, T Kudo, M Janson, R Kandori, T D Brandt, C Thalmann, D Spiegel, B Biller, J Carson, Y Hori, R Suzuki, A Burrows, T Henning, E L Turner, M W McElwain, A Moro-Martin, T Suenaga, Y H Takahashi, J Kwon, P Lucas, L Abe, W Brandner, S Egner, M Feldt, H Fujiwara, M Goto, C A Grady, O Guyon, J Hashimoto, Y Hayano, M Hayashi, S S Hayashi, K W Hodapp, M Ishii, M Iye, G R Knapp, T Matsuo, S Mayama, S Miyama, J I Morino, J Nishikawa, T Nishimura, T Kotani, N Kusakabe, T S Pyo, E Serabyn, H Suto, M Takami, N Takato, H Terada, D Tomono, M Watanabe, J P Wisniewski, T Yamada, H Takami, and T Usuda. Direct imaging of a cold jovian exoplanet in orbit around the sun-like star gj 504. *The Astrophysical Journal*, 774(1):11, September 2013.

C J Lada and B A Wilking. The nature of the embedded population in the rho ophiuchi dark cloud - mid-infrared observations. *Astrophysical Journal*, 287:610–621, December 1984.

Charles J Lada. Star formation - from ob associations to protostars. In *IN: Star forming regions; Proceedings of the Symposium*, pages 1–17. Sreward Observatory, Tucson, AZ, 1987.

David Lafrenière, Christian Marois, René Doyon, Daniel Nadeau, and Étienne Artigau. A new algorithm for point-spread function subtraction in high-contrast imaging: A demonstration with angular differential imaging. *The Astrophysical Journal*, 660(1):770–780, May 2007.

David Lafrenière, Ray Jayawardhana, and Marten H van Kerkwijk. Direct imaging and spectroscopy of a planetary-mass candidate companion to a young solar analog. *The Astrophysical Journal*, 689(2): L153–L156, December 2008.

A M Lagrange, A Boccaletti, J Milli, G Chauvin, M Bonnefoy, D Mouillet, J C Augereau, J H Girard, S Lacour, and D Apai. The position of β pictoris b position relative to the debris disk. *Astronomy and Astrophysics*, 542:A40, June 2012.

A Lawrence, S J Warren, O Almaini, A C Edge, N C Hambly, R F Jameson, P Lucas, M Casali, A Adamson, S Dye, J P Emerson, S Foucaud, P Hewett, P Hirst, S T Hodgkin, M J Irwin, N Lodieu, R G McMahon, C Simpson, I Smail, D Mortlock, and M Folger. The ukirt infrared deep sky survey (ukidss). *Monthly Notices of the Royal Astronomical Society*, 379(4):1599–1617, August 2007.

Robert Les and Min-Kai Lin. Gap formation and stability in non-isothermal protoplanetary discs. *Monthly Notices of the Royal Astronomical Society*, 450(2):1503–1513, June 2015.

D N C Lin and J Papaloizou. On the tidal interaction between protoplanets and the primordial solar nebula. ii - self-consistent nonlinear interaction. *Astrophysical Journal*, 307:395–409, August 1986a.

D N C Lin and John Papaloizou. On the tidal interaction between protoplanets and the protoplanetary disk. iii - orbital migration of protoplanets. *Astrophysical Journal*, 309:846–857, October 1986b.

Michael C Liu, Joan Najita, and Alan T Tokunaga. A survey for circumstellar disks around young substellar objects. *The Astrophysical Journal*, 585(1):372–391, March 2003.

N Lodieu, N C Hambly, R F Jameson, and S T Hodgkin. Near-infrared cross-dispersed spectroscopy of brown dwarf candidates in the uppersco association. *Monthly Notices of the Royal Astronomical Society*, 383(4):1385–1396, February 2008.

Laurent Loinard, Rosa M Torres, Amy J Mioduszewski, and Luis F Rodriguez. A preliminary vlba distance to the core of ophiuchus, with an accuracy of 4 *The Astrophysical Journal*, 675(1):L29–L32, March 2008.

M Lombardi, C J Lada, and J Alves. 2mass wide field extinction maps. ii. the ophiuchus and the lupus cloud complexes. *Astronomy and Astrophysics*, 489(1):143–156, October 2008.

Leslie W Looney, Lee G Mundy, and W J Welch. Unveiling the circumstellar envelope and disk: A subarcsecond survey of circumstellar structures. *The Astrophysical Journal*, 529(1):477–498, January 2000.

K L Luhman and G H Rieke. Low-mass star formation and the initial mass function in the ρ ophiuchi cloud core. *The Astrophysical Journal*, 525(1):440–465, November 1999.

K L Luhman, J C Wilson, W Brandner, M F Skrutskie, M J Nelson, J D Smith, D E Peterson, M C Cushing, and E Young. Discovery of a young substellar companion in chamaeleon. *The Astrophysical Journal*, 649(2):894–899, October 2006.

K L Luhman, B M Patten, M Marengo, M T Schuster, J L Hora, R G Ellis, J R Stauffer, S M Sonnett, E Winston, R A Gutermuth, S T Megeath, D E Backman, T J Henry, M W Werner, and G G Fazio. Discovery of two t dwarf companions with the spitzer space telescope. *The Astrophysical Journal*, 654 (1):570–579, January 2007.

M Malik, F Meru, L Mayer, and M Meyer. On the gap-opening criterion of migrating planets in protoplanetary disks. *The Astrophysical Journal*, 802(1):56, March 2015.

E E Mamajek. On the distance to the ophiuchus star-forming region. *Astronomische Nachrichten*, 329 (1):10–14, January 2008.

S Marino, S Perez, and S Casassus. Shadows cast by a warp in the hd 142527 protoplanetary disk. *The Astrophysical Journal Letters*, 798(2):L44, January 2015.

Christian Marois, David Lafrenière, René Doyon, Bruce Macintosh, and Daniel Nadeau. Angular differential imaging: A powerful high-contrast imaging technique. *The Astrophysical Journal*, 641(1): 556–564, April 2006.

Christian Marois, Bruce Macintosh, Travis Barman, B Zuckerman, Inseok Song, Jennifer Patience, David Lafrenière, and René Doyon. Direct imaging of multiple planets orbiting the star hr 8799. *Science*, 322(5):1348–1352, November 2008.

Kenneth A Marsh and Michael J Mahoney. Evidence for unseen companions around t tauri stars. *Astrophysical Journal*, 395:L115–L118, August 1992.

A Matter, L Labadie, J C Augereau, J Kluska, A Crida, A Carmona, J F Gonzalez, W F Thi, J B Le Bouquin, J Olofsson, and B Lopéz. Inner disk clearing around the herbig ae star hd 139614: Evidence for a planet-induced gap ? *arXiv.org*, page 3093, October 2015.

S Mayama, J Hashimoto, T Muto, T Tsukagoshi, N Kusakabe, M Kuzuhara, Y Takahashi, T Kudo, R Dong, M Fukagawa, M Takami, M Momose, J P Wisniewski, K Follette, L Abe, E Akiyama, W Brandner, T Brandt, J Carson, S Egner, M Feldt, M Goto, C A Grady, O Guyon, Y Hayano, M Hayashi, S Hayashi, T Henning, K W Hodapp, M Ishii, M Iye, M Janson, R Kandori, J Kwon, G R Knapp, T Matsuo, M W McElwain, S Miyama, J I Morino, A Moro-Martin, T Nishimura, T S Pyo, E Serabyn, H Suto, R Suzuki, N Takato, H Terada, C Thalmann, D Tomono, E L Turner, M Watanabe, T Yamada, H Takami, T Usuda, and M Tamura. Subaru imaging of asymmetric features in a transitional disk in upper scorpius. *The Astrophysical Journal Letters*, 760(2):L26, December 2012.

Satoshi Mayama, Motohide Tamura, Tomoyuki Hanawa, Tomoaki Matsumoto, Miki Ishii, Tae-Soo Pyo, Hiroshi Suto, Takahiro Naoi, Tomoyuki Kudo, Jun Hashimoto, Shogo Nishiyama, Masayuki Kuzuhara, and Masahiko Hayashi. Direct imaging of bridged twin protoplanetary disks in a young multiple star. *Science*, 327(5):306–308, January 2010.

Michel Mayor and Didier Queloz. A jupiter-mass companion to a solar-type star. *Nature*, 378(6):355–359, November 1995.

M K McClure, E Furlan, P Manoj, K L Luhman, D M Watson, W J Forrest, C Espaillat, N Calvet, P D'Alessio, B Sargent, J J Tobin, and Hsin-Fang Chiang. The evolutionary state of the pre-main sequence population in ophiuchus: A large infrared spectrograph survey. *The Astrophysical Journal Supplement Series*, 188(1):75–122, April 2010.

Michael W McElwain, Stanimir A Metchev, James E Larkin, Matthew Barczys, Christof Iserlohe, Alfred Krabbe, Andreas Quirrenbach, Jason Weiss, and Shelley A Wright. First high-contrast science with an integral field spectrograph: The substellar companion to gq lupi. *The Astrophysical Journal*, 656 (1):505–514, February 2007.

Ian S McLean, A McLean, Stangeby, P. C., Mark R McGovern, Adam J Burgasser, D Elder, J Davy Kirkpatrick, M J Schaffer, L Prato, T E Evans, L L Lao, Sungsoo S Kim, M E Austin, and J G Watkins. The nirspec brown dwarf spectroscopic survey. i. low-resolution near-infrared spectra. *The Astrophysical Journal*, 596(1):561–586, October 2003.

Bruno Merin, Joanna M Brown, Isa Oliveira, Gregory J Herczeg, Ewine F van Dishoeck, Sandrine Bottinelli, Neal J II Evans, Lucas Cieza, Loredana Spezzi, Juan M Alcalá, Paul M Harvey, Geoffrey A Blake, Amelia Bayo, Vincent G Geers, Fred Lahuis, Timo Prusti, Jean-Charles Augereau, Johan Olofsson, Frederick M Walter, and Kuenley Chiu. A spitzer c2d legacy survey to identify and characterize disks with inner dust holes. *The Astrophysical Journal*, 718(2):1200–1223, August 2010.

Farzana Meru and Matthew R Bate. Exploring the conditions required to form giant planets via gravitational instability in massive protoplanetary discs. *Monthly Notices of the Royal Astronomical Society*, 406(4):2279–2288, August 2010.

M Min, L B F M Waters, A de Koter, J W Hovenier, Keller, L. P., and F Markwick-Kemper. The shape and composition of interstellar silicate grains. *Astronomy and Astrophysics*, 462(2):667–676, February 2007.

Munetake Momose, Ayaka Morita, Misato Fukagawa, Takayuki Muto, Taku Takeuchi, Jun Hashimoto, Mitsuhiko Honda, Tomoyuki Kudo, Yoshiko K Okamoto, Kazuhiro D Kanagawa, Hidekazu Tanaka, Carol A Grady, Michael L Sitko, Eiji Akiyama, Thayne Currie, Katherine B Follette, Satoshi Mayama, Nobuhiko Kusakabe, Lyu Abe, Wolfgang Brandner, Timothy D Brandt, Joseph C Carson, Sebastian Egner, Markus Feldt, Miwa Goto, Olivier Guyon, Yutaka Hayano, Masahiko Hayashi, Saeko S Hayashi, Thomas Henning, Klaus W Hodapp, Miki Ishii, Masanori Iye, Markus Janson, Ryo Kandori, Gillian R Knapp, Masayuki Kuzuhara, Jungmi Kwon, Taro Matsuo, Michael W McElwain, Shoken Miyama, Jun-Ichi Morino, Amaya Moro-Martin, Tetsuo Nishimura, Tae-Soo Pyo, Eugene Serabyn, Takuya Suenaga, Hiroshi Suto, Ryuji Suzuki, Yasuhiro H Takahashi, Michihiro Takami, Naruhisa Takato, Hiroshi Terada, Christian Thalmann, Daigo Tomono, Edwin L Turner, Makoto Watanabe, John Wisniewski, Toru Yamada, Hideki Takami, Tomonori Usuda, and Motohide Tamura. Detailed structure of the outer disk around hd 169142 with polarized light in h-band. *Publications of the Astronomical Society of Japan*, 67(5):83, October 2015.

D Mouillet, J D Larwood, J C B Papaloizou, and A M Lagrange. A planet on an inclined orbit as an explanation of the warp in the beta pictoris disc. *Monthly Notices of the Royal Astronomical Society*, 292:896, December 1997.

G D Mulders, C Dominik, and M Min. Full two-dimensional radiative transfer modelling of the transitional disk lkca 15. *Astronomy and Astrophysics*, 512:A11, March 2010.

T Muto, C A Grady, J Hashimoto, M Fukagawa, J B Hornbeck, M Sitko, R Russell, C Werren, M Curé, T Currie, N Ohashi, Y Okamoto, M Momose, M Honda, S Inutsuka, T Takeuchi, R Dong, L Abe, W Brandner, T Brandt, J Carson, S Egner, M Feldt, T Fukue, M Goto, O Guyon, Y Hayano, M Hayashi, S Hayashi, T Henning, K W Hodapp, M Ishii, M Iye, M Janson, R Kandori, G R Knapp, T Kudo, N Kusakabe, M Kuzuhara, T Matsuo, S Mayama, M W McElwain, S Miyama, J I Morino, A Moro-Martin, T Nishimura, T S Pyo, E Serabyn, H Suto, R Suzuki, M Takami, N Takato, H Terada, C Thalmann, D Tomono, E L Turner, M Watanabe, J P Wisniewski, T Yamada, H Takami, T Usuda,

and M Tamura. Discovery of small-scale spiral structures in the disk of sao 206462 (hd 135344b): Implications for the physical state of the disk from spiral density wave theory. *The Astrophysical Journal*, 748(2):L22, March 2012.

James Muzerolle, Lori E Allen, S Thomas Megeath, Jesus Hernandez, and Robert A Gutermuth. A spitzer census of transitional protoplanetary disks with au-scale inner holes. *The Astrophysical Journal*, 708(2):1107–1118, January 2010.

Koraljka Muzic, Alexander Scholz, Vincent Geers, Ray Jayawardhana, and Motohide Tamura. Substellar objects in nearby young clusters (sonyc). v. new brown dwarfs in ρ ophiuchi. *The Astrophysical Journal*, 744(2):134, January 2012.

Joan R Najita, Stephen E Strom, and James Muzerolle. Demographics of transition objects. *Monthly Notices of the Royal Astronomical Society*, 378(1):369–378, June 2007.

Joan R Najita, Sean M Andrews, and James Muzerolle. Demographics of transition discs in ophiuchus and taurus. *Monthly Notices of the Royal Astronomical Society*, 450(4):3559–3567, July 2015.

T Nakajima, B R Oppenheimer, S R Kulkarni, D A Golimowski, K Matthews, and S T Durrance. Discovery of a cool brown dwarf. *Nature*, 378(6):463–465, November 1995.

A Natta, L Testi, and S Randich. Accretion in the ρ-ophiuchi pre-main sequence stars. *Astronomy and Astrophysics*, 452(1):245–252, June 2006.

Marie-Eve Naud, Étienne Artigau, Lison Malo, Loïc Albert, René Doyon, David Lafrenière, Jonathan Gagné, Didier Saumon, Caroline V Morley, France Allard, Derek Homeier, Charles A Beichman, Christopher R Gelino, and Anne Boucher. Discovery of a wide planetary-mass companion to the young m3 star gu psc. *The Astrophysical Journal*, 787(1):5, May 2014.

R Neuhäuser, C Ginski, T O B Schmidt, and M Mugrauer. Further deep imaging of hr 7329 a (η tel a) and its brown dwarf companion b. *Monthly Notices of the Royal Astronomical Society*, 416(2): 1430–1435, September 2011.

Daehyeon Oh, Jun Hashimoto, Motohide Tamura, John Wisniewski, Eiji Akiyama, Thayne Currie, Satoshi Mayama, Michihiro Takami, Christian Thalmann, Tomoyuki Kudo, Nobuhiko Kusakabe, Lyu Abe, Wolfgang Brandner, Timothy D Brandt, Joseph C Carson, Sebastian Egner, Markus Feldt, Miwa Goto, Carol A Grady, Olivier Guyon, Yutaka Hayano, Masahiko Hayashi, Saeko S Hayashi, Thomas Henning, Klaus W Hodapp, Miki Ishii, Masanori Iye, Markus Janson, Ryo Kandori, Gillian R Knapp, Masayuki Kuzuhara, Jungmi Kwon, Taro Matsuo, Michael W McElwain, Shoken Miyama, Jun-Ichi Morino, Amaya Moro-Martin, Tetsuo Nishimura, Tae-Soo Pyo, Eugene Serabyn, Takuya Suenaga, Hiroshi Suto, Ryuji Suzuki, Yasuhiro H Takahashi, Naruhisa Takato, Hiroshi Terada, Edwin L Turner, Makoto Watanabe, Toru Yamada, Hideki Takami, and Tomonori Usuda. Near-infrared imaging polarimetry of LkCa15: A possible warped inner disk. *Publications of the Astronomical Society of Japan*, 68(2):L3, April 2016.

Daehyun Oh. Widest separation and the lowest mass objects among planetary-mass companion candidates around young stars. *The Tenth Pacific Rim Conference on Stellar Astrophysics. ASP Conference Series*, 482:59, August 2014.

J Olofsson, J C Augereau, E F van Dishoeck, B Merín, F Lahuis, J Kessler-Silacci, C P Dullemond, I Oliveira, G A Blake, A C A Boogert, J M Brown, N J II Evans, V Geers, C Knez, J L Monin, and K Pontoppidan. C2d spitzer-irs spectra of disks around t tauri stars. iv. crystalline silicates. *Astronomy and Astrophysics*, 507(1):327–345, November 2009.

B R Oppenheimer, S R Kulkarni, K Matthews, and T Nakajima. Infrared spectrum of the cool brown dwarf gl 229b. *Science*, 270(5):1478–1479, December 1995.

J E Owen, B Ercolano, C J Clarke, and R D Alexander. Radiation-hydrodynamic models of x-ray and euv photoevaporating protoplanetary discs. *Monthly Notices of the Royal Astronomical Society*, 401 (3):1415–1428, January 2010.

James E Owen. Accreting planets as dust dams in "transition" disks. *The Astrophysical Journal*, 789 (1):59, July 2014.

James E Owen, Cathie J Clarke, and Barbara Ercolano. On the theory of disc photoevaporation. *Monthly Notices of the Royal Astronomical Society*, 422(3):1880–1901, May 2012.

S J Paardekooper and G Mellema. Dust flow in gas disks in the presence of embedded planets. *Astronomy and Astrophysics*, 453(3):1129–1140, July 2006.

Deborah L Padgett, Lucas Cieza, Karl R Stapelfeldt, Neal J II Evans, David Koerner, Anneila Sargent, Misato Fukagawa, Ewine F van Dishoeck, Jean-Charles Augereau, Lori Allen, Geoff Blake, Tim Brooke, Nicholas Chapman, Paul Harvey, Alicia Porras, Shih-Ping Lai, Lee Mundy, Philip C Myers, William Spiesman, and Zahed Wahhaj. The spitzer c2d survey of weak-line t tauri stars. i. initial results. *The Astrophysical Journal*, 645(2):1283–1296, July 2006.

Deborah L Padgett, Luisa M Rebull, Karl R Stapelfeldt, Nicholas L Chapman, Shih-Ping Lai, Lee G Mundy, Neal J II Evans, Timothy Y Brooke, Lucas A Cieza, William J Spiesman, Alberto Noriega-Crespo, Caer-Eve McCabe, Lori E Allen, Geoffrey A Blake, Paul M Harvey, Tracy L Huard, Jes K Jørgensen, David W Koerner, Philip C Myers, Annelia I Sargent, Peter Teuben, Ewine F van Dishoeck, Zahed Wahhaj, and Kaisa E Young. The spitzer c2d survey of large, nearby, interstellar clouds. vii. ophiuchus observed with mips. *The Astrophysical Journal*, 672(2):1013–1037, January 2008.

J C B Papaloizou, R P Nelson, W Kley, F S Masset, and P Artymowicz. Disk-planet interactions during planet formation. *Protostars and Planets V*, pages 655–668, 2007.

Laura M Pérez, John M Carpenter, Claire J Chandler, Andrea Isella, Sean M Andrews, Luca Ricci, Nuria Calvet, Stuartt A Corder, Adam T Deller, Cornelis P Dullemond, Jane S Greaves, Robert J Harris, Thomas Henning, Woojin Kwon, Joseph Lazio, Hendrik Linz, Lee G Mundy, Anneila I Sargent, Shaye Storm, Leonardo Testi, and David J Wilner. Constraints on the radial variation of grain growth in the as 209 circumstellar disk. *The Astrophysical Journal Letters*, 2012.

Laura M Pérez, Andrea Isella, John M Carpenter, and Claire J Chandler. Large-scale asymmetries in the transitional disks of sao 206462 and sr 21. *The Astrophysical Journal Letters*, 783(1):L13, March 2014.

Laura M Pérez, Claire J Chandler, Andrea Isella, John M Carpenter, Sean M Andrews, Nuria Calvet, Stuartt A Corder, Adam T Deller, Cornelis P Dullemond, Jane S Greaves, Robert J Harris, Thomas Henning, Woojin Kwon, Joseph Lazio, Hendrik Linz, Lee G Mundy, Luca Ricci, Anneila I Sargent, Shaye Storm, Marco Tazzari, Leonardo Testi, and David J Wilner. Grain growth in the circumstellar disks of the young stars cy tau and doar 25. *The Astrophysical Journal*, 813(1):41, November 2015.

Marshall D Perrin, Glenn Schneider, Gaspard Duchene, Christophe Pinte, Carol A Grady, John P Wisniewski, and Dean C Hines. The case of ab aurigae's disk in polarized light: Is there truly a gap? *The Astrophysical Journal Letters*, 707(2):L132–L136, December 2009.

V Piétu, S Guilloteau, and A Dutrey. Sub-arcsec imaging of the ab aur molecular disk and envelope at millimeter wavelengths: a non keplerian disk. *Astronomy and Astrophysics*, 443(3):945–954, December 2005.

V Piétu, A Dutrey, S Guilloteau, E Chapillon, and J Pety. Resolving the inner dust disks surrounding lkca 15 and mwc 480 at mm wavelengths. *Astronomy and Astrophysics*, 460(3):L43–L47, December 2006.

V Piétu, A Dutrey, and S Guilloteau. Probing the structure of protoplanetary disks: a comparative study of dm tau, lkca 15, and mwc 480. *Astronomy and Astrophysics*, 467(1):163–178, May 2007.

P Pinilla, M Benisty, and T Birnstiel. Ring shaped dust accumulation in transition disks. *Astronomy and Astrophysics*, 545:A81, September 2012a.

P Pinilla, T Birnstiel, L Ricci, C P Dullemond, A L Uribe, L Testi, and A Natta. Trapping dust particles in the outer regions of protoplanetary disks. *Astronomy and Astrophysics*, 538:A114, February 2012b.

P Pinilla, J de Boer, M Benisty, A Juhasz, M de Juan Ovelar, C Dominik, H Avenhaus, T Birnstiel, J H Girard, N Huelamo, A Isella, and J Milli. Variability and dust filtration in the transition disk j160421.7-213028 observed in optical scattered light. *Astronomy and Astrophysics*, 584:L4, December 2015.

James B Pollack, Olenka Hubickyj, Peter Bodenheimer, Jack J Lissauer, Morris Podolak, and Yuval Greenzweig. Formation of the giant planets by concurrent accretion of solids and gas. *Icarus*, 124(1): 62–85, November 1996.

Jorg-Uwe Pott, Marshall D Perrin, Elise Furlan, Andrea M Ghez, Tom M Herbst, and Stanimir Metchev. Ruling out stellar companions and resolving the innermost regions of transitional disks with the keck interferometer. *The Astrophysical Journal*, 710(1):265–278, February 2010.

Sascha P Quanz, Hans Martin Schmid, Kerstin Geissler, Michael R Meyer, Thomas Henning, Wolfgang Brandner, and Sebastian Wolf. Very large telescope/naco polarimetric differential imaging of hd100546—disk structure and dust grain properties between 10 and 140 au. *The Astrophysical Journal*, 738(1):23, September 2011.

Valerie A Rapson, Joel H Kastner, Sean M Andrews, Dean C Hines, Bruce Macintosh, Max Millar-Blanchaer, and Motohide Tamura. Scattered light from dust in the cavity of the v4046 sgr transition disk. *The Astrophysical Journal Letters*, 803(1):L10, April 2015.

S N Raymond, P J Armitage, A Moro-Martin, M Booth, M C Wyatt, J C Armstrong, A M Mandell, F Selsis, and A A West. Debris disks as signposts of terrestrial planet formation. ii. dependence of exoplanet architectures on giant planet and disk properties. *Astronomy and Astrophysics*, 541:A11, May 2012.

Bo Reipurth and Cathie Clarke. The formation of brown dwarfs as ejected stellar embryos. *The Astronomical Journal*, 122(1):432–439, July 2001.

W K M Rice, Kenneth Wood, P J Armitage, B A Whitney, and J E Bjorkman. Constraints on a planetary origin for the gap in the protoplanetary disc of gm aurigae. *Monthly Notice of the Royal Astronomical Society*, 342(1):79–85, June 2003.

W K M Rice, Philip J Armitage, Kenneth Wood, and G Lodato. Dust filtration at gap edges: implications for the spectral energy distributions of discs with embedded planets. *Monthly Notices of the Royal Astronomical Society*, 373(4):1619–1626, December 2006.

Evan A Rich, John P Wisniewski, Satoshi Mayama, Timothy D Brandt, Jun Hashimoto, Tomoyuki Kudo, Nobuhiko Kusakabe, Catherine Espaillat, Lyu Abe, Eiji Akiyama, Wolfgang Brandner, Joseph C Carson, Thayne Currie, Sebastian Egner, Markus Feldt, Kate Follette, Miwa Goto, Carol A Grady, Olivier Guyon, Yutaka Hayano, Masahiko Hayashi, Saeko S Hayashi, Thomas Henning, Klaus W Hodapp, Miki Ishii, Masanori Iye, Markus Janson, Ryo Kandori, Gillian R Knapp, Masayuki Kuzuhara, Jungmi Kwon, Taro Matsuo, Michael W McElwain, Shoken Miyama, Jun-Ichi Morino, Amaya Moro-Martin, Tetsuo Nishimura, Tae-Soo Pyo, Chunhua Qi, Eugene Serabyn, Takuya Suenaga, Hiroshi Suto, Ryuji Suzuki, Yasuhiro H Takahashi, Michihiro Takami, Naruhisa Takato, Hiroshi Terada, Christian Thalmann, Daigo Tomono, Edwin L Turner, Makoto Watanabe, Toru Yamada, Hideki Takami, Tomonori Usuda, and Motohide Tamura. Near-ir polarized scattered light imagery of the doar 28 transitional disk. *The Astronomical Journal*, 150(3):86, September 2015.

Naomi A Ridge, James Di Francesco, Helen Kirk, Di Li, Alyssa A Goodman, João F Alves, Héctor G Arce, Michelle A Borkin, Paola Caselli, Jonathan B Foster, Mark H Heyer, Doug Johnstone, David A Kosslyn, Marco Lombardi, Jaime E Pineda, Scott L Schnee, and Mario Tafalla. The complete survey of star-forming regions: Phase i data. *The Astronomical Journal*, 131(6):2921–2933, June 2006.

Eugenio J Rivera, Gregory Laughlin, R Paul Butler, Steven S Vogt, Nader Haghighipour, and Stefano Meschiari. The lick-carnegie exoplanet survey: a uranus-mass fourth planet for gj 876 in an extrasolar laplace configuration. *The Astrophysical Journal*, 719(1):890–899, August 2010.

S Roeser, M Demleitner, and E Schilbach. The ppmxl catalog of positions and proper motions on the icrs. combining usno-b1.0 and the two micron all sky survey (2mass). *The Astronomical Journal*, 139 (6):2440–2447, June 2010.

Gisela A Romero, Matthias R Schreiber, Lucas A Cieza, Alberto Rebassa-Mansergas, Bruno Merin, Analía V Smith Castelli, Lori E Allen, and Nidia Morrell. The nature of transition circumstellar disks. ii. southern molecular clouds. *The Astrophysical Journal*, 749(1):79, April 2012.

Katherine A Rosenfeld, Eugene Chiang, and Sean M Andrews. Fast radial flows in transition disk holes. *The Astrophysical Journal*, 782(2):62, February 2014.

Giovanni P Rosotti, Barbara Ercolano, James E Owen, and Philip J Armitage. The interplay between x-ray photoevaporation and planet formation. *Monthly Notices of the Royal Astronomical Society*, 430(2):1392–1401, April 2013.

Giovanni P Rosotti, Barbara Ercolano, and James E Owen. The long-term evolution of photoevaporating transition discs with giant planets. *Monthly Notices of the Royal Astronomical Society*, 454(2):2173–2182, December 2015.

V S Safronov. On the gravitational instability in flattened systems with axial symmetry and non-uniform rotation. *Annales d'Astrophysique*, 23:979, February 1960.

Shigeyuki Sako, Takuya Yamashita, Hirokazu Kataza, Takashi Miyata, Yoshiko K Okamoto, Mitsuhiko Honda, Takuya Fujiyoshi, Hiroshi Terada, Takeshi Kamazaki, Zhibo Jiang, Tomoyuki Hanawa, and Takashi Onaka. No high-mass protostars in the silhouette young stellar object m17-so1. *Nature*, 434 (7):995–998, April 2005.

S Sallum, K B Follette, J A Eisner, L M Close, P Hinz, K Kratter, J Males, A Skemer, B Macintosh, P Tuthill, V Bailey, D Defrère, K Morzinski, T Rodigas, E Spalding, A Vaz, and A J Weinberger. Accreting protoplanets in the lkca 15 transition disk. *Nature*, 527(7578):342–344, November 2015.

C Salyk, G A Blake, A C A Boogert, and J M Brown. Molecular gas in the inner 1 au of the tw hya and gm aur transitional disks. *The Astrophysical Journal*, 655(2):L105–L108, February 2007.

C Salyk, G A Blake, A C A Boogert, and J M Brown. High-resolution 5 μm spectroscopy of transitional disks. *The Astrophysical Journal*, 699(1):330–347, July 2009.

H M Schmid, F Joos, and D Tschan. Limb polarization of uranus and neptune. i. imaging polarimetry and comparison with analytic models. *Astronomy and Astrophysics*, 452(2):657–668, June 2006.

Tobias Schmidt and Ralph Neuhäuser. Finding new sub-stellar co-moving companion candidates - the case of ct cha. *Exoplanets: Detection*, 249(S249):65–69, May 2008.

G Schneider, K Wood, M D Silverstone, D C Hines, D W Koerner, B A Whitney, J E Bjorkman, and P J Lowrance. Nicmos coronagraphic observations of the gm aurigae circumstellar disk. *The Astronomical Journal*, 125(3):1467–1479, March 2003.

J Schneider, C Dedieu, P Le Sidaner, R Savalle, and I Zolotukhin. Defining and cataloging exoplanets: the exoplanet.eu database. *Astronomy and Astrophysics*, 532:A79, August 2011.

Frank Shu, Joan Najita, Eve Ostriker, Frank Wilkin, Steven Ruden, and Susana Lizano. Magnetocentrifugally driven flows from young stars and disks. 1: A generalized model. *The Astrophysical Journal*, 429:781–796, July 1994.

M Simon, A Dutrey, and S Guilloteau. Dynamical masses of t tauri stars and calibration of pre-main-sequence evolution. *The Astrophysical Journal*, 545(2):1034–1043, December 2000.

Janet P Simpson, Michael G Burton, Sean W J Colgan, Angela S Cotera, Edwin F Erickson, Dean C Hines, and Barbara A Whitney. Hubble space telescope nicmos polarization observations of three edge-on massive young stellar objects. *The Astrophysical Journal*, 700(2):1488–1501, August 2009.

M F Skrutskie, Diane Dutkevitch, Stephen E Strom, Suzan Edwards, Karen M Strom, and Mark A Shure. A sensitive 10-micron search for emission arising from circumstellar dust associated with solar-type pre-main-sequence stars. *Astronomical Journal (ISSN 0004-6256)*, 99:1187–1195, April 1990.

M F Skrutskie, R M Cutri, R Stiening, M D Weinberg, S Schneider, J M Carpenter, C Beichman, R Capps, T Chester, J Elias, J Huchra, J Liebert, C Lonsdale, D G Monet, S Price, P Seitzer, T Jarrett, J D Kirkpatrick, J E Gizis, E Howard, T Evans, J Fowler, L Fullmer, R Hurt, R Light, E L Kopan, K A Marsh, H L McCallon, R Tam, S Van Dyk, and S Wheelock. The two micron all sky survey (2mass). *The Astronomical Journal*, 131(2):1163–1183, February 2006.

Gilbert St-Onge and Pierre Bastien. A jet associated with the classical t tauri star ry tauri. *The Astrophysical Journal*, 674(2):1032–1036, February 2008.

Karen M Strom, Stephen E Strom, Suzan Edwards, Sylvie Cabrit, and Michael F Skrutskie. Circumstellar material associated with solar-type pre-main-sequence stars - a possible constraint on the timescale for planet building. *Astronomical Journal (ISSN 0004-6256)*, 97:1451–1470, May 1989.

Takeru K Suzuki, Takayuki Muto, and Shu-ichiro Inutsuka. Protoplanetary disk winds via magnetorotational instability: Formation of an inner hole and a crucial assist for planet formation. *The Astrophysical Journal*, 718(2):1289–1304, August 2010a.

Takeru K Suzuki, Takayuki Muto, and Shu-ichiro Inutsuka. Protoplanetary disk winds via magnetorotational instability: Formation of an inner hole and a crucial assist for planet formation. *The Astrophysical Journal*, 718(2):1289–1304, August 2010b.

Michihiro Takami, Yasuhiro Hasegawa, Takayuki Muto, Pin-Gao Gu, Ruobing Dong, Jennifer L Karr, Jun Hashimoto, Nobuyuki Kusakabe, Edwige Chapillon, Ya-Wen Tang, Youchi Itoh, Joseph Carson, Katherine B Follette, Satoshi Mayama, Michael Sitko, Markus Janson, Carol A Grady, Tomoyuki Kudo, Eiji Akiyama, Jungmi Kwon, Yasuhiro Takahashi, Takuya Suenaga, Lyu Abe, Wolfgang Brandner, Timothy D Brandt, Thayne Currie, Sebastian E Egner, Markus Feldt, Olivier Guyon, Yutaka Hayano, Masahiko Hayashi, Saeko Hayashi, Thomas Henning, Klaus W Hodapp, Mitsuhiko Honda, Miki Ishii, Masanori Iye, Ryo Kandori, Gillian R Knapp, Masayuki Kuzuhara, Michael W McElwain, Taro Matsuo, Shoken Miyama, Jun-Ichi Morino, Amaya Moro-Martin, Tetsuo Nishimura, Tae-Soo Pyo, Eugene Serabyn, Hiroshi Suto, Ryuji Suzuki, Naruhisa Takato, Hiroshi Terada, Christian Thalmann, Daigo Tomono, Edwin L Turner, John P Wisniewski, Makoto Watanabe, Toru Yamada, Hideki Takami, Tomonori Usuda, and Motohide Tamura. Surface geometry of protoplanetary disks inferred from near-infrared imaging polarimetry. *arXiv.org*, September 2014.

Motohide Tamura. Subaru strategic exploration of exoplanets and disks with hiciao/ao188 (seeds). In *EXOPLANETS AND DISKS: THEIR FORMATION AND DIVERSITY: Proceedings of the International Conference. AIP Conference Proceedings*, pages 11–16. National Astronomical Observatory of Japan, Mitaka, Tokyo 181-8588 motohide.tamuraatnao.ac.jp, AIP, August 2009.

Motohide Tamura, Klaus Hodapp, Hideki Takami, Lyu Abe, Hiroshi Suto, Olivier Guyon, Shane Jacobson, Ryo Kandori, Jun-Ichi Morino, Naoshi Murakami, Vern Stahlberger, Ryuji Suzuki, Alexander Tavrov, Hubert Yamada, Jun Nishikawa, Nobuharu Ukita, Jun Hashimoto, Hideyuki Izumiura, Masahiko Hayashi, Tadashi Nakajima, and Tetsuo Nishimura. Concept and science of hiciao: high contrast instrument for the subaru next generation adaptive optics. *Ground-based and Airborne Instrumentation for Astronomy. Edited by McLean*, 6269:62690V–62690V–9, June 2006.

Hidekazu Tanaka, Youhei Himeno, and Shigeru Ida. Dust growth and settling in protoplanetary disks and disk spectral energy distributions. i. laminar disks. *The Astrophysical Journal*, 625(1):414–426, May 2005.

C Thalmann, J Carson, M Janson, M Goto, M McElwain, S Egner, M Feldt, J Hashimoto, Y Hayano, T Henning, K W Hodapp, R Kandori, H Klahr, T Kudo, N Kusakabe, C Mordasini, J I Morino, H Suto, R Suzuki, and M Tamura. Discovery of the coldest imaged companion of a sun-like star. *The Astrophysical Journal Letters*, 707(2):L123–L127, December 2009.

C Thalmann, C A Grady, M Goto, J P Wisniewski, M Janson, T Henning, M Fukagawa, M Honda, G D Mulders, M Min, A Moro-Martin, M W McElwain, K W Hodapp, J Carson, L Abe, W Brandner, S Egner, M Feldt, T Fukue, T Golota, O Guyon, J Hashimoto, Y Hayano, M Hayashi, S Hayashi, M Ishii, R Kandori, G R Knapp, T Kudo, N Kusakabe, M Kuzuhara, T Matsuo, S Miyama, J I Morino, T Nishimura, T S Pyo, E Serabyn, H Shibai, H Suto, R Suzuki, M Takami, N Takato, H Terada, D Tomono, E L Turner, M Watanabe, T Yamada, H Takami, T Usuda, and M Tamura. Imaging of a transitional disk gap in reflected light: Indications of planet formation around the young solar analog lkca 15. *The Astrophysical Journal Letters*, 718(2):L87–L91, August 2010.

C Thalmann, M Janson, E Buenzli, T D Brandt, J P Wisniewski, A Moro-Martin, T Usuda, G Schneider, J Carson, M W McElwain, C A Grady, M Goto, L Abe, W Brandner, C Dominik, S Egner, M Feldt, T Fukue, T Golota, O Guyon, J Hashimoto, Y Hayano, M Hayashi, S Hayashi, T Henning, K W Hodapp, M Ishii, M Iye, R Kandori, G R Knapp, T Kudo, N Kusakabe, M Kuzuhara, T Matsuo, S Miyama, J I Morino, T Nishimura, T S Pyo, E Serabyn, H Suto, R Suzuki, Y H Takahashi, M Takami, N Takato, H Terada, D Tomono, E L Turner, M Watanabe, T Yamada, H Takami, and M Tamura. Images of the extended outer regions of the debris ring around hr 4796 a. *The Astrophysical Journal Letters*, 743(1):L6, December 2011.

C Thalmann, G D Mulders, K Hodapp, M Janson, C A Grady, M Min, M de Juan Ovelar, J Carson, T Brandt, M Bonnefoy, M W McElwain, J Leisenring, C Dominik, T Henning, and M Tamura. The architecture of the lkca 15 transitional disk revealed by high-contrast imaging. *Astronomy and Astrophysics*, 566:A51, June 2014.

C Thalmann, G D Mulders, M Janson, J Olofsson, M Benisty, H Avenhaus, S P Quanz, H M Schmid, T Henning, E Buenzli, F Ménard, J C Carson, A Garufi, S Messina, C Dominik, J Leisenring, G Chauvin, and M R Meyer. Optical imaging polarimetry of the lkca 15 protoplanetary disk with sphere zimpol. *The Astrophysical Journal Letters*, 808(2):L41, August 2015.

Alan T Tokunaga, Naoto Kobayashi, James Bell, Gregory K Ching, Klaus-Werner Hodapp, Joseph L Hora, Doug Neill, Peter M Onaka, John T Rayner, Louis Robertson, David W Warren, Mark Weber, and Tony T Young. Infrared camera and spectrograph for the subaru telescope. *Proc. SPIE Vol. 3354*, 3354:512–524, August 1998.

A Toomre. On the gravitational stability of a disk of stars. *Astrophysical Journal*, 139:1217–1238, May 1964.

K I Uchida, N Calvet, L Hartmann, F Kemper, W J Forrest, D M Watson, P D'Alessio, C H Chen, E Furlan, B Sargent, B R Brandl, T L Herter, P Morris, P C Myers, J Najita, G C Sloan, D J Barry, J Green, L D Keller, and P Hall. The state of protoplanetary material 10 million years after stellar formation: Circumstellar disks in the tw hydrae association. *The Astrophysical Journal Supplement Series*, 154(1):439–442, September 2004.

Pieter G van Dokkum. Cosmic-ray rejection by laplacian edge detection. *The Publications of the Astronomical Society of the Pacific*, 2001.

F van Leeuwen. Validation of the new hipparcos reduction. *Astronomy and Astrophysics*, 474(2):653–664, November 2007.

Kevin Wagner, Daniel Apai, Markus Kasper, and Massimo Robberto. Discovery of a two-armed spiral structure in the gapped disk around herbig ae star hd 100453. *The Astrophysical Journal Letters*, 813 (1):L2, November 2015.

Zahed Wahhaj, Lucas Cieza, David W Koerner, Karl R Stapelfeldt, Deborah L Padgett, April Case, James R Keller, Bruno Merin, Neal J II Evans, Paul Harvey, Anneila Sargent, Ewine F van Dishoeck, Lori Allen, Geoff Blake, Tim Brooke, Nicholas Chapman, Lee Mundy, and Philip C Myers. The spitzer c2d survey of weak-line t tauri stars. iii. the transition from primordial disks to debris disks. *The Astrophysical Journal*, 724(2):835–854, December 2010.

derek ward thompson and anthony p whitworth. *An Introduction to Star Formation*. Cambridge University Press, 1 edition, 2011.

D J Weights, P W Lucas, P F Roche, D J Pinfield, and F Riddick. Infrared spectroscopy and analysis of brown dwarf and planetary mass objects in the orion nebula cluster. *Monthly Notices of the Royal Astronomical Society*, 392(2):817–846, January 2009.

B A Whitney, T P Robitaille, J E Bjorkman, R Dong, M J Wolff, K Wood, and J Honor. Three-dimensional radiation transfer in young stellar objects. *The Astrophysical Journal Supplement Series*, 207(2):30, July 2013.

Barbara A Whitney and Michael J Wolff. Scattering and absorption by aligned grains in circumstellar environments. *The Astrophysical Journal*, 574(1):205–231, July 2002.

B A Wilking, M Gagné, and L E Allen. Star formation in the ρ ophiuchi molecular cloud. *Handbook of Star Forming Regions*, I:351, December 2008.

Bruce A Wilking, Thomas P Greene, and Michael R Meyer. Spectroscopy of brown dwarf candidates in the rho ophiuchi molecular core. *The Astronomical Journal*, 117(1):469–482, January 1999.

Bruce A Wilking, Michael R Meyer, John G Robinson, and Thomas P Greene. Optical spectroscopy of the surface population of the ρ ophiuchi molecular cloud: The first wave of star formation. *The Astronomical Journal*, 130(4):1733–1751, October 2005.

Jonathan P Williams and Lucas A Cieza. Protoplanetary disks and their evolution. *Annual Review of Astronomy and Astrophysics*, 49(1):67–117, September 2011.

David J Wilner, Sean M Andrews, and A Meredith Hughes. Millimeter imaging of the β pictoris debris disk: Evidence for a planetesimal belt. *The Astrophysical Journal Letters*, 727(2):L42, February 2011.

Scott J Wolk and Frederick M Walter. A search for protoplanetary disks around naked t tauri stars. *Astronomical Journal*, 111:2066, May 1996.

Edward L Wright, Peter R M Eisenhardt, Amy K Mainzer, Michael E Ressler, Roc M Cutri, Thomas Jarrett, J Davy Kirkpatrick, Deborah Padgett, Robert S McMillan, Michael Skrutskie, S A Stanford, Martin Cohen, Russell G Walker, John C Mather, David Leisawitz, Thomas N Gautier, Ian McLean, Dominic Benford, Carol J Lonsdale, Andrew Blain, Bryan Mendez, William R Irace, Valerie Duval, Fengchuan Liu, Don Royer, Ingolf Heinrichsen, Joan Howard, Mark Shannon, Martha Kendall, Amy L Walsh, Mark Larsen, Joel G Cardon, Scott Schick, Mark Schwalm, Mohamed Abid, Beth Fabinsky, Larry Naes, and Chao-Wei Tsai. The wide-field infrared survey explorer (wise): Mission description and initial on-orbit performance. *The Astronomical Journal*, 140(6):1868–1881, November 2010.

Mark C Wyatt. Evolution of debris disks. *Annual Review of Astronomy and Astrophysics*, 46(1):339–383, September 2008.

N Zacharias, C T Finch, T M Girard, A Henden, J L Bartlett, D G Monet, and M I Zacharias. The fourth us naval observatory ccd astrograph catalog (ucac4). *The Astronomical Journal*, 145(2):44, February 2013.

Zhaohuan Zhu, Richard P Nelson, Lee Hartmann, Catherine Espaillat, and Nuria Calvet. Transitional and pre-transitional disks: Gap opening by multiple planets? *The Astrophysical Journal*, 729(1):47, March 2011.

Zhaohuan Zhu, Richard P Nelson, Ruobing Dong, Catherine Espaillat, and Lee Hartmann. Dust filtration by planet-induced gap edges: Implications for transitional disks. *The Astrophysical Journal*, 755(1): 6, August 2012.

B Zuckerman and E E Becklin. Companions to white dwarfs - very low-mass stars and the brown dwarf candidate gd 165b. *Astrophysical Journal*, 386:260–264, February 1992.